UNIVERSITY OF CALIFORNIA

Los Angeles

Exoplanetary Spin States in Cool Dwarf Systems: Effects of Mean Motion Resonances and Atmospheric Tides

A dissertation submitted in partial satisfaction

of the requirements for the degree

Doctor of Philosophy in Astronomy and Astrophysics

by

Alec Matthew Vinson

2020

ABSTRACT OF THE DISSERTATION

Exoplanetary Spin States in Cool Dwarf Systems:
Effects of Mean Motion Resonances and Atmospheric Tides

by

Alec Matthew Vinson
Doctor of Philosophy in Astronomy and Astrophysics
University of California, Los Angeles, 2020
Professor Brad M.S. Hansen, Chair

One longstanding problem for the potential habitability of Earth-like planets around very small, cool dwarf stars is their perceived likelihood of being tidally locked into synchronous spin states wherein the planet's spin rate equals its orbital rate resulting in a perpetual day and corresponding night side on the planet. This problem had thus far largely been addressed by only considering two objects in the modeling: the planet under consideration and the star around which it orbits. However, many systems have been found to harbor multiple planets, with some in or near mean motion resonances. One prime example is the TRAPPIST-1 system, which contains at least seven terrestrial planets arranged compactly in a long resonant chain around a small ultra-cool dwarf star. The new Transiting Exoplanet Survey Satellite (*TESS*) also promises to reveal many new habitable zone planets around small stars. The presence of one or more nearby planetary companions near a mean motion resonance can induce oscillatory variations in the mean motion of the planet, which we show can have potentially dramatic influences on the effective spin state of a planet. In particular, we find that planetary companions can excite the spin states of planets in the habitable zone of small, cool stars, pushing otherwise synchronously rotating planets into higher amplitude librations in the spin state or even fully circulating states resulting in full stellar days. In other cases, especially those with multiple companion planets, we find that spin states are unable to sustain long-term stability, switching among quasi-stable attractor states. We also explore effects that atmospheric tides can have on the resultant spin states, finding that they can work to increase the the spin rates in many cases. Overall, we find that these effects can result in an increased illumination area on such planets, having potentially drastic consequences for habitability.

The dissertation of Alec Matthew Vinson is approved.

Mark R. Morris

Jean-Luc Margot

Smadar Naoz

Brad M.S. Hansen, Committee Chair

University of California, Los Angeles

2020

TABLE OF CONTENTS

LIST OF FIGURES

LIST OF TABLES

ACKNOWLEDGMENTS

This achievement would not have been possible without many people in my life. I would first like to thank those who directly contributed and provided thoughts, advice, and guidance for this dissertation: my advisor, Brad Hansen, and my collaborator, Dan Tamayo. Brad has provided his help and support since the beginnings of this project, and Dan provided his own academic and career advice along with direct contributions to some work presented in this dissertation. They have both been invaluable as collaborators, and I thank them very much for their support and insights.

I would also like to thank my fellow students, colleagues, and friends at both UCLA and Cal Poly Pomona for their support, especially during the most challenging moments, and for many fond memories. I would especially like to thank Mario, Chris, and Ashley for their support and friendship during our undergraduate careers. If it weren't for them, I would never have made it nearly this far, and likely would never have went to graduate school.

I also thank all my professors, at both UCLA and at Cal Poly Pomona, who helped impart not just knowledge of physics and astronomy onto me, but also how to solve problems and do research in astrophysics. In particular, I'd like to thank Alex Rudolph and Matthew Povich for their support and encouragement, as well as the CAMPARE program, which provided the support and encouragement that, in part, led to me pursuing a PhD in Astrophysics.

I also would like to thank my family for their encouragement and support, even through challenging times, and for never doubting my potential for success. In particular, I'd like to thank my dad for introducing me to Carl Sagan's Cosmos series, which I believe played a large part in instilling an interest in science in me when I was young. I also thank the Moz family for their invaluable support and generosity that allowed me the opportunity to finish high school and the early parts of college with as little stress as possible.

Finally, I would like to thank Jareni Polanco for her encouragement, support, and love during these past two and a half years, and for her eagerness to always provide help and moral support. She was always there to provide comfort and restore my spirits.

VITA

2014	Bachelor of Science in Physics with Minor in Mathematics, *magna cum laude* California State Polytechnic University, Pomona
2018	Master of Science in Astronomy University of California, Los Angeles

PUBLICATIONS

Vinson, A. M. and Hansen, B. M. S. (2017). On the spin states of habitable zone exoplanets around M dwarfs: the effect of a near-resonant companion. *Monthly Notices of the Royal Astronomical Society* 472:3217–3229.

Vinson, A. M., Tamayo, D., and Hansen, B. M. S. (2019). The chaotic nature of TRAPPIST-1 planetary spin states. *Monthly Notices of the Royal Astronomical Society*, 488(4):5739–5747.

Cheng, S. J., Vinson, A. M., and Naoz, S. (2019). Interacting young M-dwarfs in triple system - Par 1802 binary system case study. *Monthly Notices of the Royal Astronomical Society*, 489(2):2298–2306.

CHAPTER 1

Introduction

The search for habitable planets around nearby stars has spurred great interest in the lowest mass stellar hosts (see [Shields et al., 2016] for a review of habitability prospects around M dwarfs), because terrestrial planets are physically larger and more massive relative to the host as compared to higher-mass star systems, and therefore easier to detect and characterize. Furthermore, the sheer ubiquity of M dwarf stars (being by far the most common type of star), and the fact that the habitable zone is estimated to lie much closer to the fainter low mass stars, make the chance of a transit detection greater [Charbonneau and Deming, 2007]. The overall advantages that M dwarfs present for harboring and discovering habitable exoplanets are such that it can be referred to as the "small star advantage". The TRAPPIST-1 exoplanetary systems in particular has generated much interest, with seven planets observed in a compact configuration orbiting close-in to an ultra-cool dwarf star. Several of the reported planets lie in a long mean motion resonant chain, and several lie near or within the estimated habitable zone [Gillon et al., 2017].

Much of the optimism in regards to habitability prospects around such small, cool dwarfs is predicated on the assumption that a similar level of irradiation to that of the Earth correlates with habitable conditions and the existence of liquid water on the surface. However, with orbital periods on the order of just a few days, tidal interactions between the planets and the host star are expected to be significantly stronger than those the Earth experiences from the Sun. This would seem to suggest that these planets, or any planets orbiting within the habitable zone around such small and cool stars, would almost certainly be tidally locked into a synchronous spin state [Kasting et al., 1993, Turbet et al., 2018], wherein the planet's spin period and orbital period are equal to each other. This is often considered as a significant barrier to the habitability of such planets, because of the extreme temperature differences such conditions engender across the face of the planet, with predicted atmospheric collapse caused by the freezing of volatiles on the night side for planets with atmospheric compositions below certain threshold densities [Kasting et al., 1993, Joshi et al., 1997, Wordsworth et al., 2011, Wordsworth, 2015].

Alternatively, it is also possible for a planet to be trapped into higher-order, asynchronous spin-orbit resonances, depending on the degree to which the planet deviates from sphericity, the eccentricity of the orbit, and other functional dependencies of the tidal dissipation [Goldreich and Peale, 1966, Goldreich and Peale, 1968]. This is the case for Mercury within our own solar system [Margot et al., 2007].

In this work, we investigate the possibility that the tidal locking can also be affected and weakened by purely gravitational effects. The salient point to note is that most prior analyses of this problem have addressed the case of just a single planet orbiting the star (or, more generally, any satellite orbiting about another body). Yet, we know that many recently discovered planetary systems are (often highly) multiple [Lissauer et al., 2011, Fabrycky et al., 2014, Fang and Margot, 2012], even when restricting the sample to only M dwarfs (including the TRAPPIST-1 system) [Dressing and Charbonneau, 2013, Ballard and Johnson, 2016]. Thus, gravitational interactions among neighboring planets may also influence planetary spin states. One proposed way for a neighboring planet to influence the spin of another is through spin-orbit resonances of the second kind, where interactions cause the same face of the concerned planet to be oriented towards the neighboring planet at conjunction, given that the concerned planet is sufficiently deformed from sphericity [Goldreich and Peale, 1966, Goldreich and Peale, 1968]. However, this requires that the tidal torque contains a significant dependence on the synodic alignment of the planets, which is doubtful.

Instead, we will demonstrate that if a planet has one or more companion planets within the same system that are in or near a mean motion resonance with the primary, then interactions can be sufficiently strong (and sufficiently rapid if the orbital periods are short) to have a significant effect on the effective spin state. Although secular interactions can also drive changes in planetary properties, these usually occur on longer time-scales and suggest that the planetary spin would simply represent a long-term average over the secular oscillations. As we shall show, resonant interactions can drive evolution on time-scales sufficiently fast to lead to interactions with the climate system, opening up the possibility of interesting feedback between the spin evolution and climate. However, a mean motion resonance is a special configuration, and thus the model is only applicable to a fraction of the observed and postulated planetary systems. Nevertheless, such systems are known to exist. Examples include K2-21 [Petigura et al., 2015], which features two sub-Jovian planets near a 5:3 resonance orbiting around an M0 dwarf; Kepler-32 [Swift et al., 2013], an M0 star that features five planets with low-order commensurabilities between neighbors; TRAPPIST-1 [Gillon et al., 2017], with seven planets orbiting a star of $0.08 M_{\odot}$, including several that appear to be close to first-order commensurabilities; and the first habitable zone Earth-sized planet discovered by the spacecraft *TESS*, having an inner companion in a 7:3 commensurability [Gilbert et al., 2020]. Even if such systems represent only a fraction of the M dwarf planetary population, their special properties make them preferred candidates for detailed study.

For a synchronously rotating body (like the Earth's moon), its spin rate equals its orbital rate so as to always present the same face toward the primary. However, planets in, or near, a mean motion resonance undergo mean motion variations. As we will demonstrate, these variations create a moving target for the synchronicity of the spin rate to the mean motion, which can affect the spin in such a way that it stably librates about an equilibrium point in the frame co-rotating with the orbit, or else circulates completely, resulting in full, stable, stellar days.

As simple case studies, we will first consider hypothetical analogue systems based on the TRAPPIST-1 system, as well as the Kepler candidate K00255 system, which contains a star of mass $(0.53 \pm 0.06)\, M_{\odot}$, a confirmed planet of radius $R = (2.51 \pm 0.3)\, R_{\oplus}$ and orbital period of 27.52 days, and a candidate companion planet that would be near a 2:1 mean motion resonance with a radius of $(0.68 \pm 0.08)\, R_{\oplus}$ and orbital period of 13.60 days. In later chapters, we will consider a fuller treatment of the TRAPPIST-1 system, wherein we consider the full, complex effects of multiple resonant companions on the spin state. We will later also consider the TOI-700 system, containing the first Earth-sized planet in the estimated habitable zone of its system detected by *TESS*, and also happens to have a companion near a mean motion resonance.

In Chapter 2 , we will focus only how the spin of a planet would be affected by a single companion of much greater mass near resonance for illustrative purposes and to have a simple analytic formalism. To do this, we will consider a 'Pendulum Model' for the varying mean motion of the planet under the influence of a companion. This chapter will also introduce the basic formalism of our spin model, and how it incorporates orbital behaviors, which we will use in some form for future chapters as well. We will also consider a constant time-lag tidal damping model, with the tidal torque being simply proportional to spin rate of the planet in the frame co-rotating with its orbit.

In reality, planets in multi-planet systems tend to have similar masses [Millholland et al., 2017, Weiss et al., 2018], and thus mutually interact. Additionally, many planetary systems are highly multiple and can even form multi-resonant chains, with TRAPPIST-1 as the prime example. We will therefore incorporate the effects of multiple planets in a resonant chain on a planet's spin state, using the TRAPPIST-1 system to showcase our model and possible behaviors, in Chapter 3 . We will do this by utilizing N-body integrations of the TRAPPIST-1 system to extract variations in orbital parameters which can then be fed into our spin model.

In Chapter 4 we will consider a more complex tidal torque model, the 'Efroimsky Torque', which aims to more fully describe the complexities of tidal damping and can yield qualitatively different results and conclusions. We will compare this torque and the results on spin coupled with forcing as compared to the simpler tidal model that we will have used in Chapters 2 and 3. We will also include atmospheric tidal effects in our analysis, which can work to effectively weaken gravitational tides, resulting in potentially more excitation of the spin from the effects of resonant companions. Atmospheric torques can also strengthen higher-order spin-orbit resonances, or even create new, stable, non-synchronous equilibria in the spin.

Finally, Chapter 5 summarizes our findings and leaves us with concluding remarks.

CHAPTER 2

Single Companion Systems

Portions of this chapter are adapted from the publication:

Vinson, A. M. and Hansen, B. M. S. (2017). On the spin states of habitable zone exoplanets around M dwarfs: the effect of a near-resonant companion. *Monthly Notices of the Royal Astronomical Society* 472:3217–3229.

In this chapter we will introduce our spin model in Section 2.1, which is inspired largely by work presented in [Murray and Dermott, 1999], with the principal difference being that our model includes terms which allow orbital elements such as mean motion to vary. Orbital elements are allowed to vary under the influence of one companion planet. To describe variations in mean motion, we will use the so-called 'Pendulum Model' from [Murray and Dermott, 1999], which describes the mean motion as varying as something analogous to a pendulum. We will also introduce a simple tidal damping model which will be useful for illustrative purposes. Our resultant spin model will be somewhat analogous to a forced pendulum, but with key differences which we will note in Section 2.2.

We then address choices in parameters relevant for our systems of interest: those planetary systems with rocky Earth-like planets orbiting within the habitable zone of small, cool stars in Section 2.3. Finally, we will be able to showcase and analyze results in Section 2.4, as well as provide a discussion on implications and short-comings of this relatively simpler model in Section 2.5 before adding more complexity in future chapters.

Symbol	Definition
θ	inertial angle of long axis of planet
n	mean motion of primary
n'	mean motion of secondary companion
γ	Spin parameter, $\theta - nt$
ϕ	orbital resonant angle
a	semi-major axis of primary
a'	semi-major axis of secondary companion
e	eccentricity of primary
R	primary planet radius
m	primary planet mass
m'	secondary companion mass
M_*	stellar mass
A,B,C	principal moments of inertia
ω_S	natural spin angular frequency
ω_M	spin angular driving frequency
β	$2\omega_M^2/j\omega_S^2$
j	integer denoting choice in orbital resonance
σ	tidal bulk dissipation constant
Q	tidal dissipation parameter
ϵ	tidal dissipation strength parameter
year	will generally refer to a “terrestrial year” as opposed to general orbital period

Table 2.1: Symbol Definitions

2.1 Spin Model

We are principally interested in systems containing rocky Earth-like planets orbiting within the habitable zone of small cool stars. Within such systems, it has been suggested that the obliquity between a planet's spin and its orbit should erode quickly [Heller et al., 2011]. As such, we will consider a system with a planet of mass m orbiting a star of mass M_* with zero obliquity for our model. We note, however, that some more recent work (e.g. [Millholland et al., 2017]) has suggested that obliquity may vary for some planets in such systems, and thus could warrant further exploration in future work. Our assumption of zero obliquity should still be useful for many systems and for illustrative purposes while not changing many of our qualitative results.

We must allow for deviations from a perfectly spherical planet and will let A, B, and C define our principal moments of inertia of the planet, with C being the moment about the spin axis and A being the moment about the long axis of the planet lying within the orbital plane such that $B > A$. We define θ to be the angle formed between the long axis of the planet and a stationary line in the inertial frame. In anticipation of describing the spin in relation to its mean motion and to the synchronous spin state, we further define an angle $\gamma \equiv \theta - M$, where M is the mean anomaly of the planet. As such, $\dot{\gamma} = 0$ would correspond to the 1:1 synchronous spin-orbit case, and γ would also approximately define the location of substellar point in longitude on the planet at any one time (if the orbit has low eccentricity). If we assume that γ varies slowly relative to the orbit such that $\dot{\gamma} \ll n$, where n is the mean motion of the planet's orbit, then we can obtain the following equation of motion, the derivation of which can be found in [Murray and Dermott, 1999],

$$\ddot{\gamma} + \operatorname{sign}\left[H(e)\right] \frac{1}{2}\omega_S^2 \sin 2\gamma + \dot{n} = 0, \tag{2.1}$$

where $H(e)$ is a power series in orbital eccentricity e and $\omega_S^2 = 3n^2 \left(\frac{B-A}{C}\right) |H(e)|$. However, there is a crucial difference between equation 2.1 presented here and that presented in other sources, that difference being that we do not dispose of the $\dot{n}$ term on the presumption that it should be zero or insignificant. The key insight in this work is that $\dot{n}$ can vary due to strong mutual interactions with nearby companions in resonance, which we will show can then affect the behavior of γ under certain circumstances.

We further note that equation 2.1 resembles that of a pendulum (if we ignore $\dot{n}$ for now) with a natural spin frequency ω_S, except that here we have two stable equilibria at $\gamma = 0$ and $\gamma = \pi$. These equilibria correspond to the two possible orientations in which the long axis of the planet points towards the central star as the planet orbits. Under tidal damping forces, this would result in eventual synchronicity as γ damps to either 0 or π. This model, with an accompanying tidal damping model, is the standard way of modeling spin evolution of such planets, and can incorporate synchronous as well as asynchronous equilibria by using using more general forms of $H(p, e)$ where p is an integer multiple of 1/2 which corresponds to the spin-orbit resonance under consideration, and by further generalizing $\gamma \equiv \theta - pM$. In this work, we are concerned with objects at or near synchronicity and thus always set $p = 1$.

We can now consider variations in mean motion to determine how the $\dot{n}$ term in equation 2.1 may drive the evolution of spin in γ.

2.1.1 Mean Motion Variations Due to Companion in Resonance

For this work, we allow mean motion n to vary by first considering the consequences of adding just one companion planet such that it lies in or near a first-order mean motion resonance with the primary planet. We can then describe the variations in n via the 'Pendulum Model' described in detail by [Murray and Dermott, 1999]. This model describes variations of a resonant angle ϕ, with $\dot{\phi} = (j+1)n' - jn - \bar{\omega}$, where n and n' are the mean motions of the primary and secondary companion planets, respectively, and $\bar{\omega}$ is the primary planet's longitude of periastron. j is an integer which denotes the specific choice of resonance. With this formulation, we can describe the evolution of the planet in the context of the circular restricted three-body problem, where the secondary planet is on a perfectly circular, fixed orbit in the same orbital plane as the primary. This model is most directly applicable when the perturber is substantially more massive than the primary planet since it ignores any gravitational effects that the primary exerts on the secondary, but can still generally capture proper qualitative behavior. The evolution of n can then be described by

$$\dot{n} = -\frac{1}{j}\omega_M^2 \sin\phi, \tag{2.2}$$

with the equation of motion for resonant angle ϕ being

$$\ddot{\phi} = -\omega_M^2 \sin\phi, \tag{2.3}$$

where $\omega_M^2 = -3j^2 C_r n e$ and $C_r = \frac{m'}{m}\frac{a}{a'} n f_d$ is a constant depending on the nature of the perturber and the resonance, with a and a' being the semi major axis of the orbit of the primary and secondary companion, respectively, and f_d a function of the ratio a/a' arising from direct terms in the expansion of the disturbing function outlined and tabulated in [Murray and Dermott, 1999]. For instance, for the 2:1 and 3:2 resonant cases, $\frac{a}{a'} f_d = -0.7500$ and -1.5455, respectively.

With this, we now have a full description of how mean motion n varies in time, and with equation 2.2 describing the $\dot{n}$ term in equation 2.1 we have a more complete description of the evolution of the spin:

$$\ddot{\gamma} + \mathrm{sign}\left[H(e)\right] \frac{1}{2}\omega_S^2 \sin 2\gamma - \frac{1}{j}\omega_M^2 \sin\phi = 0, \tag{2.4}$$

We note that the above equation can now be seen as analogous to a forced pendulum, with the $\dot{n}$ from equation 2.1 becoming a forcing term with a frequency of ω_M. The forced pendulum is a model that arises in a variety of contexts, and is indeed one of the favorite subjects of dynamical systems studies (e.g. [Baker and Blackburn, 2005]) because it can yield a range of interesting chaotic and resonant behaviors when the two frequencies ω_S and ω_M are close in value. The principal differences between equation 2.4 and a standard forced pendulum are that 1) there are two stable equilibria in γ at 0 and π, 2) the forcing is itself a pendulum, not a simple sinusoid as commonly analyzed in the harmonic forcing case, and 3) the forcing strength is a function of the forcing frequency. The second and third points are important, as ϕ could itself be allowed to circulate or librate, and as increasing forcing frequency can also increase overall forcing strength.

Conceptually, γ can be thought of as always trying to track to either 0 or π, under the influence of tidal damping forces, such that $\dot{\gamma} = 0$ and hence $\dot{\theta} = n$. However, as n varies at some frequency, γ may be excited as it attempts to track to a moving target in n, especially if the natural spin frequency and the forcing frequency are close in value such that $\omega_S \approx \omega_M$.

2.1.2 Tidal Damping

Tides and their effects on spin and orbit are a long-studied subject (see [Ogilvie, 2014] for a review). There has also been growing literature on the mechanisms of tidal dissipation in Earth-like planets Notably for this work, tidal forces between planets and their host star are expected to be exceptionally strong in small cool dwarf systems, such as in the TRAPPIST-1 system, due to the relatively close proximity between the planets and the host star. This is thought to very likely lead to synchronous spin states for planets within the habitable zone of such systems in previous unforced considerations. For now, we will use the simpler 'constant time-lag' formalism, which should be sufficient for illustrative purposes and has the attractive quality that it avoids unphysical discontinuities by having tidal torque go to zero as $\dot{\gamma} \to 0$. In particular, we wish to focus on the spin behavior driven by changes in the forcing without contamination by spin flips associated with abrupt changes in the sign of the spin damping forces. In Chapter 4, we will revisit tidal modeling and consider a more complex model from [Makarov, 2012].

Tidal strengths and effects can be calibrated for giant planets (see [Hansen, 2010]), however the data for lower mass planets is not sufficient for direct calibration and we will draw on the additional calibration relative to the strength of tides on Earth. This is often expressed in terms of the 'tidal Q' parameter, but we wish to retain the functional form of our prior formulation based on the work of [Hut, 1981] and [Eggleton et al., 1998] because it has the attractive property that $\ddot{\gamma} \to 0$ as $\dot{\gamma} \to 0$. This allows a simple formulation, with damping being proportional to $\dot{\gamma}$. Using the formulation from [Hansen, 2010], we may describe the evolution of γ under the action of tides with

$$\ddot{\gamma}_{\text{tides}} = -\frac{15}{2}\dot{\gamma}\frac{M_*}{m}\left(\frac{R}{a}\right)^6 M_* R^2 \sigma, \tag{2.5}$$

where R is the planetary radius, and where we express the strength of dissipation in terms of a bulk dissipation constant, σ. Since much of the literature phrases the discussion in terms of the tidal dissipation factor Q, we will translate the bulk dissipation constant σ into a form in terms of an equivalent tidal Q, while still formally using the aforementioned convention that describes tidal dissipation in terms of a bulk dissipation constant. We can choose an equivalent tidal Q under the specific forcing applied to the Earth to describe the tidal damping strength on these Earth-like planets, with

$$\sigma = \frac{1}{2Q}\left(\frac{G}{\Omega R^5}\right), \tag{2.6}$$

wherein we set tidal forcing frequency $\Omega = 2\pi/day$, approximately equal to the tidal frequency exerted on the Earth by the Moon.

We can now write our full equation of motion for γ by adding the torque from equation 2.5 to equation 2.4:

$$\ddot{\gamma} + \frac{1}{2}\omega_S^2 \sin 2\gamma - \frac{1}{j}\omega_M^2 \sin\phi + \epsilon\dot{\gamma} = 0, \tag{2.7}$$

where we let damping strength be represented by $\epsilon = \frac{15}{2}\frac{M_*}{m}\left(\frac{R}{a}\right)^6 M_* R^2 \sigma$.

2.2 Comparisons to Standard Forced Pendulum

With equation 2.7, we can now make some qualitative comparisons to similar systems and make some approximations to yield a qualitative sense of how γ behaves under the influence of forcing and damping, and how that compares to the behavior of a standard forced pendulum.

Recall that one of the important differences between the standard pendulum and our treatment is that the amplitude of the forcing strength in our treatment depends directly on the forcing frequency, increasing as we increase forcing frequency. We will show that this has some potentially dramatic consequences. Let us first simplify the full equation of motion by using small angle approximations in γ and ϕ. This approximation will break down in our short study in this section, however we will later show that the approximation still gives insightful results that are qualitatively similar to the full results. Under this approximation, we can rewrite equation 2.7 as

$$\ddot{\gamma} + \omega_S^2 \gamma - \frac{1}{j}\omega_M^2 \phi + \epsilon \dot{\gamma} = 0 \tag{2.8}$$

Equation 2.8 is functionally very similar to a standard forced harmonic oscillator, except that the forcing term varies as $\frac{1}{j}\omega_M^2 \phi$, as opposed to a simple sinusoid, e.g. $\phi_0 \sin \omega_M t$ with ϕ_0 being the amplitude of the forcing. Figures 2.1 and 2.2 depict the qualitative differences between these two treatments. We note that, in our treatment, we can expect elevated amplitudes for γ and $\dot{\gamma}$ even as ω_M increases far from resonance. This is not totally unexpected since the forcing *strength* continually increases with forcing *frequency*, resulting in the forcing being the dominant term as forcing frequency increases. This can result in continued high-amplitude libration, or even circulation depending on other factors in the forcing and damping. We also note that there is also still expected to be a strong peak near the resonance at $\omega_M \approx \omega_S$, yielding higher likelihoods of circulation.

To further confirm any qualitative assessment of our treatment via the small-angle approximation, we also present actual results and compare to the small-angle approximation predictions in Figures 2.3 and 2.4. In these figures, we present how γ behaves as we fully integrate the full equation 2.7 for different values of ω_M and damping strengths ϵ. For these treatments, we also choose a small librating amplitude in ϕ so that the small approximation in ϕ is somewhat appropriate, even if it is not for γ. We also show the same results for the small-angle approximations. We can see that, while having slightly different amplitudes and having a different location in the resonance peak, that there are strong qualitative similarities.

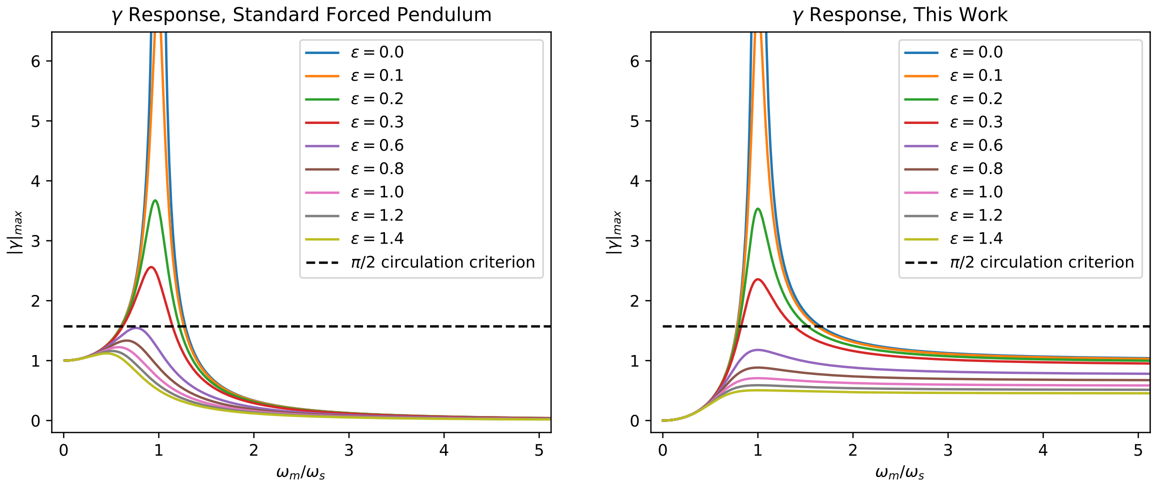

Figure 2.1: Here we plot the amplitude of γ as we vary forcing frequency ω_M with respect to natural frequency ω_S for the long-term behavior (time $\to \infty$) for various damping strengths ϵ (which are in units normalized the natural spin frequency ω_S). The left panel shows results for the standard forced harmonic oscillator, and the right for our work under the small angle approximations in γ and ϕ. We also depict the theoretical 'circulation criterion', above which we would expect circulation in γ and below which we would expect libration. Note that the differences are primarily evident in the limits as $\omega_M \to \infty$, with our work showing γ continuing to remain elevated as ω_M increases far from the resonance.

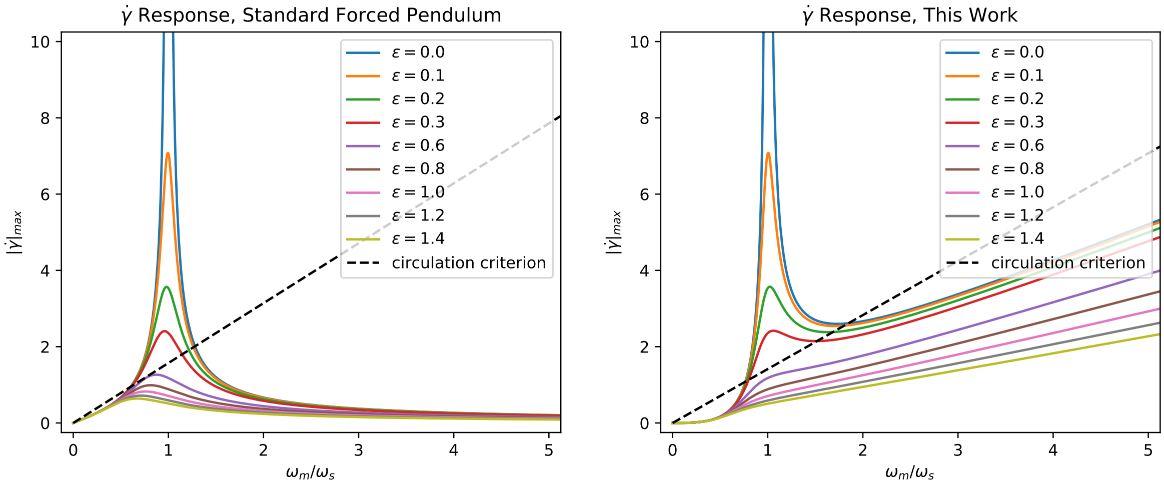

Figure 2.2: Here we plot the amplitude of $\dot{\gamma}$ as we vary forcing frequency ω_M with respect to natural frequency ω_S for the long-term behavior (time $\rightarrow \infty$) for various damping strengths ϵ (which are in units normalized the natural spin frequency ω_S). The left panel shows results for the standard forced harmonic oscillator, and the right for our work under the small angle approximations in γ and ϕ. We also depict the theoretical 'circulation criterion', above which we would expect circulation in γ and below which we would expect libration. Note that the differences are primarily evident in the limits as $\omega_M \rightarrow \infty$ and as $\omega_M \rightarrow 0$, with our work showing elevated amplitudes in γ even as ω_M increases far from the resonance.

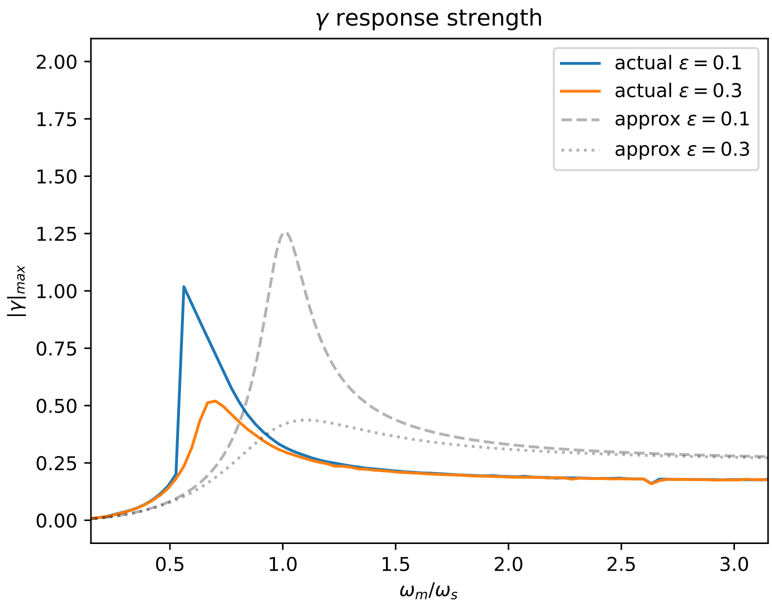

Figure 2.3: Here we plot the maximum value of the absolute value of γ as we vary forcing frequency ω_M with respect to natural frequency ω_S for the long-term behavior (time $\to \infty$) for various scenarios. Dashed and dotted lines represent the theoretical behavior for γ under small-angle approximations in γ and ϕ, where the damping strength is 0.3 and 0.1, normalized to natural frequency ω_S, respectively. The blue and orange lines show actual results without the small-angle approximations. We note that the small-angle approximations can at least show qualitatively useful information.

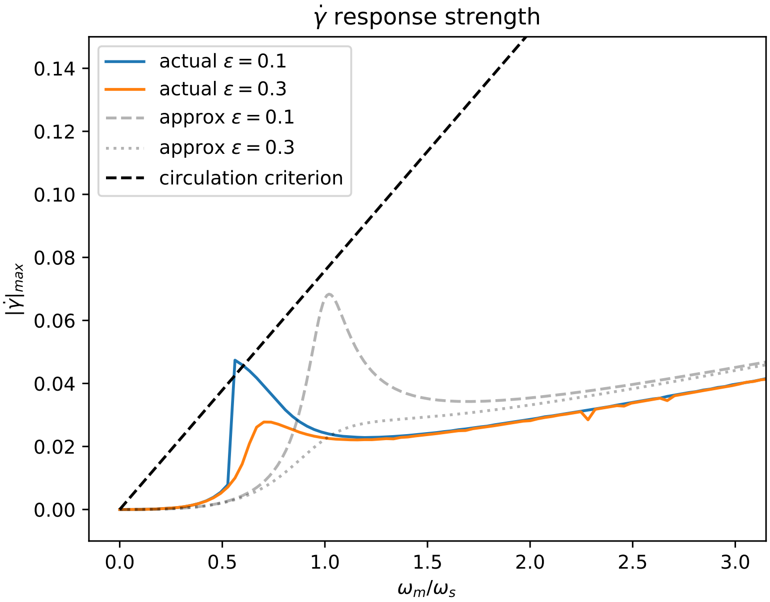

Figure 2.4: Here we plot the amplitude of $\dot{\gamma}$ as we vary forcing frequency ω_M with respect to natural frequency ω_S for the long-term behavior (time $\to \infty$) for various scenarios. Dashed and dotted lines represent the theoretical behavior for $\dot{\gamma}$ under small-angle approximations in γ and ϕ, where the damping strength is 0.3 and 0.1, normalized to natural frequency ω_S, respectively. The blue and orange lines show actual results without the small-angle approximations. We also depict the theoretical 'circulation criterion', above which we would expect circulation in γ and below which we would expect libration. We note that the small-angle approximations can at least show qualitatively useful information.

2.3 Setup

As shown in Section 2.2, the driving frequency should ideally have a value of similar order, or even larger, to the natural spin frequency, if we wish the driving to have significant implications on the evolution of the spin argument γ. Comparing the strengths of the two terms can characterize much of the behavior of the system:

$$\frac{2\omega_M^2}{j\omega_S^2} = 2|f_d| \left(\frac{j^{5/2}}{j+1}\right) \left(\frac{m'}{M_*}\right) \left(\frac{e/H(e)}{(B - A/C)}\right) \tag{2.9}$$

With this, we can determine what relative values of system parameters can lead to excited spin behavior. We can first make a simplifying assumption that $H(e) \sim 1$, appropriate for low eccentricity. We can further choose a value of $(B - A)/C$, which describes the asphericity of the planet, consistent with Earth-like planets of primary concern for this work. We therefore choose a value of $(B - A)/C = 2 \times 10^{-5}$ as our default value based on available empirical evidence determined for the Earth, Mars, and Mercury [Edvardsson et al., 2002, Margot et al., 2012, Chen et al., 2015]. We note, however, that estimates of the maximum probable triaxiality suggest that a value of ~ 10 times higher is possible depending on mass and ocean depth [Zanazzi and Lai, 2017]. If we set equation 2.9 to unity, we can rearrange to then solve for secondary mass m', choosing default parameter values consistent with our systems of interest

$$m' \sim 3 \left(\frac{(B - A)/C}{2 \times 10^{-5}}\right) \left(\frac{M_*}{0.5 M_\odot}\right) e M_\oplus, \tag{2.10}$$

implying that, ideally, values of secondary mass and eccentricity should together be such that $m'/e \sim 3M_\oplus$. Eccentricities for low-mass planetary systems can be quite difficult to determine empirically, but estimates based on transit timing variations (TTVs) (e.g. [Wu and Lithwick, 2013, Van Eylen and Albrecht, 2015, Hadden and Lithwick, 2014]) suggest that the majority have non-zero but small eccentricities, with estimates ranging from $e \sim 0.01$ up to as much as 0.1. Such values are also consistent with the level of eccentricity expected from *in situ* assembly models [Hansen and Murray, 2013, Hansen and Murray, 2015] or the requirement that many escape capture into resonant chains during an extended period of inward migration [Goldreich and Schlichting, 2014]. Thus, we will adopt a default value of $e \sim 0.05$, suggesting an optimal perturber mass of $m' \sim 50M_\oplus$ for a $0.5m_\odot$ stellar host. We note that this 'optimal value' for the secondary's mass decreases as the stellar host's mass decreases, so that if we were to choose a stellar host mass of $0.1M_\odot$ (closer to that of a system such as TRAPPIST-1), then the estimated 'optimal mass' for the perturber drops to $\sim 10M_\oplus$. Through this short analysis, it appears as though, by simple numerical coincidence, the susceptibility of a terrestrial planet to spin perturbations in compact, small star systems is such that Neptune-mass companions, which have been observed in such systems, can drive interesting spin dynamics.

One such example of a such a system that we can consider is the *Kepler* candidate system K00255, which contains a star of mass $M_* = (0.53 \pm 0.06)\, M_\odot$, a confirmed planet K00255.01 of radius $R = 2.51 \pm 0.3R_\oplus$ and orbital period $T = 27.52$ days, and a candidate planet K00255.02 of radius $R = 0.68 \pm 0.08R_\oplus$ and orbital period $T = 13.60$ days. This would imply a system near a 2:1 mean motion resonance. This system would be almost perfect for our needs except that the larger outer planet is actually closer to the habitable zone than the inner smaller planet. Even so, the system can serve as a useful illustration of the kinds of behavior we may observe for more Earth-like planets in other systems. To estimate planetary mass, [Lissauer et al., 2011] and [Fabrycky et al., 2014] suggest a mass-radius relation of $M_p = M_\oplus \left(R_p/R_\oplus\right)^{2.06}$ for $R_p > R_\oplus$, which fits well within the solar system. Adopting this scaling relation for the outer planet yields a mass of $m' = 7M_\oplus$.

Another system of interest is the TRAPPIST-1 system [Gillon et al., 2017], which contains at least seven transiting planets orbiting compactly around a very low mass ($\sim 0.08M_\odot$) star in a long resonant chain. At least three planets lie within or close to the estimated habitable zone. Radii and mass estimates (constrained by TTVs) suggest that these planets are also rocky, making them an excellent case study for our model.

In our analysis in future sections in this chapter, we will take inspiration from the K00255 and TRAPPIST-1 systems in choosing input parameter values. For all of our analysis, we will choose an Earth-sized planet of mass $m = M_\oplus$ and radius $R = R_\oplus$ as our primary planet.

The semi-major axis of the primary planet and its outer secondary companion will be taken from the K00255 and TRAPPIST-1 systems, where for TRAPPIST-1, we consider only two planets at a time: a primary planet and its nearest outer companion. A more complete treatment wherein we consider multi-planet influences will be discussed in Chapter 3. For tidal damping strengths, we will examine two scenarios: a higher tidal damping strength corresponding to $Q = 10$, and a smaller damping strength corresponding to $Q = 100$.

For all results in the following section, we solve for γ with equation 2.7 using the Runge-Kutta fourth-order method of integration. Time steps adapt to the highest value of ω_S and ω_M, taking 70 time steps in the period corresponding to the highest frequency.

2.4 Results

In this section, we present results in the absence of tidal damping before we present how tidal forces affects the evolution in Section 2.4.2. This way we can more directly observe the affects of forcing due to mean motion variations in Section 2.4.1.

2.4.1 Without Tidal Damping

We will first focus on a hypothetical system based on the properties of the K00255 system. This system contains both an Earth-like interior planet and an external companion, which we will take as mass $m' = 7\ M_\oplus$, near the 2:1 commensurability around a 0.53 $M_\odot$ dwarf. For illustrative purposes, we choose to place the spin $1 M_\oplus$ planet at a location farther from the star ($0.15AU$) such that it receives the same stellar flux as the Earth, with $e = 0.05$ and $(B - A)/C = 2 \times 10^{-5}$. These parameters yield $\beta = \frac{2\omega_M^2}{j\omega_S^2} = 0.11$ (recalling that $\beta \sim 1$ is ideal for a larger spin response).

The dynamics of a pendulum also requires specifications of initial conditions. In this case, we require initial conditions not only in γ and $\dot{\gamma}$, but also ϕ and $\dot{\phi}$. Starting with the latter, pair, we choose $\phi(0) = 0$ for all runs, while varying $\dot{\phi}(0)$. The value of $\dot{\phi}(0)$ will then characterize the orbital dynamics of the resonant pair – small enough values will yield libration of ϕ and larger values will result in circulation.

For $\gamma - \dot{\gamma}$, we set $\gamma(0) = 0$ for all runs. The natural (no forcing) separatrix between circulation and libration would occur at $\dot{\gamma}(0) = 0.33$ yr^{-1} for this system. With this in mind, we consider three representative initial states consisting of small amplitude libration ($\dot{\gamma}(0) = 0.02$ yr^{-1}) , large amplitude libration ($\dot{\gamma}(0) = 0.25$ yr^{-1}), and circulation ($\dot{\gamma}(0) = 0.38$ yr^{-1}), and examine how each responds to different levels of forcing as determined by the amplitude of ϕ. For all these cases, we let the integrations runs for 10^5 years to allow sufficient time to approach any final spin state.

Figure 2.5 shows the evolution for the spin for the initial large amplitude libration case ($\dot{\gamma}(0) = 0.25$ yr^{-1} in response to four different levels of forcing as determined by $\dot{\phi}(0)$. To better characterize the behavior, we highlighted in red the values of γ and $\dot{\gamma}$ that occur when $\phi - 0$ and $\dot{\phi} > 0$ on the left-hand panels, known as a Poincare section (e.g. [Baker and Blackburn, 2005]). In panel a), we see that the behavior is qualitatively similar to what we would observe if there was no forcing. In panel b, however, we see that the spin behavior becomes chaotic, now switching between circulation and libration about both $\gamma = 0$ and $\gamma = \pi$. It is worth noting that, in the integration depicted in panel b, $\dot{\phi}(0) = 0.21$ yr^{-1} and resonant angle ϕ is circulating since the separatrix for ϕ would occur at $\dot{\phi}(0) = 0.11$ yr^{-1}. Thus, the most dramatic effects actually occur for ϕ *near* resonance, but not actually in it. As $\dot{\phi}(0)$ continues to increase in panel c, γ no longer evolves chaotically, though we see a slight increase in the libration amplitude as compared to natural libration without forcing; we also observe that the Poincare section is a smaller closed curve as compared to panel a, suggesting an approximate commensurability between the period of libration for γ and the period of circulation for ϕ. As we continue to increase $\dot{\phi}(0)$ into panel d, this commensurability becomes weaker and the surface of section expands, eventually enclosing the origin again. We can further summarize this behavior in Figure 2.6, in which we show the values of γ corresponding to the surface of section at $\phi = 0$ and $\dot{\phi} > 0$ plotted against initial $\dot{\phi}(0)$.

The large amplitude libration may be especially susceptible to showing chaotic behavior, since the natural oscillations (in the absence of forcing) are still a non-negligible amplitude

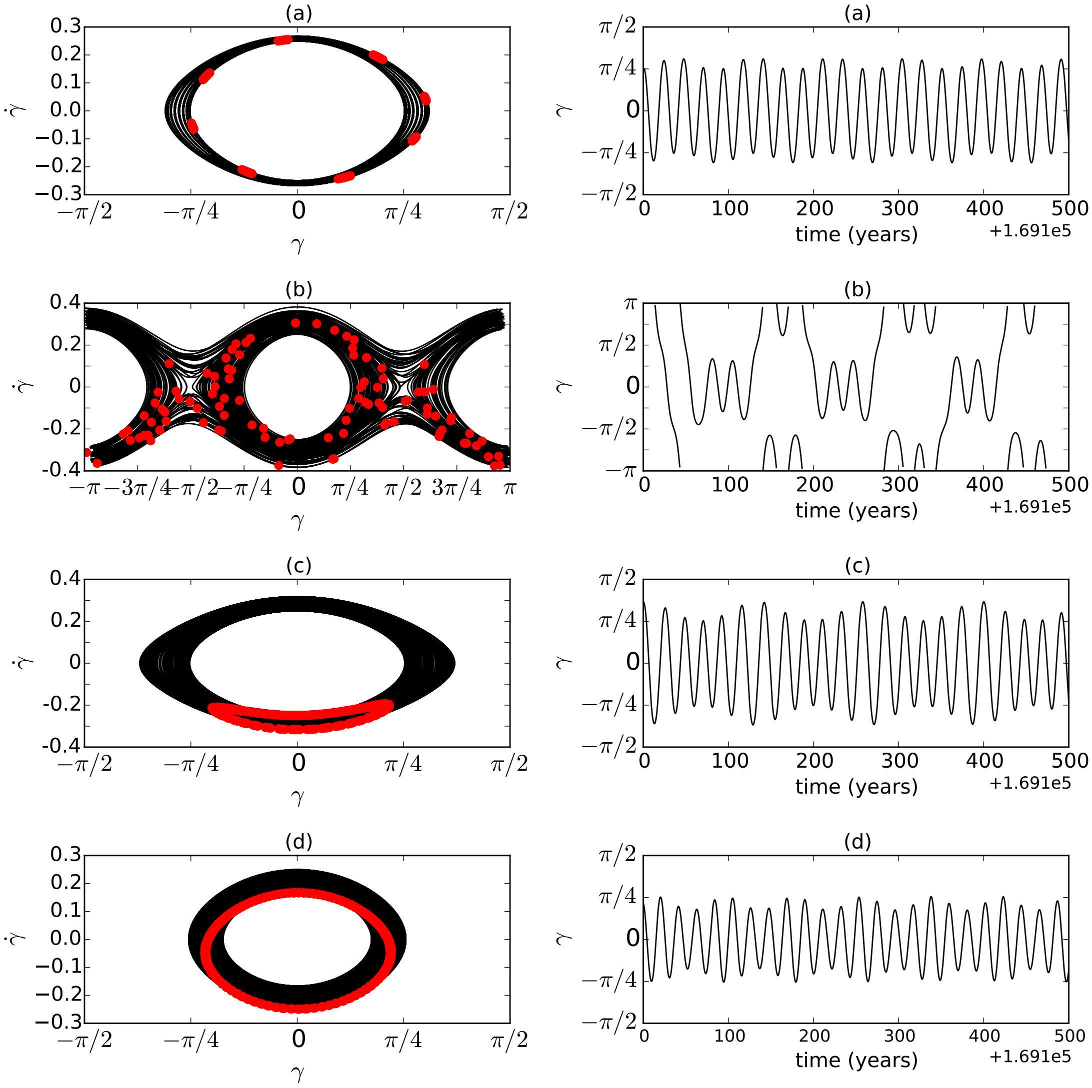

Figure 2.5: Here we depict four scenarios for the evolution of γ for our K00255 analogue system subject to driving without dissipation ($\epsilon = 0$). Each row panel depicts one integration, with left panels plotting results in $\dot{\gamma}$ - γ state space in black, with the surface of section plotted in red taken when $\phi = 0$ and $\dot{\phi} > 0$. The corresponding evolution of γ in time is shown on the right. Panels labeled a) have $\dot{\phi}(0) = 0.09$ yr^{-1}, b) have $\dot{\phi}(0) = 0.21$ yr^{-1}, c) have $\dot{\phi}(0) = 0.29$ yr^{-1}, and d) have $\dot{\phi}(0) = 0.39$ yr^{-1}. We set $\dot{\gamma}(0) = 0.25$ yr^{-1}, $\gamma(0) = 0$, and $\phi(0) = 0$ for each integration, with fiducial parameters chosen such that $\beta = 0.11$. We note the chaos that can be inherent in such systems, as seen in panel b.

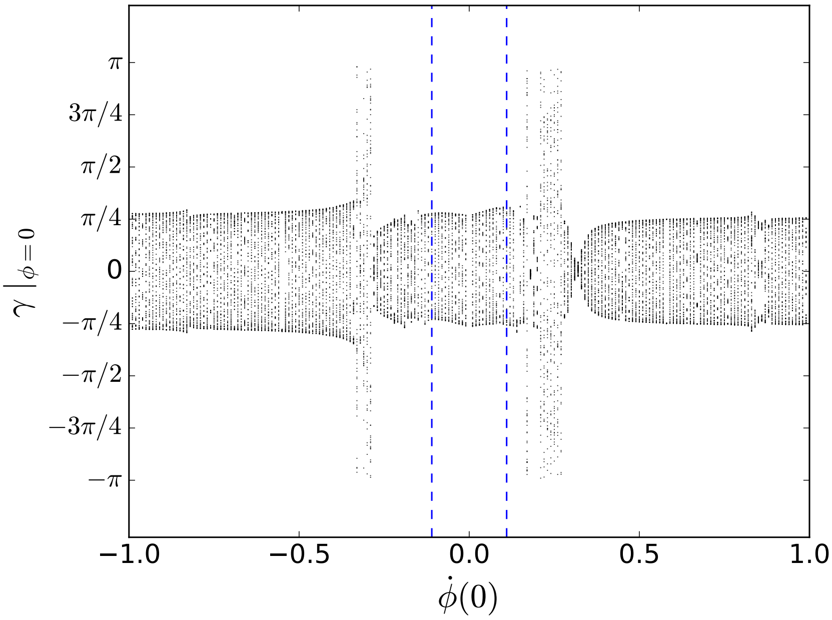

Figure 2.6: The points depict the values of γ in the surface of section defined by $\phi = 0$, and $\dot{\phi}$ with the sign of its initial value, for each value of the initial forcing $\dot{\phi}(0)$ when $\dot{\gamma}(0) = 0.25$ yr^{-1} for our K00255 analogue system, yielding $\beta = 0.11$, in the absence of damping ($\epsilon = 0$). The vertical dashed lines indicate the separatrix between libration and circulation (to the far left and right) of the external forcing resonant argument. Being in between these dashed lines is thus when the system is *in* a mean-motion resonance, with a librating resonant angle ϕ. We see that the character of the behavior is the same for both negative and positive values of $\dot{\phi}(0)$, but that it is not entirely symmetric.

relative to the separatrix value. Thus, in Figure 2.7 we consider the effect of a similar range of forcing, but now our initial $\dot{\gamma}(0) = 0.02$ yr^{-1}, so that the natural libration is of a much smaller amplitude. Once again, the effect of a librating ϕ is minimal, with the libration in γ not significantly affected, but with a circulating ϕ, with $\dot{\phi}(0) \sim \pm 0.3$ yr^{-1}, we again see stronger effects, with larger-amplitude librations. Thus, the character of the forced solution for a librating γ is similar regardless of amplitude – the effects are strongest for ϕ circulating at about twice the separatrix distance from exact resonance.

The character of the behavior for an initially circulating γ is different. This is shown in Figure 2.8 by depicting values of $\dot{\gamma}$ against $\dot{\phi}(0)$, which presents a more useful picture than the Poincare projection in this specific case. Here, the effect of a librating ϕ is to enforce intermittent libration of γ as well, but only if $\dot{\gamma}(0)$ and $\dot{\phi}(0)$ have the same sign. This is evident from the fact that Figure 2.8 shows far less symmetric behavior about the origin than either of Figure 2.6 or Figure 2.7. In this case the influence of the perturber is stronger if the system is closer to resonance.

Overall, these estimates suggest that a system with the parameters of the K00255 system could experience episodes of chaotic spin evolution if close to a mean-motion resonance. We can infer what a likely $\dot{\phi}$ is from observation, with $\dot{\phi} = (j+1)n - jn'$ assuming $\bar{\omega} = 0$, and let $\dot{\phi}(0)$ equal this. For the observed K00255 period ratio of 2.024, we infer $\dot{\phi}(0) = 2.0$ yr^{-1}, which is probably too distant from resonance to produce large effects. However, a less triaxial planet, with $(B-A)/C \sim 10^{-6}$, would lie within the chaotic zone at these periods.

Given the uncertainty in the eccentricity, perturber mass, and especially $(B-A)/C$ in the K00255 system, it is also worth considering the sensitivity of the system to changes in β. If we fix $\dot{\phi}(0) = 2.0$ yr^{-1}, consistent with the currently observed value based on period ratio, we can characterize the evolution of the spin for different values of β. For the case where $\dot{\gamma}(0) = 0.25$ yr^{-1}, Figure 2.9 shows how the spin-state varies with forcing amplitude β. We see that this system doesn't begin to undergo circulation, or chaotic motions, until $\beta > 12.5$. The character of the spin evolution is the same for larger values of β, except that the rotation gets progressively more rapid. From the threshold value of $\beta \sim 12.5$, we can estimate that a perturber mass of $(55/eM_{\oplus})\,|H(e)|$, with our fiducial $(B-A)/C = 2 \times 10^{-5}$, is required for

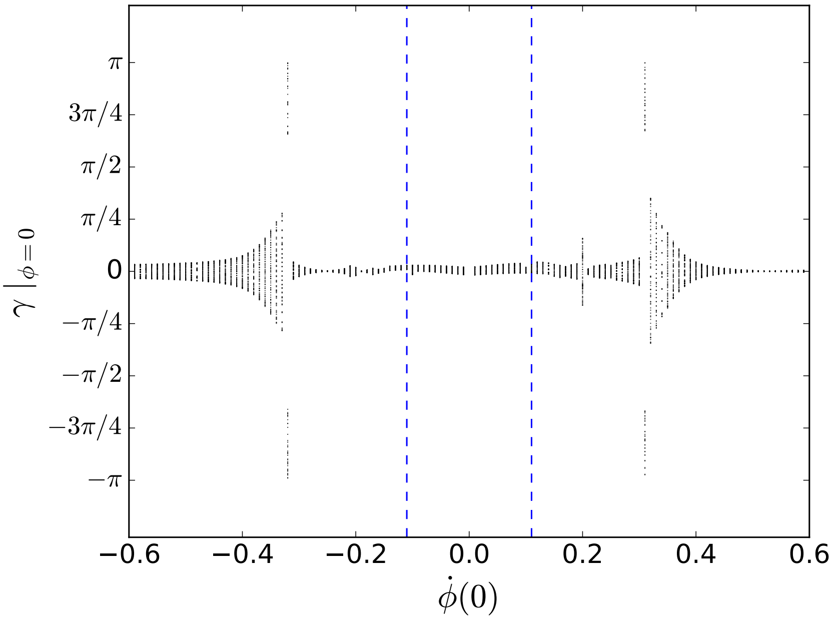

Figure 2.7: The points depict the values of γ in the surface of section defined by $\phi = 0$, and $\dot{\phi}$ with the sign of its initial value, for each value of the initial forcing $\dot{\phi}(0)$ when $\dot{\gamma}(0) = 0.02$ yr^{-1} for our K00255 analogue system, yielding $\beta = 0.11$, in the absence of damping ($\epsilon = 0$). The vertical dashed lines indicate the separatrix between libration and circulation (to the far left and right) of the external forcing resonant argument. Being in between these dashed lines is thus when the system is *in* a mean-motion resonance, with a librating resonant angle ϕ. We see that the character of the behavior is the same for both negative and positive values of $\dot{\phi}(0)$, but that it is not perfectly symmetric.

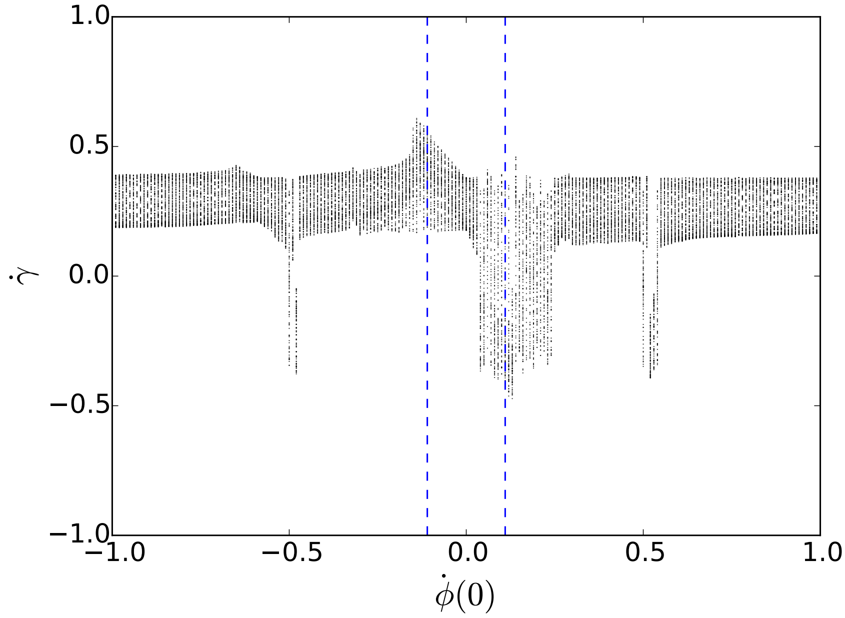

Figure 2.8: The points depict all $\dot{\gamma}$ (not just the surface of section) depending on the different initial forcing $\dot{\phi}(0)$ among our simulations for our nominal K00255 values ($\beta = 0.11$) in the absence of damping $\epsilon = 0$ with $\dot{\gamma}(0) = 0.38$ yr^{-1} (such that γ is initially circulating). The vertical dashed lines indicate the separatrix between libration and circulation of the external forcing resonant argument. Being in between these dashed lines is thus when the system is *in* a mean-motion resonance, with the resonant angle ϕ librating instead of circulating. We note the asymmetry, finding more dramatic effects near the separatrix for positive $\dot{\phi}(0)$, where γ evolution enters a wide chaotic regime.

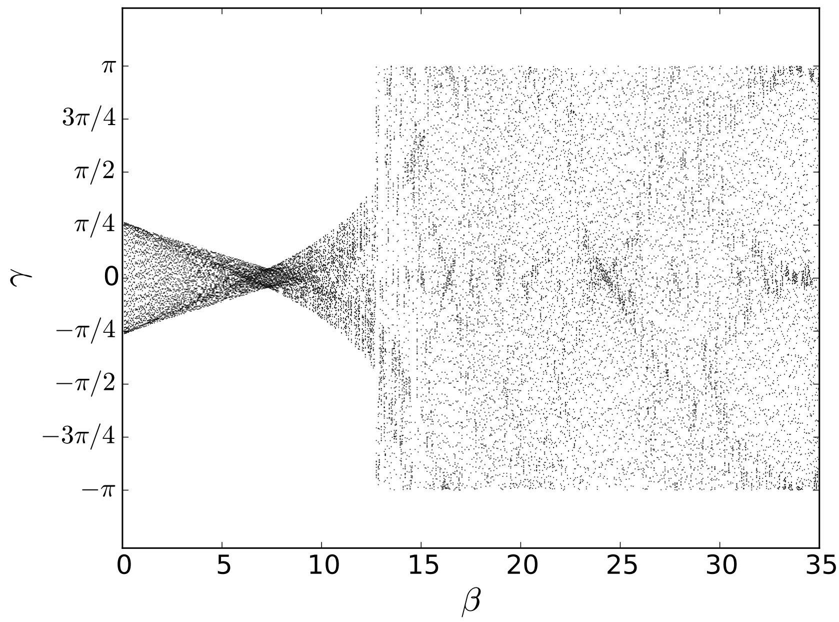

Figure 2.9: The points show the range of values for γ in our simulations for each value of β, fixing $\dot{\phi}(0) = 2.0\ \mathrm{yr}^{-1}$ implied by observation of the K00255 system, and with our nominal values for our K00255 system analogue. Here there is no damping term ($\epsilon = 0$), and $\dot{\gamma}(0) = 0.25\ \mathrm{yr}^{-1}$. We find that γ does not begin to circulate until $\beta \gtrsim 12.5$, though we do find higher amplitude libration of γ for lower values of β.

K00255.01 in order to get circulation. If we set a limit of $e < 0.6$ to avoid orbit crossing, this gives us a strict lower limit of 17 $M_\oplus$, although it is likely larger than this. For our nominal value of $e = 0.05$, this would imply a larger mass of 555 $M_\oplus$ to yield circulation in γ. These masses are much larger than the radius of the companion would suggest, and show that the K00255 system is likely too far from a mean-motion resonance for these effects to be very significant. If the planet is less triaxial, with $(B - A)/C = 2 \times 10^{-6}$, these values change to a lower limit of $m' = 1.7$ $M_\oplus$, and an implied mass of $m' = 56$ $M_\oplus$, still somewhat larger than the radius of the companion would imply. Nevertheless, for a similar system closer to a mean-motion resonance, circulation or larger amplitude oscillations in γ could be possible. To know at what level high amplitude librations or even circulation is possible, we must now also consider tidal damping, which will do in Section 2.4.2.

First, we will introduce another potential application of this model, which is to the TRAPPIST-1 planetary system. In this case, there are several planets arranged in a chain, with several near commensurabilities. If we focus on the planet TRAPPIST-1d, which has the most Earth-like stellar irradiation levels, and is found in a mean motion resonance with planet TRAPPIST-1e, we find that $\beta \sim 1$ for the nominal choices of $e = 0.05$, $(B - A)/C = 2 \times 10^{-5}$, and our estimated mass for TRAPPIST-1e (0.62 $M_\oplus$). Other contributing factors to larger β parameter include the fact that they are near a 3:2 resonance, which increases j and C_r, and that the host star is of very low mass.

We infer $\dot{\phi}(0) = 3.0$ yr^{-1} from the observed period ratio of the two planets if we assume $\dot{\phi}$ is currently at the maximum value in its oscillation. In Figure 2.10, we demonstrate our results for the evolution for γ in this system if we choose $\dot{\gamma}(0) = 0.3$ yr^{-1} (small-amplitude in natural libration). The red dots in the left-hand panel depict the Poincare points, recorded after each driving cycle, with their random placement illustrating the chaotic nature of that we happen to observe with these parameters. the right-hand panel shows a snapshot in a small time range, showing how γ chaotically switches between libration about 0 or π and circulation with either prograde or retrograde motion. For a broader picture, Figure 2.11 shows the effect of the driving for different $\dot{\phi}(0)$ for this system, starting with $\dot{\gamma}(0) = 0.3$ yr^{-1}. We see again a substantial effect around the separatrix ($\dot{\phi}(0) = 4.1$ yr^{-1}).

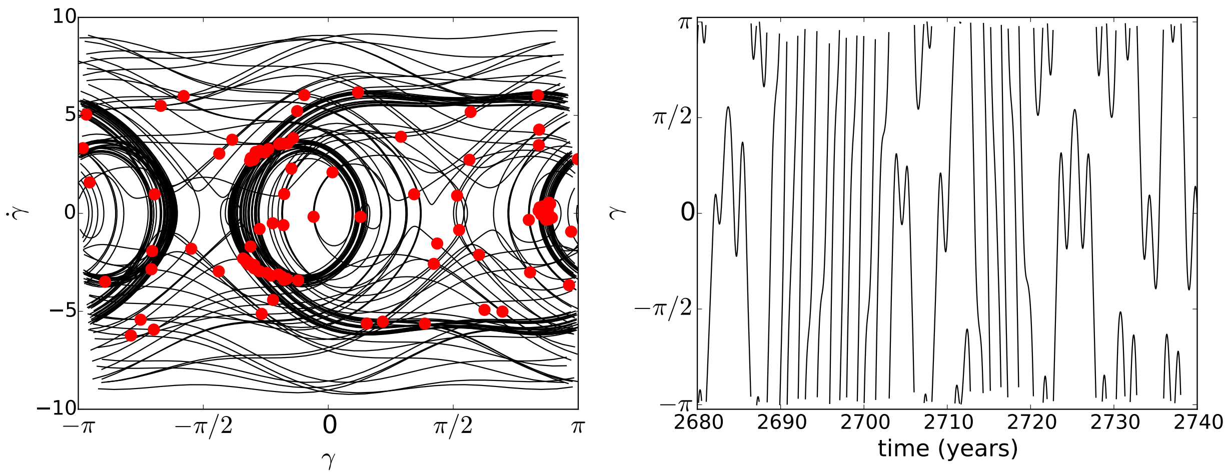

Figure 2.10: We show the evolution of γ for nominal values of our TRAPPIST-1d system with $\beta = 1.0$ and no damping. We choose $\dot{\phi}(0) = 3.0$ yr^{-1} based on the observed period ratio, and $\dot{\gamma}(0) = 0.3$ yr^{-1}. On the left we depict the evolution of γ in $\dot{\gamma} - \gamma$ space, and the surface of section is depicted with red dots. On the right we show γ as a function of time for a small snippet of time.

It can be shown that the separatrix in ϕ occurs at $\dot{\phi} = \omega_S\sqrt{j\beta}$ and $\phi = 0$. With the knowledge that the largest effects occur near the separatrix of ϕ, or around twice the separatrix in the 2:1 mean-motion resonance case, we can summarize the applicable range of parameters in Figure 2.12. Here we show how the separatrix of ϕ shifts as we vary β. For maximum effect, we would like to a find a system which lies roughly around the separatrix. We find that the K00255 system is likely too far from this range to yield interesting behavior, but the TRAPPIST-1d system lies squarely in this range, and indeed many of our simulations yield a circularized γ near the implied ϕ separatrix based on observation.

The Planet TRAPPIST-1d is the one with the most earth-like insolation, but other planets in the system also reside close to mean motion resonances. Both TRAPPIST-1e and TRAPPIST-1f are also close to 3:2 and 4:3 commensurabilities respectively, and we estimate $\beta = 0.39$ and $\beta = 2.65$ for these planets under the same assumptions as above. The large value of the latter is the result of both larger j and C_r and also a larger perturber mass. Our model can also potentially apply to TRAPPIST-1c, which lies near a second order (5:3)

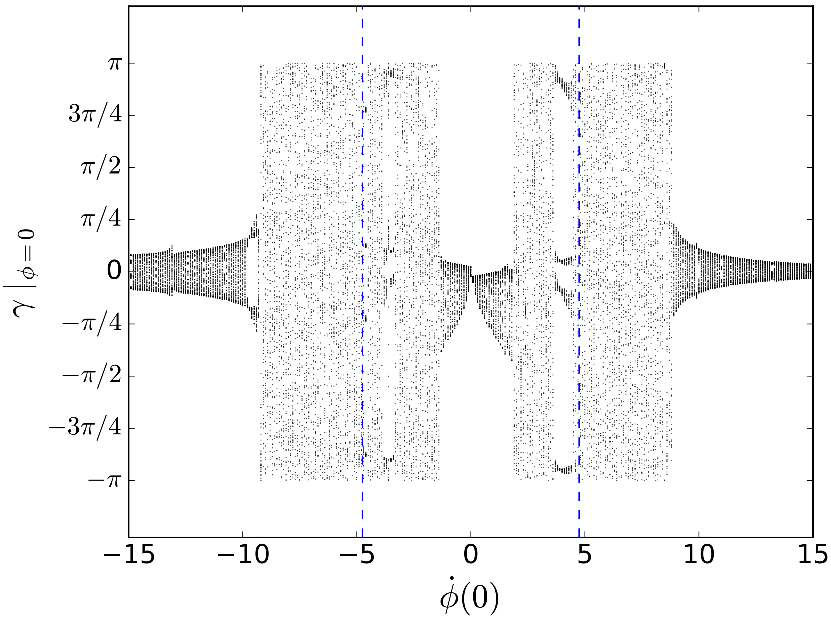

Figure 2.11: The points show the values of γ in the surface of section defined by $\phi = 0$, and $\dot{\phi}$ with the sign of its initial value, for each value of the initial forcing $\dot{\phi}(0)$ with our nominal values for the TRAPPIST-1d system with $\beta = 1.0$. Here there is no damping term, and $\dot{\gamma}(0) = 0.3\ \mathrm{yr}^{-1}$. The vertical dashed lines indicate the separatrix between libration and circulation (to the far left and right) of the external forcing resonant argument. We can see that the behavior is not symmetric about $\dot{\phi}(0) = 0$, since the circulation of γ imposes a preferred direction. We also observe a wide range of applicable $\dot{\phi}(0)$ as compared to the K00255 2:1 system.

resonance. However, in this case ω_M^2 (and thus β) acquires an extra factor of eccentricity, making the estimated value smaller ($\beta = 0.04$). A further point to note for this system is that its extreme compactness also implies short tidal synchronization *and* circularization times. If we repeat the analysis above, we estimate synchronization and circularization times $\sim 3 \times 10^4$ years and $\sim 8 \times 10^6$ years, respectively, for TRAPPIST-1d. This would suggest that perhaps we should set eccentricity equal to zero for these systems. However, resonant chains with more than two planets can excite eccentricities through zeroth order resonances not available to the two planet case, as is known to occur in the Laplace resonance of the Galilean moons [Yoder and Peale, 1981]. This combination can potentially lead to a non-negligible contribution to the planetary heat budget due to tidal dissipation [Barnes et al., 2013, Van Laerhoven et al., 2014, Bolmont et al., 2013, Driscoll and Barnes, 2015], which may shift the optimal conditions of habitability in this system from planet d to e or f. This system clearly warrants a more detailed investigation, but, for now, we simply assume that the more extended interactions generate eccentricity but that the spins can be described in the two planet formalism. In Chapter 3, however, we will more fully explore the multi-planet effects for TRAPPIST-1, and compare to the simpler formalism in this chapter.

2.4.2 Full Results with Tidal Dissipation

The preceding discussion focused on the interaction between the spin state and the external driving, in order to illustrate the kinds of effects that the driving can have on the spin. In the true physical situation, we must also account for the damping effects of tides, which would drive the planet to synchronous rotation in the absence of an external forcing. When a forcing is present, we then expect the system to evolve to a finite amplitude limit cycle, or a stable circulation. In studies of harmonically driven damped pendula, the properties of this limit cycle can often be a sensitive function of the system parameters [Baker and Blackburn, 2005].

To examine the consequences of this, we now evolve equation 2.7 for our nominal K00255 analogue parameters (yielding $\beta = 0.11$ and $\epsilon = 6 \times 10^{-8}$ yr^{-1}), assuming initially a large $\dot{\gamma}$,

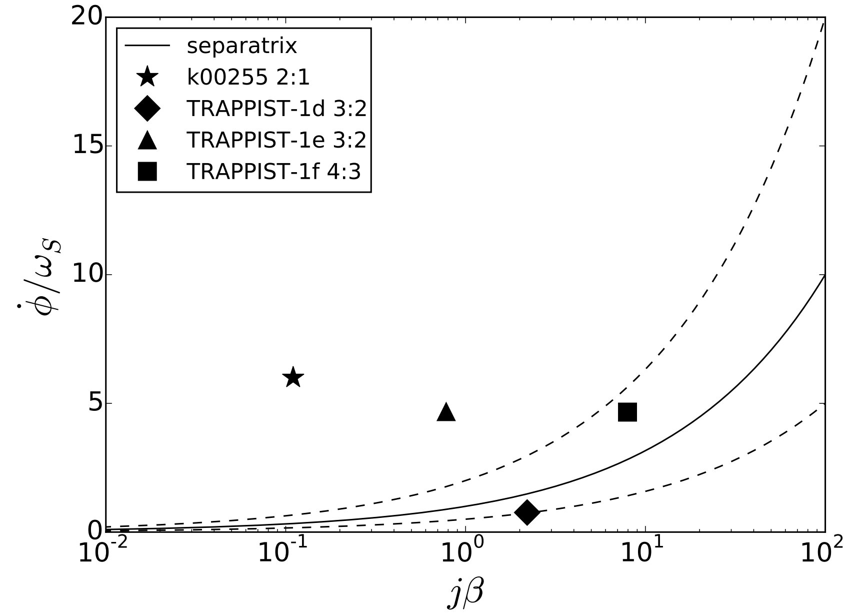

Figure 2.12: We show how the location of the separatrix in the $\dot{\phi} - \phi$ system varies with β, depicting the value of $\dot{\phi}$ at the separatrix when $\phi = 0$. We also show the locations of the our K00255 and TRAPPIST-1d example systems, based on our normal parameters and implied $\dot{\phi}$ values from observation. The dashed lines depicted the location at twice and half the separatrix. Lying near or within the dashed lines imply higher potential for variance in γ.

for a range of initial $\dot{\phi}(0)$, to examine the properties of the family of resulting limit cycles. Figure 2.13 shows our results with the points plotted depicting the full range (i.e. not just the Poincare section) of γ probed by the solution at late times only ($> 10^8$ yrs). Thus, these represent the final limit cycles and indeed show a great deal of sensitivity to the nature of the driving via $\dot{\phi}(0)$. The system can librate about either $\gamma = 0$ or $\gamma = \pi$, and it can also circulate. The final pattern of the limit cycle seems quite sensitive to the imposed conditions. As mentioned previously, the observed period ratio for the K00255 system suggests $\dot{\phi}(0) = 2.0$ yr^{-1}. The solutions in this part of the diagram can exhibit limit cycle behavior anywhere from complete circulation to low amplitude librations. We note that this is different than our solution for an initially librating γ, as shown in Figure 2.7, without damping. This suggests that the initial conditions of the spin state, along with the strength of the forcing term, can dramatically alter the resulting limit cycle, even relatively far from the $\phi - \dot{\phi}$ separatrix and with subtle variations of these initial conditions, with higher $\dot{\gamma}(0)$ giving a larger range of interesting behaviors.

Figure 2.14 shows the same for the TRAPPIST-1d system. In this case, both the forcing and the damping are stronger, yielding $\beta = 1.0$ and $\epsilon = 8 \times 10^{-3}$ yr^{-1} for our nominal system parameters, and we set $\dot{\gamma}(0) = 5.0$ yr^{-1} (natural moderate-amplitude libration in γ). Once again we see similar behavior, with more extensive regions where the limit cycle yields circulation. It is also interesting to note that $\dot{\phi}(0) = 3.0$ yr^{-1} is implied from observation, which yields a libration with amplitude $\sim 42°$, implying that approximately 73% of the planet would receive at least some level of illumination. Furthermore, this is on the edge of the regime where the limit cycle circulates. If $\dot{\phi}(0)$ were only slightly larger, or $(B - A)/C$ slightly smaller, then the entire planet could potentially also receive substantial illumination, and slight changes in parameters can yield wildly different results. Indeed, the evolution of ϕ is likely to be more complicated in this resonant chain system, and the planet may move between spin regimes. We will further investigate this in future chapters.

Figure 2.15 shows two examples of the evolution to the limit cycle for the TRAPPIST-1d system near the separatrix of the $\phi - \dot{\phi}$ system. The top panels depict results with $\dot{\phi}(0) = 3.4$ yr^{-1} and $\dot{\gamma}(0) = 5$ yr^{-1}, where we see that γ damps into a limit cycle librating about $\gamma = \pi$

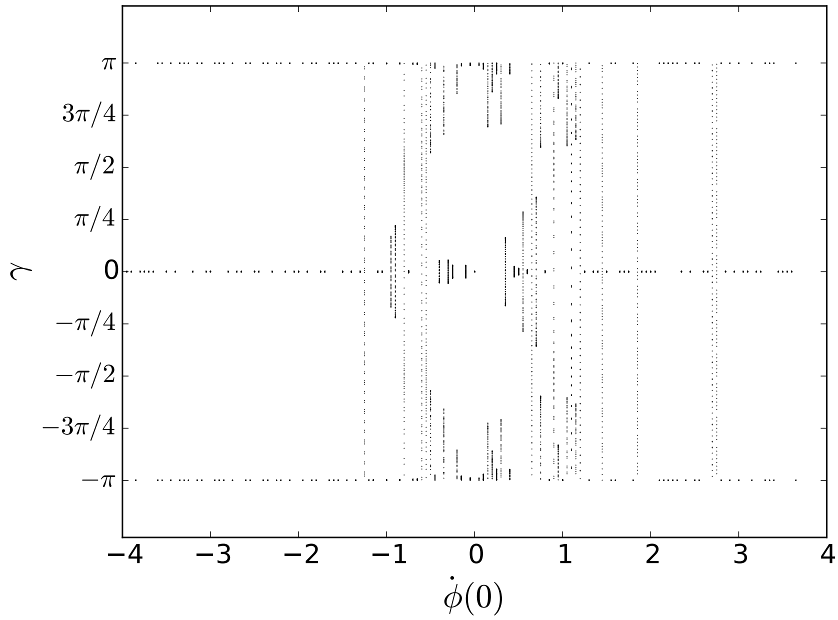

Figure 2.13: We show all values of γ (not just the surface of section) executed by the limit cycle at late times as we vary initial conditions of $\dot{\phi}$ for nominal values of our K00255 system with $\beta = 0.11$ and dissipation factor $\epsilon = 6.0 \times 10^{-8}$. We also assign a relatively high value of $\dot{\gamma}(0) = 1.5\ \mathrm{yr}^{-1}$. We find regions where γ either circulates (where γ spans the full range of $-\pi$ to π), or librates about 0 or π, with final results being very sensitive to initial conditions.

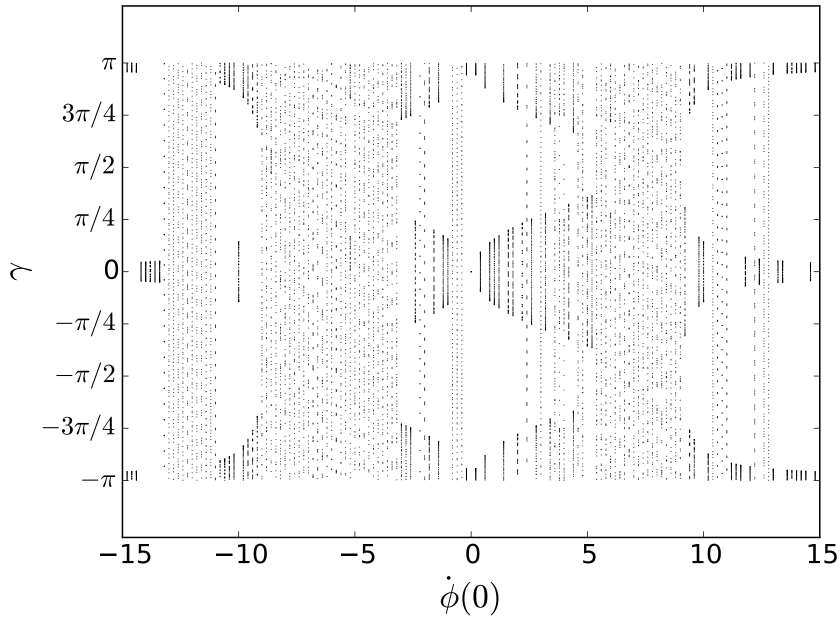

Figure 2.14: The points show all values of γ (not just the surface of section) executed by the limit cycle at late times under the influence of tidal damping, given the nominal values of the TRAPPIST-1d planetary system with $\beta = 1.0$ and $\epsilon = 8 \times 10^{-3}$, and $\dot{\gamma}(0) = 5.0\ \mathrm{yr}^{-1}$. We see that, once again, there are large zones where the planet can undergo circulation in the limit cycle (where γ spans the range from $-\pi$ to π), ensuring that the full planet surface receives some level of illumination.

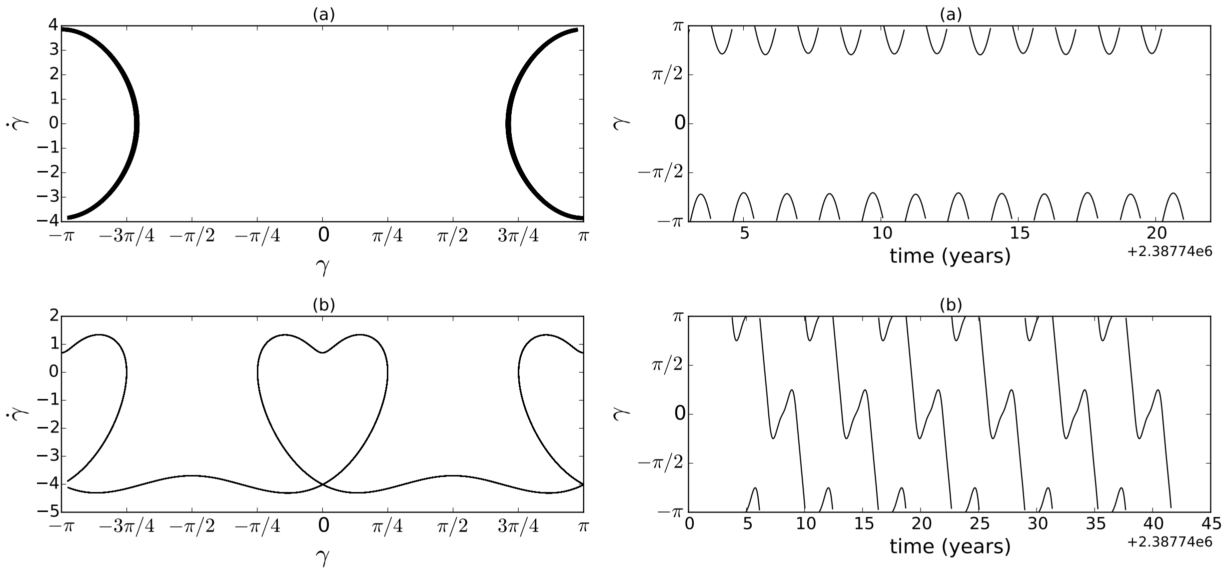

Figure 2.15: The curves show the evolution of γ over time, presented in $\dot{\gamma}$ vs. γ space in the left panels, and alternatively γ vs. time on the right. Given our nominal values for the TRAPPIST-1d planetary system damping ($\epsilon = 8 \times 10^{-3}$), $\beta = 1.0$, and $\dot{\gamma} = 5.0$ yr^{-1}, we compare two cases of slightly different $\dot{\phi}(0)$. In panels labeled (a), $\dot{\phi}(0) = 3.4$ yr^{-1} and we observe libration about $\gamma = \pi$. In panels labeled (b), $\dot{\phi}(0) = 3.8$ yr^{-1} and we observe elements of both libration and circulation. In both cases, we only see the behavior after the simulation has run for much longer than the dissipation timescale to allow the system to reach its limit cycle. The time after the start of the simulation is indicated in the bottom right of the time axes as 2.3877×10^6 years.

with an amplitude of 60°. The bottom panels of Figure 2.15 shows the limit cycle with the same parameters except that $\dot{\phi}(0) = 3.8$ yr^{-1}. In this case the limit cycle exhibits features of both circulation and libration – in essence the circulation is interrupted by a two beat libration at both $\gamma = 0$ and $\gamma = \pi$ before resuming.

2.4.3 Timescales

In order to determine the effects on climate, we must also determine typical timescales on which the spin states drift. The definition of $\dot{\gamma}$ implies the degree of mismatch between the spin of the planet and the orbital frequency, so the planet still rotates *almost* synchronously unless $\dot{\gamma}$ is quite large. However, a small finite mismatch means that the pattern of illumination will slowly drift over the surface of the planet, and the timescale over which it does this will determine the nature of the atmospheric response. If it occurs very slowly, the atmosphere should adjust to the change in illumination at each location, and should therefore present a similar atmospheric state to that of a synchronous planet, with the only likely variations due to ocean distribution and topographical distribution. On the other hand, if the drift is sufficiently rapid, the effect of the insolation is averaged over the surface of the planet. The most interesting cases are when the drift occurs on a timescale comparable to the atmospheric response time, as this can lead to nonlinear feedback.

Specifically, we are interested in the time in which γ spans the entire range within its limit cycle (i.e. the time for the substellar point to return to the same physical location on the planet and begin a new cycle). For circulating cases, this corresponds to the time in which γ goes from $-\pi$ to π, after spanning all γ in between. So we can say that this yields an effective length of a stellar day on the planet in these circulating cases. Meanwhile, for librating cases, it yields the time in which γ makes a full oscillation with its maximum amplitude. We will define this as our relevant "spin period."

In the case of our K00255 analogue, the large scale librations and circulations shown in Figure 2.13 have characteristic timescales $\sim$10–25 years. We summarize this in Figure 2.16, where we show what our relevant spin period is for each simulation, where red dots depict drift periods for librating cases, and blue depicts circulating cases.

If we consider the two limit cycles for TRAPPIST-1d shown in Figure 2.15, the period for the libration for the case in the top panel is 1.5 years. This suggests that portions of a planet in such a configuration could experience variations in levels of illumination not unlike the seasonal variations experienced on Earth because of the obliquity of Earth's spin. In the case of the hybrid libration-circulation limit cycle shown on the bottom panels of Figure 2.15, the period of the libration episodes is similar, and the period of a full cycle, including the circulation, is 6 years. We can again summarize this in Figure 2.17, with red dots depicting librating cases, and blue dots circulating cases. This shows that the TRAPPIST-1d system

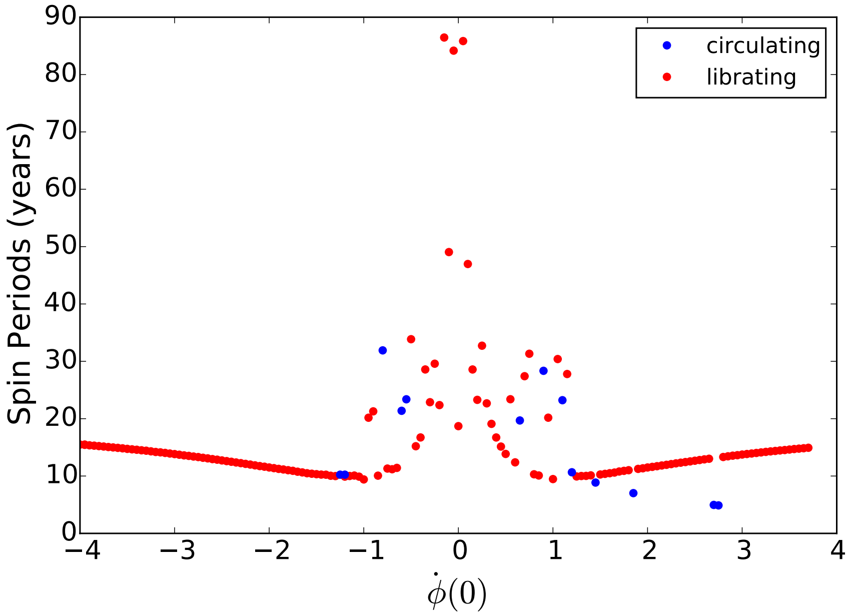

Figure 2.16: Here we show how the spin period varies as we change initial conditions in $\dot{\phi}(0)$ from the same simulations depicted in Figure 2.13. Each red dot depicts the values for simulations which yield librating spin states for γ, while blue points depict simulations which yield circulating γ states. We observe that this system yields mostly librating states, though a few circulating cases exist, notably around the implied $\dot{\phi}(0) = 2.0$ yr^{-1} from observation. These spin period timescales, however, are on the order of decades.

has much shorter spin periods than our K00255 system analogue, with many periods on the order of just a year, as well as having far more circulating cases.

Overall, the large scale librations and circulations in the limit cycles of equation 2.7 have characteristic timescales in the range $\Delta\tau \sim 1$–25 years, which can imply different real-world timescales depending on the triaxiality and orbital period, but which are approximately decades for Earth-like planets in the habitable zones of M0 stars, and of order years for those in the habitable zones of very low mass stars, like TRAPPIST-1.

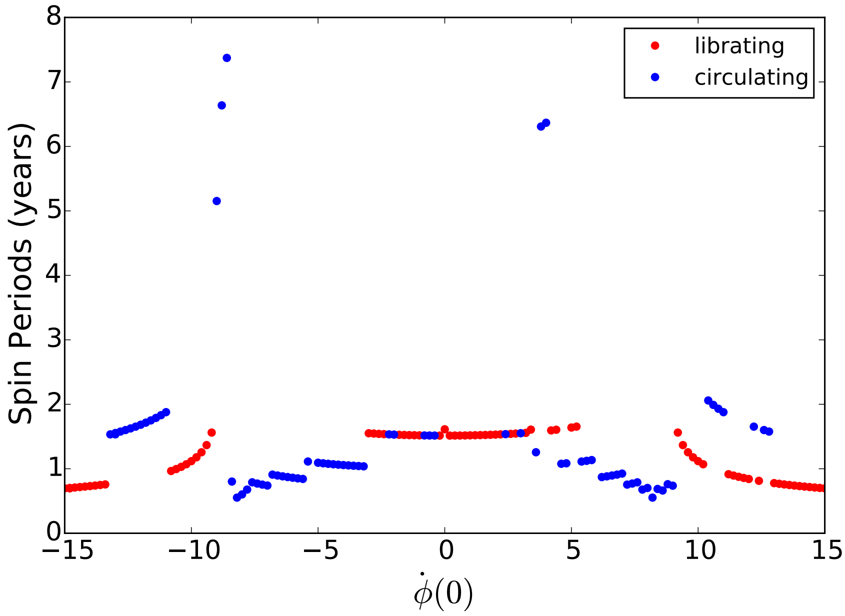

Figure 2.17: Here we show how the spin period varies as we change initial conditions in $\dot{\phi}(0)$ from the same simulations depicted in Figure 2.14. Each red dot depicts the values for simulations which yield librating spin states for γ, while blue points depict simulations which yield circulating γ states. We note that abundance of simulations which yielded circulating spin states, with typical timescales on the order of a year.

2.5 Implications

Our single-companion spin model introduced in this chapter demonstrates that the presence of a companion in, or near, a mean motion resonance can perturb a planets spin sufficiently, even in the presence of tidal dissipation, to place it in a non-synchronous limit cycle. This can result in substantial drift, and even circulation, of the planetary spin. A consequence of this is that a greater fraction of the planetary surface can receive some level of illumination, relative to that expected from a planet tidally locked to a synchronous spin. Furthermore, the timescales for this drift are approximately years to decades, depending on the particular configuration. This could have profound implications for the climate, and thus the habitability, of such a planet. The response of a planetary atmosphere and surface conditions to variations in level of illumination is very complex and an entire subject of study in itself. Nevertheless, we can anticipate the broadest atmospheric consequences of our new spin dynamics by studying the one-dimensional energy balance models used to estimate the breadth of stellar habitable zones [Kasting et al., 1993, Kopparapu, 2013, e.g]. In particular, if we consider the models of [Spiegel et al., 2008], the atmospheric thermal response times for Earth-like planets range from years to decades, depending on the level of surface water (more water implies more thermal inertia and longer response times). This is comparable to the characteristic timescales estimated above for variations in the level of illumination, which implies that the atmospheric dynamics could be quite complex, as the conditions change on similar timescales to the response.

In the context of exoplanet habitability then, our results suggest one more avenue that may allow a planet to avoid the consequences of tidal synchronism close to low mass stars [Kasting et al., 1993]. Indeed, our model need not be exclusive of other proposals to avoid this fate. The formation of thick clouds near the substellar point [Yang et al., 2014] will presumably still be a part of the evolving climate dynamics, and the operation of strong atmospheric tides [Leconte et al., 2015] may also operate, introducing an additional torque component into the spin dynamics that might also be worthy of consideration in the future. We began our consideration of this problem motivated by the anticipation of future discoveries of planetary systems around M dwarfs, and use the K00255 system as a prototype for the kinds of host stars likely to dominate magnitude limited samples of this type. However, the discovery of the planetary system around the very low mass ($\sim 0.08 M_{\odot}$) star TRAPPIST-1 illustrates that such models have a potentially very broad scope, and the presence of several near-commensurabilities in that system suggest that the configurations considered here are not rare. The fact that the drift timescales discussed above scale relative to the orbital period also suggests that the particular atmospheric responses may vary with stellar host mass too, with the habitable planets around the lowest mass stars like TRAPPIST-1 experiencing variations quite similar to the seasonal variations on Earth. In near resonant chains like the TRAPPIST-1 system, the variation in the spin dynamics may have an influence on the relative habitability of each of the systems as well. Figure 2.18 shows the limit cycle for the three planets TRAPPIST-1d, TRAPPIST-1e and TRAPPIST-1f, that lie near first order resonances. In each case we have considered only the effects from the external neighbor, even though the inner companion may also provide non-negligible perturbations. In each case, there is a reason to suggest that the external perturber is more significant (the coupling between c-d is second order, and the external perturber is more massive in the case of planets e and f). We have performed this calculation assuming the nominal triaxiality and $Q_{\oplus}$ for each planet. We see that TRAPPIST-1e executes moderate libration under these conditions, and TRAPPIST-1f a much smaller libration, both about $\gamma = \pi$. On the other hand, TRAPPIST-1d has a limit cycle that circulates and features an intermittent, wide-angle libration as well. The characteristic timescale for the full cycle is ~ 1.1 years in this case. This demonstrates that planets in the same system can occupy different spin states, with some being essentially synchronized, while others experience a more distributed irradiation. Although the arrangement in Figure 2.18 counter-intuitively suggests increased synchronism away from the star, this more has to do with our exact choices in initial conditions, with strong sensitivity to $\dot{\gamma}(0)$ and especially $\dot{\phi}(0)$ within these regimes that could result in significantly different limit cycles. The general effect is typically regulated by the value of β, but the solutions could still change dramatically within certain regimes if we adjust $\dot{\phi}(0)$ or $\dot{\gamma}(0)$, as can be seen in Figures 2.13 and 2.14.

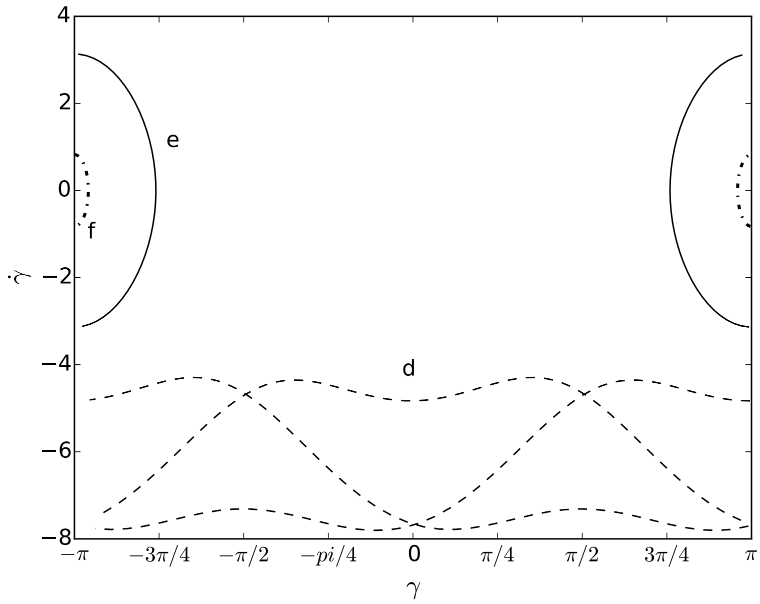

Figure 2.18: We show the limit-cycle solution for 3 different planets inspired by the TRAPPIST-1 system (TRAPPIST-1 d, e, and f), considering only the effects of the immediate outer companion for each and using initial conditions in $\dot{\phi}(0)$ that would be suggested from current observation of the respective period-ratios. The dashed line depicts the solution for TRAPPIST-1d, which shows a circulation of the spin state. Meanwhile, TRAPPIST-1e, depicted by the solid line, has reached a moderate-amplitude librating state about π. TRAPPIST-1f, depicted by the dashed-dotted line, librates about a much π at a much smaller amplitude, and thus represents a nearly perfect synchronous spin state.

Such spin states have potentially both direct and indirect observational consequences. The most obvious indirect consequence is simply the fact that spreading the stellar illumination over more of the surface area will help to make a planet more temperate and increase the fraction of the planet that is habitable. Figure 2.19 demonstrates this by comparing the average flux received at each point on a planet for the limit cycles shown in Figure 2.18. In the case of libration for TRAPPIST-1d, we see a moderate increase in the average value of the flux and in the surface area irradiated. For the circulating case, the differences are much more dramatic, with a substantial averaging observed. More direct observational consequences may emerge if the observing technology reaches the point of identifying signals from surface features [Ford et al., 2001, Kawahara and Fujii, 2011, Cowan et al., 2012, Crossfield, 2013, e.g.], because then one could potentially identify the years-to-decades drift on surface features over the course of many orbits.

Finally, we note some of the limitations of our spin model presented in this chapter. Namely, that it doesn't include the possible effects of multiple resonant companions, and the complex interactions that can result from such a scenario. Moreover, considering multiple companion effects may prove to be very important for known systems such as TRAPPIST-1. As such, a more complete pictures of the mutual gravitational interactions of the planets is required, and we will address this in Chapter 3 by considering N-body simulations of different possible TRAPPIST-1 configurations. Finally, another possible limitation is our choice of a simple tidal dissipation model, which is useful for illustrative purposes, but a more realistic model may also provide further insights. Considerations of atmospheric torques may also prove to be essential for sufficiently dense atmospheres. We will thus provide a more complex tidal model as well as consider atmospheric torques in Chapter 4.

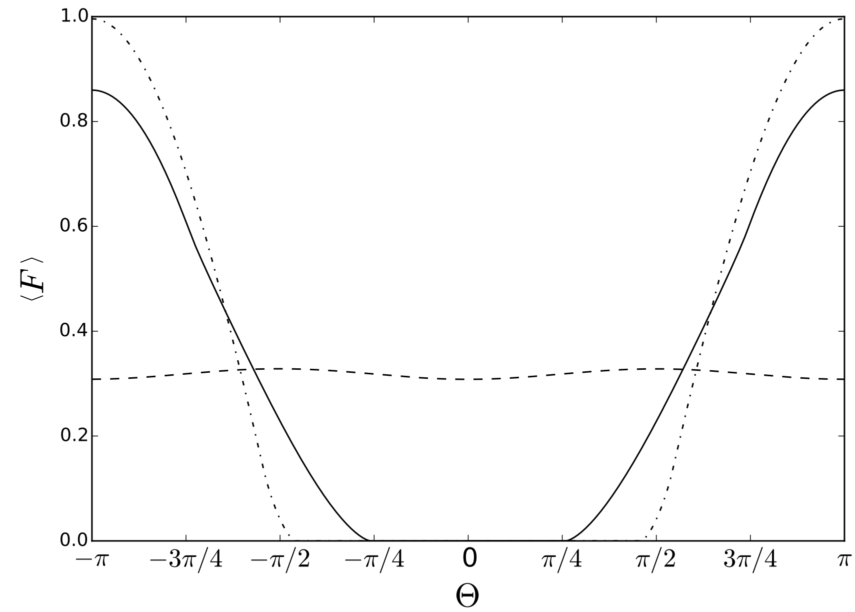

Figure 2.19: Here we show the average flux received, normalized to the flux at the substellar point, at each longitude Θ of the planets depicted in Figure2.18 over time (with corresponding line styles). We see that, in the circulating case (planet d), all longitudes receive approximately the same amount of stellar radiation over time, with some slight variations. The other two are both librating cases, with planet f representing a nearly perfect synchronous spin state about π. We observe a widening for the higher-amplitude case (planet e) as compared to the more perfectly synchronous planet f, with a higher portion of the planet receiving at least some stellar coverage.

CHAPTER 3

Multiple Companion Systems

Portions of this chapter are adapted from the publication:

Vinson, A. M., Tamayo, D., and Hansen, B. M. S. (2019). The chaotic nature of TRAPPIST-1 planetary spin states. *Monthly Notices of the Royal Astronomical Society*, 488(4):5739–5747.

In Chapter 2, we addressed how the spin of a planet can be affected by just one companion planet near resonance. However, systems have been discovered which have more than two planets, some in resonant chains. One prime example is the TRAPPIST-1 system, containing seven planets arranged compactly in a long resonant chain, some in or near the estimated habitable zone within the ultra-cool dwarf system. All of these planets then may have the opportunity to mutually interact in a significant matter in the context of our spin model.

This chapter addresses these considerations by taking N-body orbital simulations of the TRAPPIST-1 system. We can then directly input orbital variations from such simulations into our spin model, as we will describe in Section 3.1. We then will address assumptions and choices in parameters in Section 3.2 before presenting results in Section 3.3, and then concluding with a discussion of implications of our results in Section 3.4.

3.1 Mean Motion Variations

We describe the planetary spins using the same basic framework presented in Chapter 2. Thus we will consider a system with a planet of mass m orbiting a star of mass M_*, with zero obliquity between the planet's spin and its orbit. Recall also that we let A, B, and C be the principal moments of inertia of the planet with C being the moment about the spin axis and A being the moment about the long axis of the planet in the plane of the orbit such that $B > A$. We define θ to be the angle formed between the long axis of the planet and a stationary line in an inertial frame within the plane of the orbit, and another angle $\gamma \equiv \theta - M$, where M is the mean anomaly. γ then roughly corresponds to the longitude of the substellar point for a planet on a near-circular orbit. We then apply the equation of motion for γ as derived and presented in [Goldreich and Peale, 1966, Goldreich and Peale, 1968] and [Murray and Dermott, 1999], under the assumption that $\dot{\theta} \simeq n$, while including the $\dot{n}$ term as we did in Chapter 2, which is usually disposed of. Including tidal damping from section 2.1.2, we get the same as equation 2.7

Previously in Chapter 2, we applied the "pendulum model" presented in [Murray and Dermott, 1999] to describe the $\dot{n}$ term in equation 2.7, wherein n evolved as a simple pendulum under the effects of a single companion planet in resonance. Thus, equation 2.7 described something analogous to a forced pendulum for the evolution of γ, with the simple case having two stable equilibria corresponding to opposite faces of the planet along the planet's long axis pointing to the host star. The main difference from a typical forced pendulum is that our forcing term itself behaved like a pendulum instead of the more typical case of a simple sinusoid. The forced pendulum is a popular topic in dynamical studies due to its interesting chaotic behaviors when the natural and driving frequencies are close in value. Indeed, after incorporating tidal damping effects in the model, our results in Chapter 2 depicted a wide range of interesting limit cycles for example systems based on the TRAPPIST-1 and K00255 planets.

However, many systems are found to be highly multiple, including the TRAPPIST-1 system that inspired much of our work. To have a fuller understanding of the possible behaviors of the spin, we must then expand the model to incorporate the effects of multiple resonant companions. This is the main difference between the work presented in this chapter and our previous one: we now consider the effects of *multiple*, mutually interacting companions in or near mean motion resonances in order to understand how our model applies to resonant-chain systems such as TRAPPIST-1, wherein there are seven planets compactly arranged into a long resonant chain. This introduces a more difficult problem in describing how exactly the mean motion of any particular planet varies in time, with interactions from many companions. We therefore use N-body integrations of the TRAPPIST-1 system by [Tamayo et al., 2017] to calculate the variations in the orbital eccentricities and mean motions numerically.

TRAPPIST-1 presents a very attractive system as a compact analog of the inner Solar System, with the seven planets contained within the system receiving between about 10% and 400% the stellar irradiation of the Earth. As first announced by [Gillon et al., 2017], the inner six planets in the system form the longest known near-resonant chain of exoplanets, with orbital period ratios of approximately 8/5, 5/3, 3/2, 3/2, and 4/3 between planets c, d, e, f, and g, respectively, and their nearest inner companion. We also note that the period ratios of of e to d, f to e, and g to f, suggest that the resonances are of first-order, which also suggest larger variations in $\dot{n}$ as can be seen in the model described in Chapter 1.

3.2 Setup

To extract orbital parameters, we use the numerical integrations of [Tamayo et al., 2017], which simulated a range of initial conditions near the observed resonant configurations of TRAPPIST-1. These spanned configurations at or near the centers of the observed resonant chain where eccentricities and mean motions remain nearly constant (i.e., low spin forcing), to ones near their separatrices where the orbits undergo larger, chaotic oscillations (i.e., strong spin forcing). These integrations thus can span a range of dynamical behaviors, but we note that other works have determined better fits to the actual TRAPPIST-1 system [Gillon et al., 2017, Grimm et al., 2018, e.g.]. However, we wish to illustrate behaviors for a wide range of possibilities that can be applied not only to TRAPPIST-1, but to similar systems as well.

The integrations in [Tamayo et al., 2017] were performed using the `WHFAST` integrator [Rein and Tamayo, 2015] in the REBOUND N-body package [Rein and Liu, 2012], with a time step of 7% of the innermost planet's orbital period. Details of their initialization by migrating them into the observed resonant chain with parameterized disk forces can be found in [Tamayo et al., 2017]. We extracted their publicly available[1] `SimulationArchives`, which allow for fast, parallel extraction of system parameters at arbitrary times [Rein and Tamayo, 2017], and sampled eccentricities and mean motions at a cadence of 10% of the orbital period for each planet. With the mean motion and eccentricity histories, we then used spline interpolation so that we could extract values of mean motion n, $\dot{n}$, and eccentricity e, at arbitrary times to feed into our equation of motion and perform an adaptive time-step, Fourth-Order Runge-Kutta integration to find the evolution of the spin parameter γ. The equation of motion, similar to equation 2.7, is as follows

$$\ddot{\gamma} + \frac{1}{2}\omega_S^2 \sin 2\gamma - \frac{1}{j}\omega_M^2 \sin\phi + \epsilon\dot{\gamma} = 0 \tag{3.1}$$

Choices also need to be made in regards to assumptions about the planets and their tidal damping strengths, which can result in different behaviors. We choose to calibrate equation 2.5 to two different damping strengths represented by the tidal Q parameter via equation 2.6. Studies suggest a tidal parameter $Q \sim 10$ for the Earth, exerted primarily by pelagic turbulence in the oceans [Egbert and Ray, 2000], so we will take this as our stronger damping estimate. For a water-poor terrestrial planet, we adopt $Q = 100$ as our weaker damping, based on estimates for Mars [Lainey et al., 2007]. We also choose a triaxiality factor of $(B - A)/C = 10^{-5}$ based on considerations of empirical evidence determined for the Earth, Mars, and Mercury [Chen et al., 2015, Edvardsson et al., 2002, Margot et al., 2012]. We note that reasonable assumptions on this triaxiality factor can vary among planets in the Solar System by up to an order of magnitude, and can thus have an effect on the natural spin frequency ω_S by up to a factor of ~ 3. Meanwhile, it's not unreasonable to assume that

[1] `https://github.com/dtamayo/trappist`

this range could be wider for planets in other systems which contain such close-in planets. We find, however, that our overall results do not change very dramatically within this range of reasonable triaxiality assumptions.

Finally, we focus on the spins of planets d, e, and f (while under the influence of all other companions in the system). Much of our interest in this problem is motivated by habitability questions, and these three planets all lie within the estimated habitable zone [Kopparapu et al., 2013, Kopparapu et al., 2016]. These planets, while likely to have experienced water loss during the host star's ~ 1 Gyr long pre-main sequence phase, are also likely to still have been able to retain significant oceans depending on initial water levels [Bolmont et al., 2017].

3.3 Results

We use various outcomes from different initial conditions of REBOUND simulations of the orbital parameters of the TRAPPIST-1 system, picked to span a range in forcing strength from negligible to strong (see Appendix A), and use these as inputs for our own spin model detailed in this work. Many of the simulations are dominated by a primary frequency of the mean motion variations, with many others manifesting strong secondary frequencies. We use eighteen different simulations as input for our spin model, ranging from very low amplitude librations of the mean motion to higher amplitude variations, all of which are long-lived configurations [Tamayo et al., 2017].

In this work we look at those planets closest to the estimated habitable zone: planets d, e, and f. With 18 different REBOUND simulations to apply to each of these planets, coupled with two different tidal strengths we choose to test ($Q = 10$ and $Q = 100$), we have a total of 36 different simulations of the spins of each of these three planets. We observe a variety of different behaviors that emerge from different integrations. These include integrations wherein the spin of the planet remains effectively purely synchronous, with very small librating amplitudes. Other simulations depict higher amplitude librations in the spin, while others even exhibit periods of complete circulation. However, most of the realizations we studied exhibit chaotic evolution, with the spin often alternating between periods of libration and circulation. There is a small subset of integrations with approximately regular orbital behavior that do stably librate over long timescales.

3.3.1 High Amplitude, Irregular Forcing

One representative example is presented in Figure 3.1, with variations in mean motion attained from the corresponding REBOUND simulation presented in Figure 3.2. We can see a variety of behaviors in just this one simulation. First we notice that, due to the inherent chaos of the behavior of the orbital parameters from the input taken from the REBOUND simulation, the spin state also never reaches a true stable equilibrium. In this particular simulation, we see switching among different quasi-stable states, which each last on the order of a few thousand to tens of thousands of years. Some of these states include moderate-amplitude librations of γ about either 0 or π, while others are states of complete circulation, wherein we observe full stellar coverage on the surface of the planet.

3.3.2 Regular Forcing

Other simulations can depict far more regular behavior if the behavior of the driving (i.e. the mean motion) is also very stable. One such example is shown in Figure 3.3, where we show the evolution of γ, $\dot{\gamma}$, and n, for a small period of time during the simulation (though the entire simulation depicts the same, stable behavior). We note the very regular behavior of the mean motion n, especially as compared to the evolution of n for our other example shown Figure 3.2. In fact, the example depicted in Figure 3.3 is among the closest to our classical case presented in Chapter 2, where behavior of mean motion n can largely be described as a simple pendulum with a single frequency. This can also be compared in Figures 3.4 and 3.5, which depict the Fourier Transforms of the mean motion shown in Figure 3.2 and Figure 3.3, respectively. Where Figure 3.4 exhibits multiple frequencies in the mean motion, in Figure 3.5 we see that the mean motion is dominated by just one. As a result of a more stable mean motion evolution, we observe a stable libration of γ in the 3.3 with an amplitude of about 0.4 radians about π.

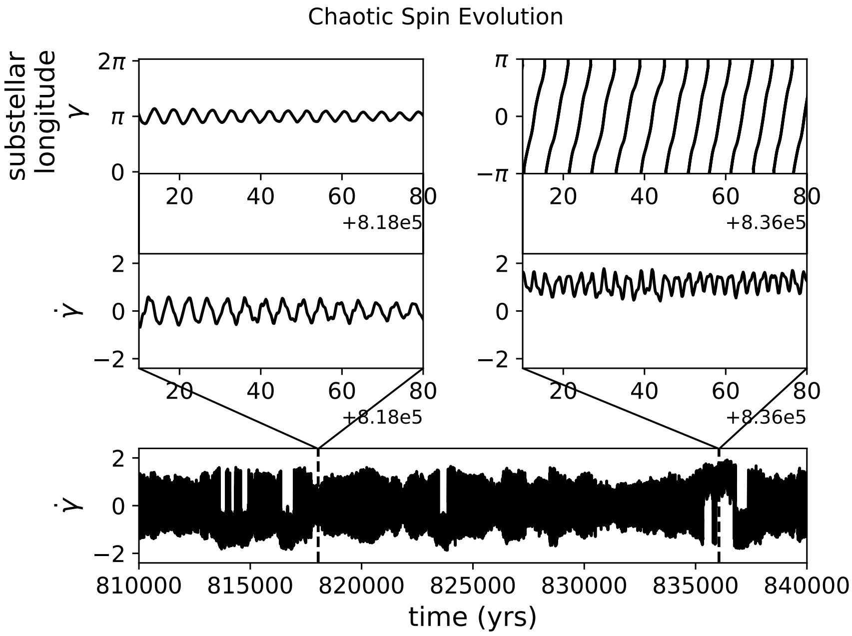

Figure 3.1: Example simulation of spin of planet f with $\dot{\gamma}$ plotted against time, wherein we set $Q = 100$. Years are used for units involving time. The bottom panel depicts the long-term evolution of $\dot{\gamma}$ over 30,000 years. The top four panels zoom in to depict two different types of behavior that occurs in this particular simulation, with the middle panels depicting evolution of $\dot{\gamma}$ and the top panels depicting evolution of γ. On the left panels we observe libration of γ about π. On the right panels we observe a time when there is full circulation of γ, which can remain quasi-stable for approximately 10^3 years. Overall, this simulation depicts a chaotic evolution of the spin state, switching among librating and circulating states.

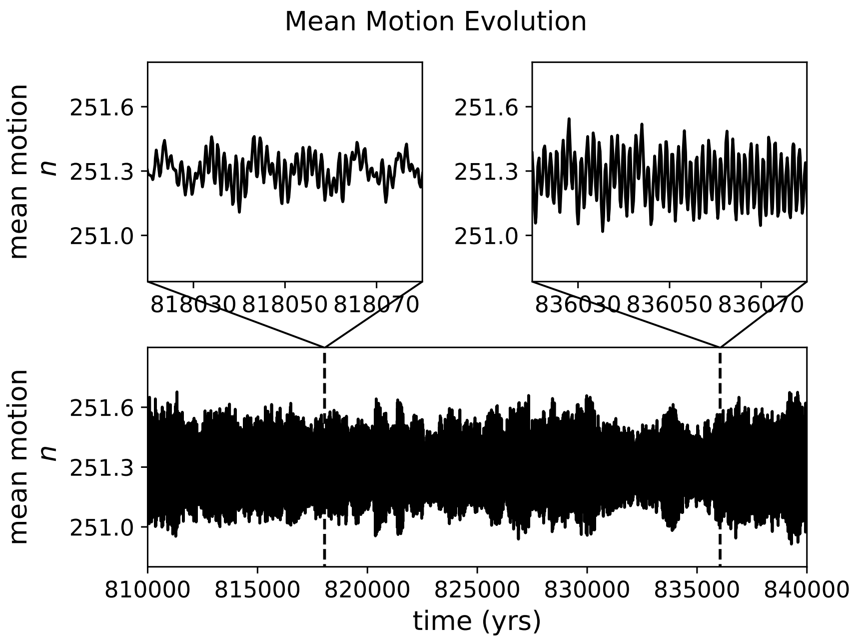

Figure 3.2: Example simulation of planet f depicting evolution of mean motion n versus time taken from a REBOUND simulation. This is used as input for our spin model, a corresponding simulation of which is shown in Figure 3.1. The bottom panel presents long-term evolution of n, while the top two panels zoom in to depict behavior at different instances in time. We can compare this to Figure 3.1 to see how the mean motion input affects the spin state. We find that the most dominant frequency when performing a Fourier Transform on n is $\omega_M = 5.1$ yr^{-1}. We also find that the standard deviation of $\dot{n}$, which we can use as a proxy for overall forcing strength, is $\sigma(\dot{n}) = 0.55$ yr^{-2}. We note, however, that $\sigma(\dot{n})$ varies throughout the simulation, and we can observe here that the mean motion has larger variations in the top right panel than in the top left panel, corresponding to circulating and librating states for the spin argument γ as seen in Figure 3.1, which is suggestive that the behavior of the spin depends strongly on the strength of mean motion variations.

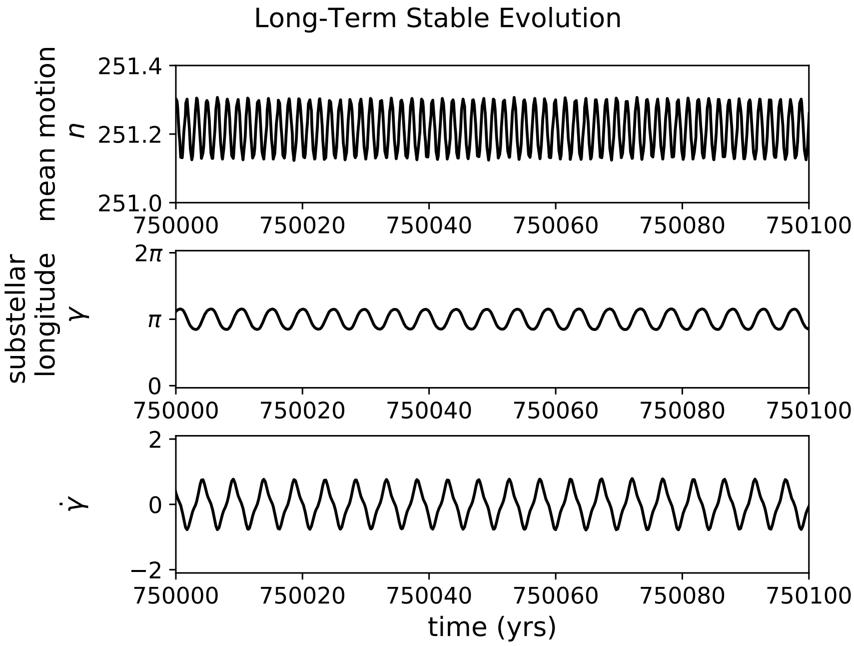

Figure 3.3: Example simulation of planet f depicting evolution of mean motion n in the top panel, γ in the middle panel, and $\dot{\gamma}$ in the bottom panel. This is an example of a simulation which has a very stable evolution in mean motion which is strongly dominated by just one frequency, $\omega_M = 4.18$ yr^{-1}, as shown in the Fourier transform in Figure 3.5. Thus, we also observe a stable evolution of the spin argument γ, wherein we observe a stable libration of γ about π. We also note that the standard deviation of $\dot{n}$, which we use as a proxy for forcing strength, is $\sigma(\dot{n}) = 0.26$ yr^{-2}.

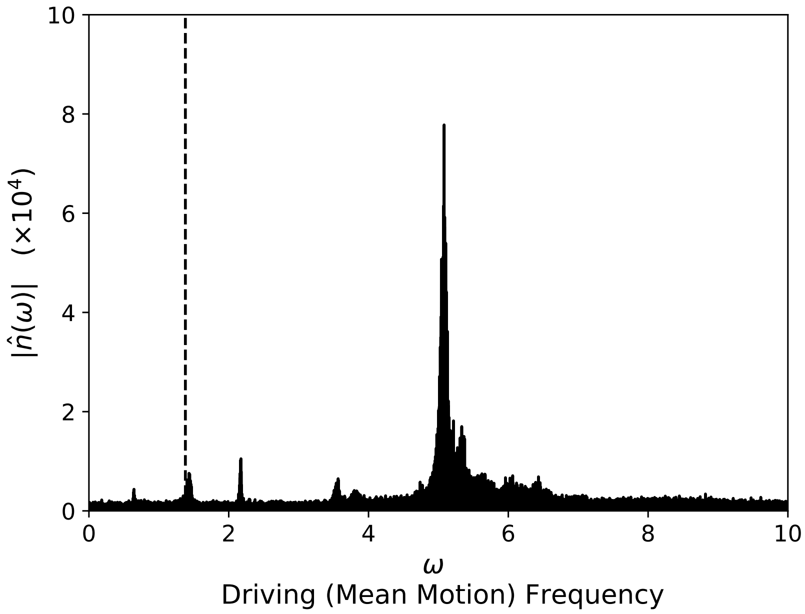

Figure 3.4: Absolute value of the frequency spectrum of the mean motion $n(t)$, denoted $|\hat{n}|$, for the entire time range of the simulation corresponding to Figure 3.2. Here we see that, while there is a primary frequency which dominates in the behavior of $n(t)$, $\omega_M = 5.1$ yr^{-1}, there are also secondary frequencies which can change the behavior of n, and thus its influences on the spin argument γ. We also plot vertical dashed lines to indicate the spin frequency for natural libration for planet f, $\omega_S = 1.38$ yr^{-1} for our assumed triaxiality $(B - A)/C$. Here we note that ω_S happens to line up approximately with one of the secondary driving frequencies.

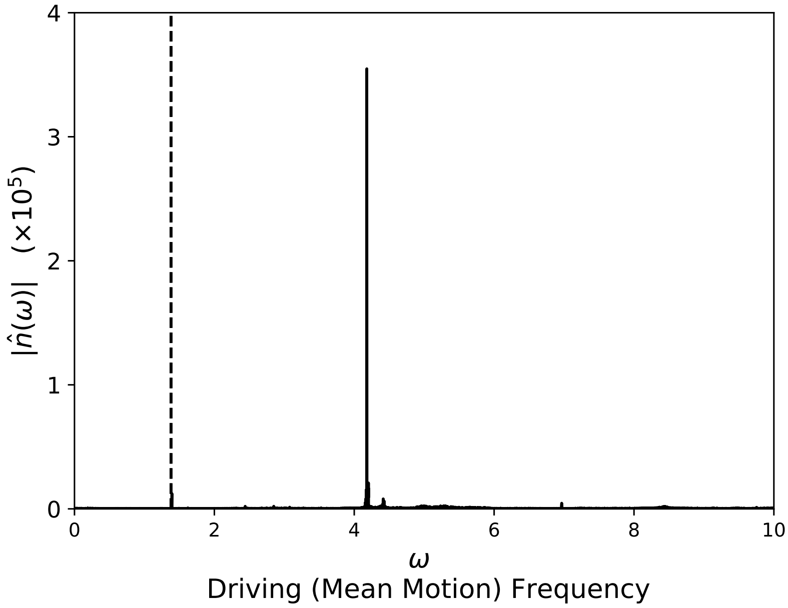

Figure 3.5: Absolute value of the frequency spectrum of the mean motion $n(t)$, denoted $|\hat{n}|$, for the entire time range of the simulation corresponding to Figure 3.3. We also plot vertical dashed lines to indicate the natural spin frequency for planet f, $\omega_S = 1.38$ yr^{-1} for our assumed triaxiality $(B - A)/C$. Here we see that the evolution of n can largely be described in terms of just one dominant frequency, $\omega_M = 4.18$ yr^{-1}, which is approximately three times the natural spin frequency ω_S.

3.3.3 Correlations

We can attempt to characterize the results of all of our 108 planetary history integrations in terms of the variance of γ and $\dot{\gamma}$. This can be difficult given the changing nature of individual simulations, but higher standard deviation of $\dot{\gamma}$ about 0 (i.e. the *root mean squared*), and higher standard deviation of $|\gamma|$ about its mean, would generally indicate cases of higher amplitude librations, or else even complete circulation that would result in effective stellar days. We denote our measures of the variance of γ and $\dot{\gamma}$ as $\sigma(\gamma)$ and $\sigma(\dot{\gamma})$, respectively.

We can also attempt to characterize the REBOUND simulations via terms that we would expect to have the strongest effects on the evolution of γ. In our previous work, we could largely describe the driving on the spin argument γ from the varying mean motion in terms of both the frequency and of amplitude or strength of the mean motion variations. In this work, the actual behavior of the driving is clearly more complex, but we can still attempt to largely characterize the simulations in terms of a frequency and of an amplitude of the driving. In reality, the chaotic behavior would result in varied amplitudes and multiple frequencies. But we can expect, and largely observe, a dominant frequency manifesting along with a typical amplitude.

We will therefore characterize the typical amplitude of the forcing as the standard deviation of $\dot{n}$, denoted $\sigma(\dot{n})$. We also take a Fourier Transform to retrieve a primary frequency of oscillation from each of the REBOUND simulations, which we denote as ω_M. As these values change depending on the REBOUND simulation, we can then relate these terms related to the driving to trends observed in the evolution of the spin argument γ. Finally, as we considered different forcing strengths and frequencies, we must also consider damping strengths. We will consider two tidal scenarios: strong damping with tidal $Q = 10$, and weak damping with $Q = 100$.

In Figure 3.6, we demonstrate how variations in $\dot{\gamma}$ respond to different levels of forcing by plotting $\sigma(\dot{\gamma})$ versus a proxy for the amplitude of the forcing term in equation 3.1, $\sigma(\dot{n})/\omega_S^2$, for different tidal damping strengths, $Q = 10$ and $Q = 100$, respectively. We normalize $\sigma(\dot{n})$ to ω_S^2, as this nondimensionalizes $\sigma(\dot{n})$ to the torques on the spin and allows us to plot results

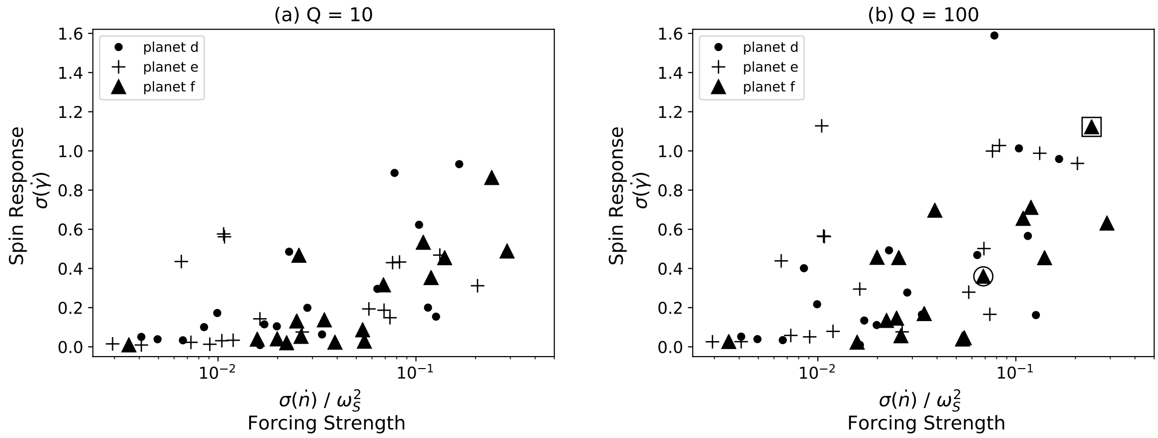

Figure 3.6: Standard deviation of $\dot{\gamma}$ versus standard deviation of $\dot{n}$ normalized to ω_S^2 for each of our integrations with tidal factor $Q = 10$ (i.e. higher tidal damping) depicted in panel (a) on the left, and tidal factor $Q = 100$ depicted in panel (b) on the right. Integrations for planets d, e, and f, are represented by dots, plus signs, and triangles, respectively. The cases studied from Figures 3.1 and 3.3 are enclosed in a square and a circle, respectively. We see an overall trend that variations in $\dot{\gamma}$ increase with variations in $\dot{n}$. Higher variations in $\dot{\gamma}$ indicate larger responses to the driving of the spin argument γ, and thus would suggest the potential for larger total stellar coverage. Years are used for units with time.

from each of planets d, e, and f, on the same plot in a consistent manner, with $\omega_S \simeq 3.08$ yr^{-1}, 2.05 yr^{-1}, and 1.38 yr^{-1} for planets d, e, and f, respectively, if eccentricity is small (valid for all these simulations). We note that these plots indeed show a correlation that as variations in $\dot{n}$ grow, (i.e. the forcing strength in equation 3.1 increases), the spin responds more strongly with higher variations in $\dot{\gamma}$. There is also a clear dependence on tidal damping strengths, with higher tidal damping strength ($Q = 10$) suppressing variations in $\dot{\gamma}$ as compared to lower tidal damping strength ($Q = 100$). We also note that each of these plots, while manifesting a correlation of $\dot{\gamma}$ with $\dot{n}$, have a quite a bit of scatter. This is expected due to different dependencies with how the spin argument responds to the frequencies of variations in the mean motion, which adds many complexities due to the chaotic nature of the mean motion evolution in many of REBOUND integrations of the orbital parameters.

As we are largely interested in how the behavior of the spin affects the total stellar coverage of these planets, we also plot variations in the spin argument γ, which we denote with $\sigma(\gamma)$, versus $\sigma(\dot{n})/\omega_S^2$ in Figure 3.7 for different tidal factor assumptions, $Q = 10$ and $Q = 100$. This demonstrates how much the substellar point on these planets is varying in longitude over the course of our integrations. We expect $\sigma(\gamma)$ to be about equal to zero for purely synchronous cases, and $\sigma(\gamma) = \pi/2$ for cases where the spin exhibits full, regular, stellar days over the entire integration. In Figure 3.7 we notice that many simulations have planets effectively still experiencing spin-orbit synchronicity with low variance in γ and low forcing strength. As the forcing strength increases, the variance in γ also tends to increase, depicting higher amplitude librations in the spin. We also notice a clustering at higher forcing strengths where the γ variations are much stronger. This cluster represents cases wherein γ is undergoing full circulation at least a large fraction of the time, or where the amplitudes of libration are large enough to cause switching between libration of γ about 0 and about π. This depicts how there is a certain threshold in libration amplitude beyond which circulation becomes much more likely, and causes this clustering at larger $\sigma(\gamma)$.

Finally, we also note that there are likely to be larger variations in γ for lower tidal damping strengths (i.e. larger tidal factor Q), as we would still expect very low variance in γ in the limit of very high tidal damping strength.

3.3.4 Best-Fit for Real System

While our ultimate goal is to characterize how the spin of a planet may respond to a variety of possible dynamical behaviors, we may also wish to know what is likely for the real TRAPPIST-1 system. We therefore reproduced the best-fit orbital solutions from [Grimm et al., 2018] and inputted the orbital histories into our spin model using the same assumptions outlined in 3.2 and with tidal factor $Q = 100$. Our results are shown for planets d, e, and f in Figures 3.8, 3.9, and 3.10. We can see that, indeed, the spins of each planet in the real system may respond very strongly to the mutual interactions with the other planets. We find high amplitude libration in planet d, with switching among circulation and libration in planets e and f. The spin of planet f in particular seems likeliest to respond to the strongest

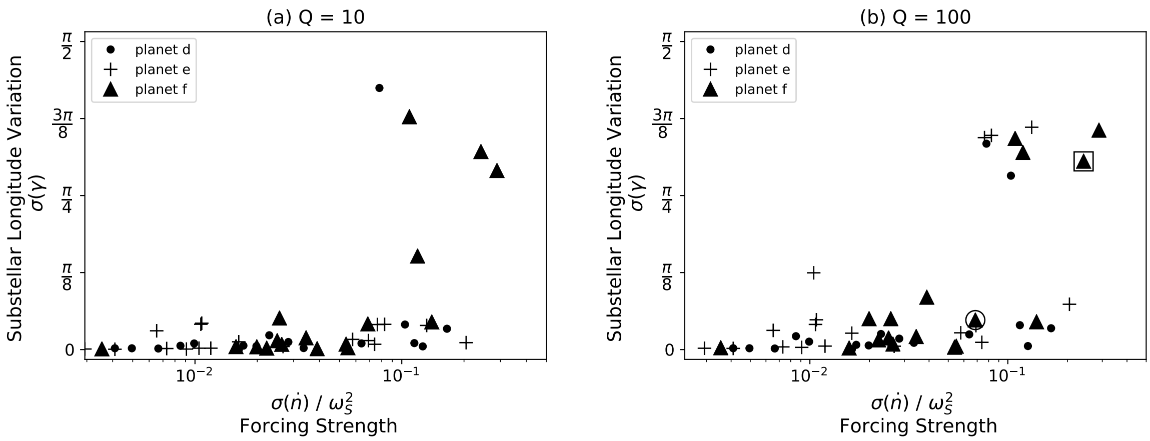

Figure 3.7: Standard deviation of γ versus standard deviation of $\dot{n}$ normalized to ω_S^2 for each integration with tidal parameter $Q = 10$ (i.e. higher tidal damping) being depicted in panel (a) on the left and tidal factor $Q = 100$ being depicted in panel (b) on the right (i.e. lower tidal damping). Planets d, e, and f, are represented with dots, plus signs, and triangles, respectively. The cases studied from Figures 3.1 and 3.3 are enclosed in a square and a circle, respectively. Higher variations in γ suggest larger, or even complete, stellar coverage over time on the planet. We see clearly that there is higher probability of large variations in γ beyond a certain threshold in the standard deviation of $\dot{n}$. We also can see that circulation becomes more common for lower tidal damping strengths (higher Q). Years are used for units with time.

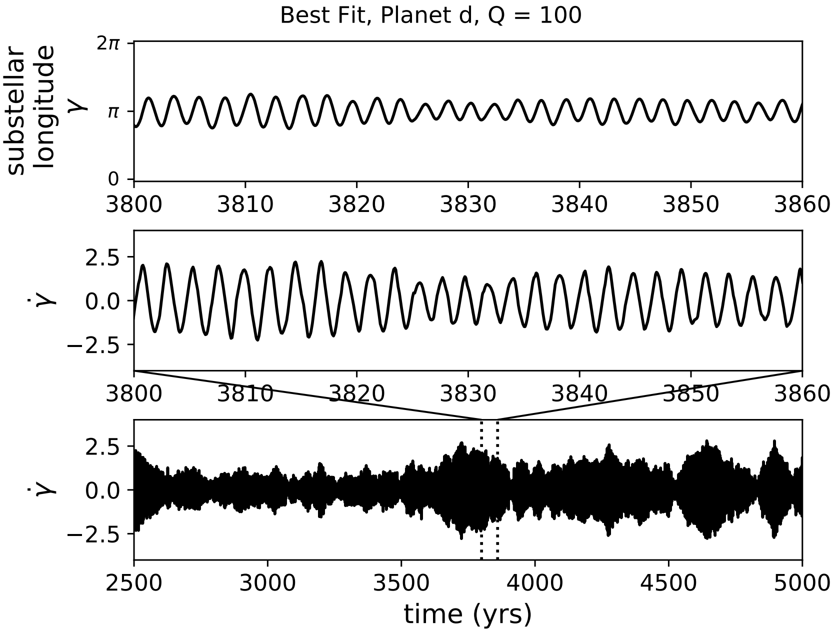

Figure 3.8: Best-fit results for planet d, assuming tidal factor $Q = 100$. Bottom panel shows evolution of $\dot{\gamma}$. Upper panels zoom in to show the behavior of γ and $\dot{\gamma}$ on a shorter timescales, where we see high-amplitude libration in the spin.

to the mutual interactions.

While these results can give as strong qualitative sense of how the spins of the planets may behave, we caution that, due to its chaotic nature, exact solutions for the spin cannot be inferred. We can, however, posit that these planets may likely be effectively non-synchronous, with a high amplitude libration in the spin and with potential for circulation at certain times, resulting in more stellar coverage over their surfaces.

3.3.5 Timescales

There are two timescales which are of primary concern in our results for the spin evolution: one is the libration or circulation timescales, and the other is the duration of quasi-stable states, that we observe in many of our simulations. These timescales both would have profound implications for climate and thus for habitability.

The duration of quasi-stable states varies among our simulations from just a few thousand

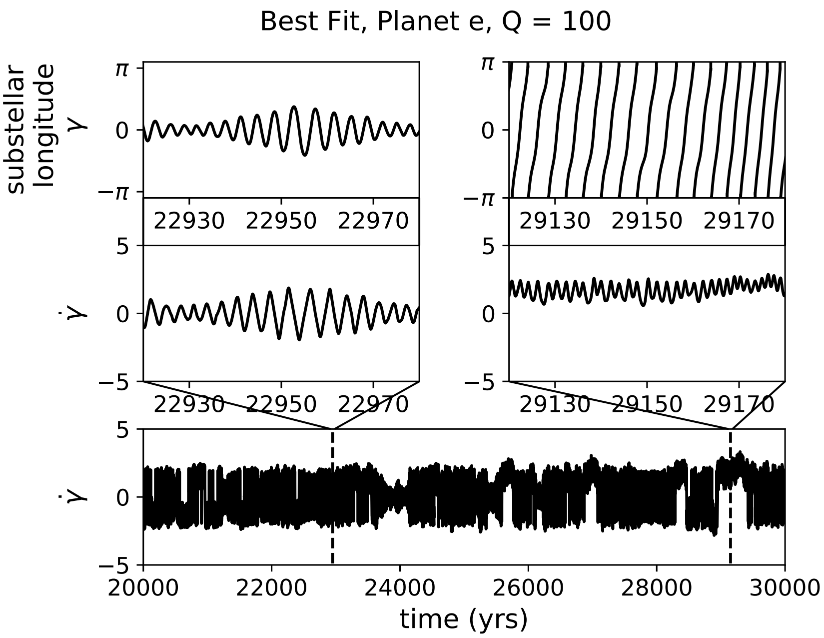

Figure 3.9: Best-fit results for planet e, assuming tidal factor $Q = 100$. Bottom panel shows evolution of $\dot{\gamma}$. Upper panels zoom in to show the behavior of γ and $\dot{\gamma}$ at different times, where we see libration on the left and circulation on the right.

years to hundreds of thousands of years. In the example presented in Figure 3.1, we determine that the circulating and librating states endure on timescales on the order of 10^4 years. The planet would undergo long periods of moderate-amplitude librations of its spin argument γ, while occasionally switching to other quasi-stable states, some where spin argument γ can "flip" such that the side that was previously the "night side" becomes the "day side" and vice versa, and other states where the spin argument γ can fully circulate for a few thousand years.

The other important timescale to note here is the period of the libration or circulation while in a quasi-stable state. Figure 3.11 depicts the average timescale for libration and circulation for each of our integrations for tidal factors $Q = 10$ and $Q = 100$. Here we see typical timescales on the order of a few years for both librating and circulating cases. This implies, for the circulating cases, full stellar days, wherein the planet makes a full rotation in its co-rotating frame, which last on the order of a few years (while the system lasts in such a circulating quasi-stable state). We note that these stellar days last far longer than the

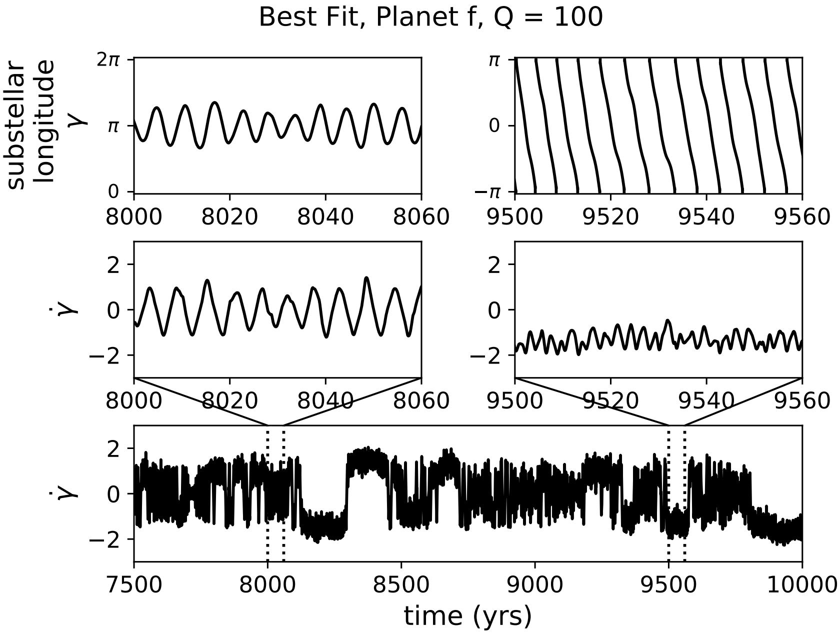

Figure 3.10: Best-fit results for planet f, assuming tidal factor $Q = 100$. Bottom panel shows evolution of $\dot{\gamma}$. Upper panels zoom in to show the behavior of γ and $\dot{\gamma}$ at different times, where we see libration on the left and circulation on the right.

orbital period of the planet, with the planet's spin still being effectively synchronous over one orbit. We also note that circulating behavior is more common for lower tidal damping strengths (corresponding to larger tidal factor Q), and also appears to be more common for the outer-most planet we simulated, planet f, and less common for inner-most simulated planet, planet d. This would also be expected, as the tidal damping strength, as well as depending on Q, also depends strongly on distance from the central star, with tidal damping increasing with decreased distance from the star. We note that circulation is still a possibility even for planet d under the right circumstances.

3.4 Implications

Our model depicts how much more complicated the spin states of planets in compact, multi-planet systems can be than what one might naively infer from simple tidal theory. The chaotic configuration of a system such as TRAPPIST-1 can lead to a chaotic driving of the spin

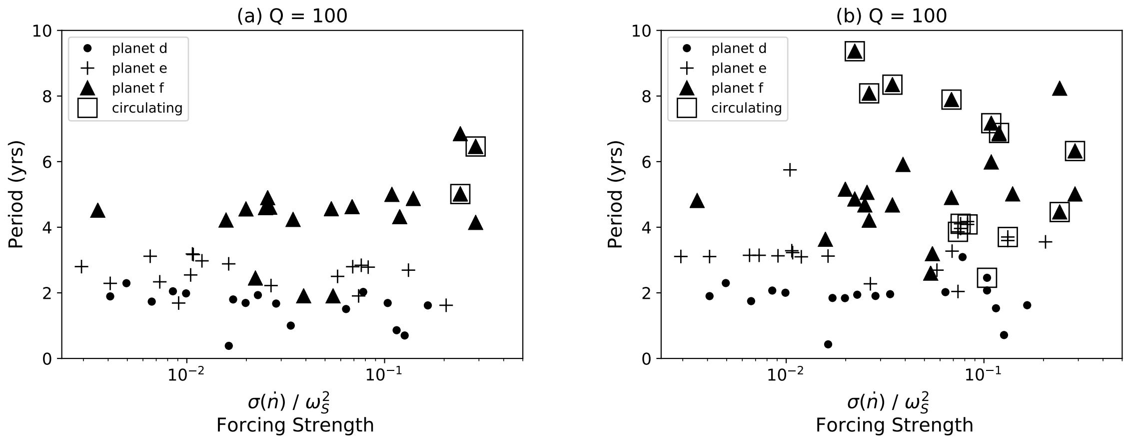

Figure 3.11: Periods of libration or circulation in γ plotted against variations in $\dot{n}$ normalized to ω_S^2 for our integrations with tidal factor $Q = 10$ in panel (a) on the left and tidal factor $Q = 100$ in panel (b) on the right. Integrations for planets d, e, and f, are represented by dots, plus signs, and triangles, respectively. A square around one of these markers indicates a circulating timescale for the respective planet. We find that the timescales are all on the order of a few years, with higher likelihood for periods of circulation for larger Q. We also note that circulation in γ is most likely in planet f, and least likely in planet d.

argument γ, resulting in a variety of possible chaotic behaviors in the spin. Some simulations exhibit small or moderate amplitude librations of γ, while other depict full circulation, with many others exhibiting switches among different quasi-stable states. This can clearly have dramatic potential consequences on climate, and thus on habitability prospects.

From Section 3.3.5, we noted that the spin timescales for libration or circulation are on the order of a few years, as also seen in Figure 3.11 . These timescales are shorter than the expected atmospheric response time of $\lesssim 10$ years for Earth-like planets as calculated by [Spiegel et al., 2008], and thus can help prevent atmospheric collapse on the night-side of the planet if the spin is circulating or undergoing high-amplitude libration.

We also note that state switching could also be likely, wherein the spin state changes behavior by abruptly transitioning from librating to circulating, circulating to librating, or else the planet swapping day and night sides for librating cases (e.g. switching from librating about γ at 0 to librating about π on the opposite face of the planet). The longevity of these quasi-stable states can be on the order of a few thousand years, though the time it takes to switch from one state to another is on the order of tens of years. This can result in relatively stable climate states that last for a few thousand years, but that can then intermittently switch.

That the libration and circulation timescales are less than the expected atmospheric response times of these planets would seem to bode well for habitability prospects on these planets, if the response of the spin to the driving of mean motion variations caused by neighboring planets is strong enough to produce high-amplitude librations in γ, or even complete circulation. The effects of the intermittent changes in climate, due to switches among quasi-stable spin states, is less certain. The time for the switches to occur would provide a period of transition on the order of tens of years from one quasi-stable climate period to another, likely giving the atmosphere enough time to respond gradually enough. More work is necessary to fully explore the effects on climate and the resultant effects on potential habitability.

With the new Transiting Exoplanet Survey Satellite (*TESS*), which aims to perform a near-full sky survey designed for detecting small exoplanets in tight configurations, there comes the opportunity of discovering many similar systems in which our model may be applicable. Already, *TESS* has discovered that the small-dwarf system TOI-700 contains two planets, one of which is terrestrial and in the estimated habitable zone, very near a 7:3 commensurability. We will further use this system as a case study in Chapter 4. We should note, however, that even given the optimistic scenario of obtaining many relevant analogue systems from *TESS* which could be used observe spin states, we would not expect to be able to observe any spin transitions occurring. Rather, we would observe a snapshot of the system during its evolution within one of potentially multiple quasi-stable states .

CHAPTER 4

Considering the Efroimsky Tidal Torque and Atmospheric Tides

Thus far, we have modeled the effects that one or more resonant companions can have on the effective spin states of planets within certain kinds of systems, wherein one would otherwise expect the planets to be tidally locked into synchronous spin states. The principal mechanism that leads to this tidal locking is tidal dissipation, causing the planet to eventually "lock on" to a stable equilibrium (e.g. the synchronous spin-orbit state). In the previous two chapters, we considered a relatively simple tidal dissipation model with the assumption that tidal torque is simply proportional to, and acting against, the spin rate in the co-rotating orbital frame (i.e. $\ddot{\gamma}_{\text{tide}} \propto -\dot{\gamma}$). The simplicity allowed us to easily illustrate how the driving of the spin by resonant companions can be a dramatic factor for the resultant spin state. It also forced synchronicity absent of driving forces.

A more realistic tidal model may yet provide additional insights, being able to more accurately provide tidal torques as we vary $\dot{\gamma}$ and also depict higher-order spin-orbit resonances, as we will see that dependence on the spin rate can actually be quite a bit more complex than a simple proportionality.

Another factor not yet considered which can affect the net torque on the planet is that due to atmospheric tides. Atmospheric tides are caused by an asymmetric temperature gradient when viewing a planet from directly over its substellar point due to thermal inertia while the planet spins, further causing an asymmetric mass redistribution. Due to this asymmetric mass distribution in the atmosphere with respect to the substellar point, a nonzero net torque results which can accelerate or decelerate the spin. This is thought to cause a stable, slightly retrograde, spin for Venus within our own solar system [Ingersoll and Dobrovolskis, 1978], aided by Venus's especially thick atmosphere. However, it has also been shown that the same effect may be relevant for habitable-zone planets around very cool dwarf stars [Leconte et al., 2015].

In this chapter, we will introduce a more complex tidal model due known as the "Efroimsky Torque" in Section 4.1. We will also introduce atmospheric tides to our modeling, as will be discussed in Section 4.2, which we will show can lead to a net weakening of the torques working to damp the spin. We will describe our setup with assumptions and parameter choices in Section 4.3 before presenting some key results from these effects coupled with our spin driving model in Section 4.4, with a discussion of implications in Section 4.5

4.1 Efroimsky Torque

For our new tidal model, we will incorporate the so-called "Efroimsky Torque", which applies a comprehensive development of Kaula and Darwin's harmonic decomposition of the tidal torque [Efroimsky and Lainey, 2007, Efroimsky and Williams, 2009, Efroimsky, 2012b, Efroimsky, 2012a]. This is a more realistic, albeit more complex, way of modeling the tidal torques acting on the planet than we have used thus far.

The simplified expression for the secular part of the Efroimsky Torque from [Makarov, 2012] can be written as

$$\ddot{\gamma}_{\text{efr}} = \frac{3}{2} G \frac{M_*^2}{m} \frac{R^3}{a^6} \frac{1}{\zeta} \sum_{q=-1}^{4} G_{20q}^2(e) K_c(2, \chi_{220q}) \text{sign}(\omega_{220q}), \tag{4.1}$$

where ζ is a moment of inertia coefficient which we will simply take as $\zeta = 2/5$, χ_{220q} is the positively defined forcing frequency $|\omega_{220q}| = |(2+q)n - 2\dot{\theta}|$, $G_{20j}(e)$ is a power series in eccentricity via the "Hansen coefficients" as found in [Murray and Dermott, 1999], and K_c is a so called "quality function" whose relation can be found by

$$K_c(l, \chi) = -\frac{3}{2(l-1)} \frac{\Lambda_l \chi \Im(\chi)}{\left(\Re(\chi) + \Lambda + l\chi\right)^2 + \Im^2(\chi)}, \tag{4.2}$$

with

$$\Lambda_l = \frac{4\pi\left(2l^2+4l+3\right)R^4\mu}{3lGM_2^2}, \tag{4.3}$$

and

$$\Re(\chi) = \chi + \chi^{1-\alpha}\tau_A^{-\alpha}\cos\left(\frac{\alpha\pi}{2}\right)\Gamma(1+\alpha) \tag{4.4}$$

$$\Im(\chi) = -\tau_M^{-1} - \chi^{1-\alpha}\tau_A^{-\alpha}\sin\left(\frac{\alpha}{2}\right)\Gamma(1+\alpha), \tag{4.5}$$

where τ_A and τ_M refer to the Andrade and Maxwell times, respectively, α is the tidal lag responsitivity, and μ is the unrelaxed rigidity modulus. The symbols $\Re$ and $\Im$ indicate the "real part" and "imaginary part", respectively. The characteristic Andrade time is frequency dependent and, according to [Makarov, 2012], can be modeled as

$$\tau_A(\chi) = \left((5\times10^4\ \text{yrs})e^{-\chi/0.2} + \tau_M\right), \tag{4.6}$$

which becomes large as frequency χ becomes small, but can otherwise often be taken as $\tau_A \approx \tau_M$.

We can compare the complexities of the Efroimsky Torque and our previously-used constant time lag model from Chapters 2 and 3 by observing how each varies with $\dot{\gamma}$ under a set of assumptions on the system we are applying the models to. Applying to a typical system relevant to our considerations (i.e. an Earth-sized planet within the habitable zone of a cool dwarf system), we compare the two torques in Figures 4.1. Here we see the dramatic differences between the two. Our previous, simpler treatment varies linearly with $\dot{\gamma}$ and has only one stable equilibrium. Meanwhile, the Efroimsky torque is far more complicated; while the torque does go to zero as $\dot{\gamma}$ goes to zero, the torque can still get quite large as we approach this limit, before quickly turning to approach zero. In this particular example, we also observe another stable equilibrium with Efroimsky torque at a $\dot{\gamma}$ corresponding to a 2:1 spin-orbit resonance. Whether or not the resonance at this location is strong enough for capture is sensitive to particular choices in parameters for our system of interest.

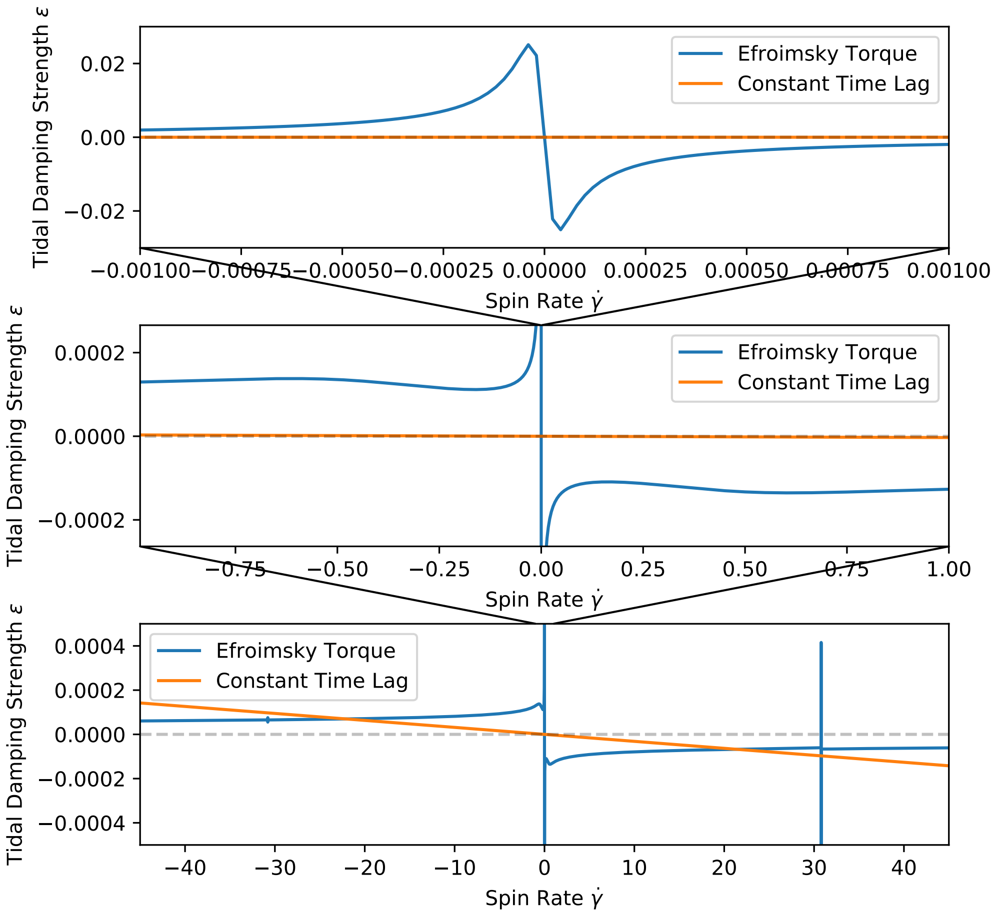

Figure 4.1: Here we present an example of how the tidal damping strength varies as we vary $\dot{\gamma}$ for both the new Efroimsky torque tidal treatment, and for the constant time lag torque we used in Chapters 2 and 3 wherein the tidal torque was exactly proportional to $\dot{\gamma}$. Top panel zooms in on the center of the middle panel, which zooms in on the center of the bottom panel. Note the different scale on the y-axis as well. We see more complex behavior for the Efroimsky Torque, also viewing different stable spin-orbit resonances away from $\dot{\gamma} = 0$. This example applies to an Earth-sized planet with mean motion $n = 61.58$ yr^{-1} and eccentricity $e = 0.04$ orbiting a star of mass $M_* = 0.416 M_\odot$. We further assume $\mu = 80 \times 10^{10}$ Pa, and choose a tidal $Q = 5$ to illustrate the differences.

We note that, while the Efroimsky torque can showcase various other non-synchronous spin-orbit resonances, we are primarily concerned with behavior near the synchronous 1:1 case given that we are interested in how the perturbations from other planets can push an otherwise synchronous planets out of pure synchronicity, as planet within our systems of interest are typically believed to not be captured into higher order resonances. We also note, however, that our forcing model can potentially affect these other spin-orbit resonances as well by affecting their stability.

4.2 Atmospheric Tides

Atmospheric thermal tides have been used to explain the slight retrograde motion of Venus, but have also been shown to be potentially significant for planets in the habitable zone of cool dwarf systems [Leconte et al., 2015]. For a circular orbit with zero spin-orbit obliquity, the atmospheric torque on a planet of mass m and radius R can be written as

$$mR^2\ddot{\gamma}_{\mathrm{atm}} = -\frac{3}{2}Kb(2\dot{\gamma}), \tag{4.7}$$

where

$$K \equiv \frac{3M_* R^3}{5\rho a^3}, \tag{4.8}$$

and ρ is the mean density of the planet. $b(\omega)$ is a function characterizing the frequency-dependent response of the planetary atmosphere. Using the same method used by [Leconte et al., 2015], wherein we can utilize empirically quantified amplitudes of torques induced by thermal tides as predicted by global climate models, we can further write $b(2\dot{\gamma})$ as

$$b(2\dot{\gamma}) = -\sqrt{\frac{10}{3\pi}}\Im\left[\tilde{q}(\dot{\gamma})\right], \tag{4.9}$$

where $\Im$ indicates the 'imaginary part of', and where

$$\tilde{q}(\omega) = -\frac{q_0}{1 + i\omega/\omega_0}, \tag{4.10}$$

$i^2 \equiv -1$, ω_0 is the inverse of the timescale to reach thermal equilibrium, and q_0 is the amplitude of the quadrupole term of the pressure field at zero frequency.

In Figure 4.2, we give an example comparing the atmospheric tidal torque to the Efroimsky torque, and how they may add to create stable equilibria outside of the standard spin-orbit resonances which occur due to the Efroimsky torque alone. In this example, we see additional equilibria on the prograde as well as retrograde sides of the plot, indicating how, e.g., Venus can have a stable and slow retrograde orbit.

Even if the atmospheric and bodily tidal torques do not create these additional equilibria, the atmospheric tide will typically work *against* the bodily tides acting on the body of the planet, effectively weakening the net tidal torque acting on the planet. This may have potential consequences for systems of interest for this work, wherein the atmospheric torque can work to lessen the net tidal damping torques, which can lead to heightened effects by the resonant spin forcing in our spin model. An exception to this is at higher-order spin-orbit resonances expressed by the Efroimsky torque, which the atmospheric torque can act to further strengthen.

4.3 Setup

One recently discovered system that we will examine in this Chapter is TOI-700, which contains the first habitable zone Earth-sized planet discovered by *TESS* [Gilbert et al., 2020]. The system contains a star of mas $M_* = 0.416$ with three planets, one of which (planet TOI-700 d) has an estimated radius of 1.19 $R_\oplus$ residing in estimated habitable zone at a semi-major axis of 0.163 AU and is in a 7:3 commensurability with an inner planet (TOI-700 c) of radius 2.63 $R_\oplus$ at a semi-major axis of 0.0637 AU. We will consider this analogue system (ignoring any potential effects from the third planet in the system, which is not near a resonance) when considering the spin of planet d under the influence of planet

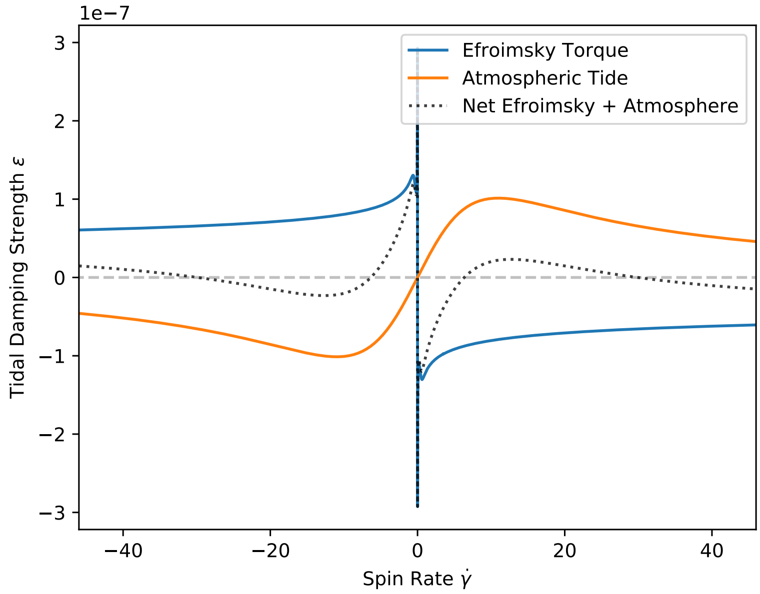

Figure 4.2: Here we present an example of how atmospheric torque may vary as we vary $\dot{\gamma}$, along with the Efroimsky torque. We also show the torques added together with the dotted black curve, which shows that the torques may add together to create additional equilibria if the relative strengths are of similar order in certain $\dot{\gamma}$ regimes. In this example, we observe the normal synchronous stable equilibrium at $\dot{\gamma} = 0$, but also observe a pair of stable and unstable equilibria both on the prograde ($\dot{\gamma} > 0$) and retrograde ($\dot{\gamma} < 0$) sides of this plot. For this purely illustrative example, we apply an Earth-sized planet with $e = 0.07$ and $n = 7.0$ yr^{-1} orbiting around a Sun-like star. For the atmospheric torque, we applied $q_0 = 200$ Pa and $\omega_0 = 11$ yr^{-1}, which is taken from [Leconte et al., 2015] and corresponds to a Venus-like atmosphere. For the Efroimsky torque, we assumed $\mu = 8.0 \times 10^{10}$ kg m^{-1} s^{-2}.

c via our spin model. We will additionally consider the Efroimsky tidal torque as well as the atmospheric torque in place of the simpler constant-lag tidal torque considered in Chapters 2 and 3. As such, our equation of motion may be written, similar to equation 2.7, as

$$\ddot{\gamma} + \frac{1}{2}\omega_S^2 \sin 2\gamma - \frac{1}{j}\omega_M^2 \sin\phi + \left(\ddot{\gamma}_{\mathrm{efr}} + \ddot{\gamma}_{\mathrm{atm}}\right) = 0, \tag{4.11}$$

but where the net tidal torque in the parentheses is given by the Efroimsky torque $\ddot{\gamma}_{\mathrm{efr}}$ and atmospheric torque $\ddot{\gamma}_{\mathrm{atm}}$ as defined in equations 4.1 and 4.7, respectively.

We must now choose appropriate parameters which will govern the evolution of the spin, including parameters which govern the tidal torques. First, since we are considering the effects on an Earth-like planet, we will retain our previous fiducial choice in $(B - A)/C = 1.0 \times 10^{-5}$, and will also choose $e = 0.04$ as a fiducial value. From the radii estimates, we can further assume that planet d has a mass of $m = 1.5\ M_\oplus$ while the inner perturber, planet c, has a mass of $m' = 7.3\ M_\oplus$.

For the Efroimsky Torque, we choose parameters appropriate for rocky terrestrial planets within the solar system by using values presented in [Makarov, 2012], with a Maxwell time of $\tau_M = 500$ years, tidal lag responsitivity $\alpha = 0.2$ from equations 4.4 and 4.5, and a fiducial unrelaxed rigidity modulus $\mu = 8.0 \times 10^{10}$ kg m^{-1} s^{-2}. For the atmospheric torque, we also choose parameters appropriate for rocky terrestrial planets with an atmosphere thicker than Earth's (10 bar) within the habitable zone by using values presented in [Leconte et al., 2015], with $q_0 = 3000$ Pa and $\omega_0 = 22$ yr^{-1}. This will be to better illustrate potential effects as it allows the atmospheric torque to be more significant without the atmosphere being inhospitably thick.

Finally, we note that a commensurability of 7:3 corresponds to a value of $j = 3$ in equation 4.11, which we choose for the sake of analogy to TOI-700. The behavior of the forcing under this commensurability is similar to, e.g., a 2:1 or 3:2 first-order resonance in that it still behaves like a pendulum. The only differences arise in the strength of such a forcing as coefficients change within ω_M and change the width of a resonance in semi-major axis, with a tighter range for higher-order resonances. Since we can vary the strength of the forcing in other ways (e.g. by changing ω_M or initial conditions in ϕ), the conclusions we reach on the behaviors of the spin should be qualitatively similar than if we choose different commensurabilities, but keeping in mind that strengths can change holding other parameters constant and that conditions for mean motion resonance can become more stringent as the order of the resonance increases.

In section 4.4.1 we will present results given our choices in parameters presented here except without atmospheric effects, while varying certain choices to demonstrate how the spin responds to different choices in parameters under the influence of just the Efroimsky torque. Our integrations will solve equation 4.11 via the Runge Kutta Fourth Order method of integration with adaptive time steps depending on a convergence criterion of γ where $\gamma_{i+1} - \gamma_i < |10^{-8}\gamma_i|$, with subscripts i representing some arbitrary step in the integration. An integration in ϕ must also be used alongside to feed into the overall integration of γ.

In Section 4.4.2, we will then present results when adding effects of significant atmospheric torques.

4.4 Results

4.4.1 Efroimsky Torque Only

To explore effects of the Efroimsky torque coupled with spin driving we will use the TOI-700 system as inspiration, with parameters laid out in the previous section. We will ignore atmospheric tidal effects for now, adding effects from atmospheric tides in Section 4.4.2 We first present two case examples in Figures 4.3 and 4.4, being examples resulting in full stellar coverage and moderate-amplitude libration, respectively. We note that we used a higher perturbing mass m' than observations suggest in order to better illustrate the two case behaviors. Initial conditions are set such that the planet begins at synchronicity ($\gamma(0) = 0$, $\dot{\gamma}(0) = 0$) so that we may see how the spin deviates starting from there. We also let $\phi(0) = 3.0$, and $\dot{\phi}(0) = 0$, suggesting an orbital resonance with reasonably high-amplitude librations in resonant angle ϕ.

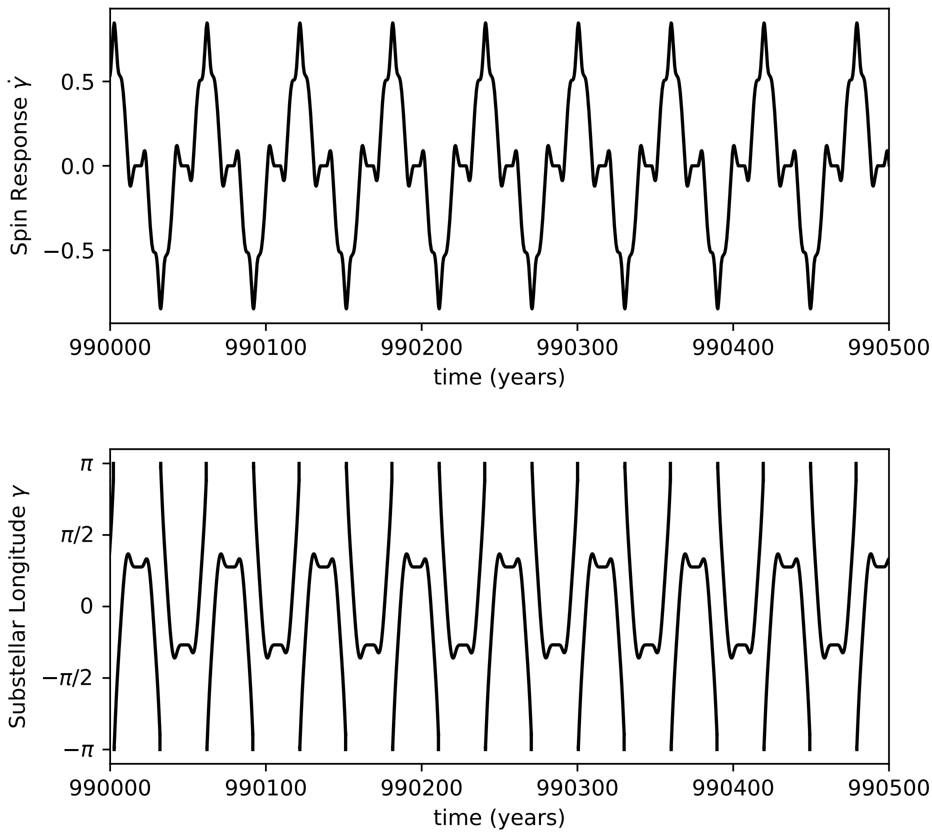

Figure 4.3: Here we present one example of how the spin might evolve for a system inspired by TOI-700 wherein the spin results in full stellar coverage of planet d over time. In the top panel we plot $\dot{\gamma}$ versus time, and in the bottom panel we plot the substellar longitude γ versus time, after the evolution reached a limit cycle. This is then the final behavior of the spin for this particular system. We chose our fiducial parameters for our TOI-700 analogue system, except with an unrealistically high perturber mass of 100 $M_\oplus$ for purely illustrative purposes to indicate dependence on ω_M as compared to Figure 4.4. These parameters yield a forcing frequency of $\omega_M = 0.584$ yr^{-1} and a natural spin frequency of $\omega_S = 0.336$ yr^{-1}. Initial conditions were chosen as $\gamma(0) = 0$, $\dot{\gamma}(0) = 0$, $\phi(0) = 3.0$, and $\dot{\phi}(0) = 0$.

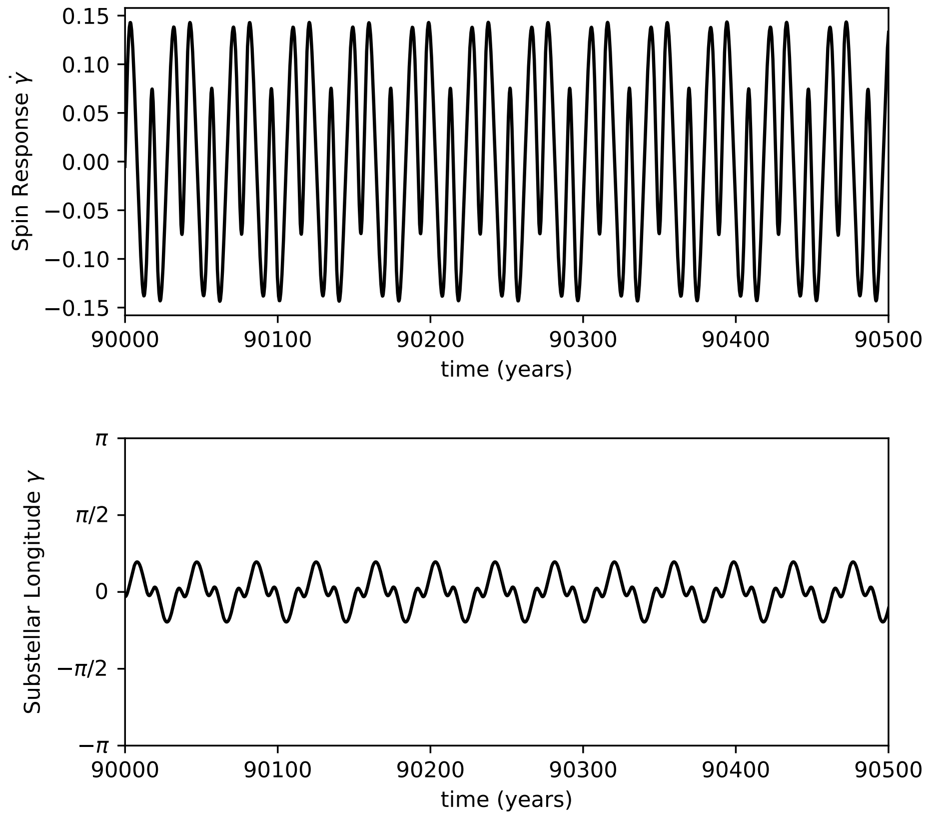

Figure 4.4: Here we present one example of how the spin might evolve for a system inspired by TOI-700 wherein the spin results in moderately high amplitude librations in γ. In the top panel we plot $\dot{\gamma}$ versus time, and in the bottom panel we plot the substellar longitude γ versus time, after the evolution reached a limit cycle. This is then the final behavior of the spin for this particular system. We chose our fiducial parameters for our TOI-700 analogue system, except with an unrealistically high perturber mass of 40 $M_\oplus$, but still lower than that of Figure 4.3, to indicate how lowering ω_M affects the limit cycle. These parameters yield a forcing frequency of $\omega_M = 0.413$ yr^{-1} and a natural spin frequency of $\omega_S = 0.336$ yr^{-1}. Initial conditions were chosen as $\gamma(0) = 0$, $\dot{\gamma}(0) = 0$, $\phi(0) = 3.0$, and $\dot{\phi}(0) = 0$.

The case presented in Figure 4.4 has a higher value of ω_M than that presented in Figure 4.3, resulting in a stronger spin response which leads to complete circulation. We note that, if we had used the fiducial value of perturbing mass $m' = 7.3\ M_\oplus$, a lower value of ω_M would have resulted, yielding near-perfect synchronicity of the spin and suggesting that the perturbing planet may need a larger mass to push planet d out of synchronicity in the real system. Clearly, the ratio ω_M/ω_S is an important factor in the resultant behavior of the spin, as it was in previous chapters and depicted in Figures 2.1, 2.2, 2.3, and 2.4.

Under our new tidal damping treatment in this chapter, we can similarly plot the spin response for various integrations as we vary ω_M/ω_S, as seen in Figure 4.5 where we choose our fiducial parameters for TOI-700 except for m', which we vary in order to vary ω_M. We also choose initial conditions of $\phi(0) = 0.25$, and $\dot{\phi}(0) = 0$, indicating a system very close to a perfect orbital resonance with small amplitude librations in the resonant angle ϕ, and also choose $\gamma(0) = 0$, $\dot{\gamma}(0) = 0$. (As such, the small angle approximation in ϕ discussed in Section 2.2 would be valid). We observe some expected similarities to Figures 2.3 and 2.4. However, we note an important difference: there appears to be a threshold in ω_M/ω_S below which the tidal damping becomes so strong that any librations in the spin become insignificant, resulting in near-perfect synchronicity in the spin. Above the threshold, we observe a stronger response from the spin as a result of a relaxed damping. The response of the spin is complicated by the manner in which the Efroimsky torque depends on $\dot{\gamma}$, becoming quite strong at relatively low $\dot{\gamma}$ (see Figure 4.1 or Figure 4.2). There is a feedback in that $\dot{\gamma}$ depends on tidal damping (as well as ω_M), and tidal damping itself depends on $\dot{\gamma}$. As such, if the forcing is too small, the tidal damping more actively suppresses the spin. If the forcing reaches a high enough threshold, then the spin can effectively break past this barrier and $\dot{\gamma}$ vary strongly enough to sustain weaker tidal damping strengths, further allowing the spin to be excited by the forcing.

These results may also be sensitive to choices in initial conditions. For results depicted in Figure 4.5, we chose a small librating condition in ϕ as well as small initial conditions in γ. If we increase the initial conditions in ϕ such that the resonant angle librates at a higher amplitude, this would effectively lead to a higher amplitude in forcing across all of our integrations. Results of a higher $\phi(0) = 1.0$ are shown in Figure 4.6, where we again plot the spin response $|\dot{\gamma}|_{max}$ as well as amplitude of the substellar longitude $|\gamma|_{max}$ as a function of ω_M/ω_S.

We notice some qualitative differences between results depicted in Figure 4.6 and those depicted previously in Figure 4.5. The spin responds more unpredictably as there is likely more chaotic behavior at early times before the individual integrations settle into a limit cycle. We also find that the spin response is generally far stronger than the corresponding integrations for lower $\phi(0)$.

Finally, we also note the much lower threshold in ω_M/ω_S at which the integrations go from depicting almost-pure synchronicity to higher amplitude librations. This therefore shows how strongly our results depend on the exact proximity to a mean motion resonance. As discussed in previous chapters, planets should ideally should be *near* a perfect mean motion resonance to yield the largest response from the spin, but not in an *exact* commensurability, which would lead to little-to-no variations in mean motion.

In order to observe how the spin may also respond in initial conditions in γ, we also show results from a set of integrations in which we now increase the initial condition in γ to $\gamma(0) = 1.4$ in Figure 4.7, which would yield a high amplitude libration in γ in the absence of forcing and damping. Here we observe even more unpredictable final limit cycles, with even some integrations resulting in low-to-moderate librations below the ω_M/ω_S threshold which tends to lead to pure synchronicity. We also observe what appear to be two clear outliers from the trends in $|\gamma|_{max}$ (as we also did in Figure 4.6) with very large amplitudes. These integrations do not actually depict correspondingly large deviations from the trend in $|\dot{\gamma}|_{max}$, but are just near a threshold which results in very large amplitude librations that cause full stellar coverage on the planet. Each particular integration's variation in γ and $\dot{\gamma}$ in time can be found in the subplots shown in Figures 4.8 and 4.9, respectively, where we can find these two particular integrations' unique behavior in γ.

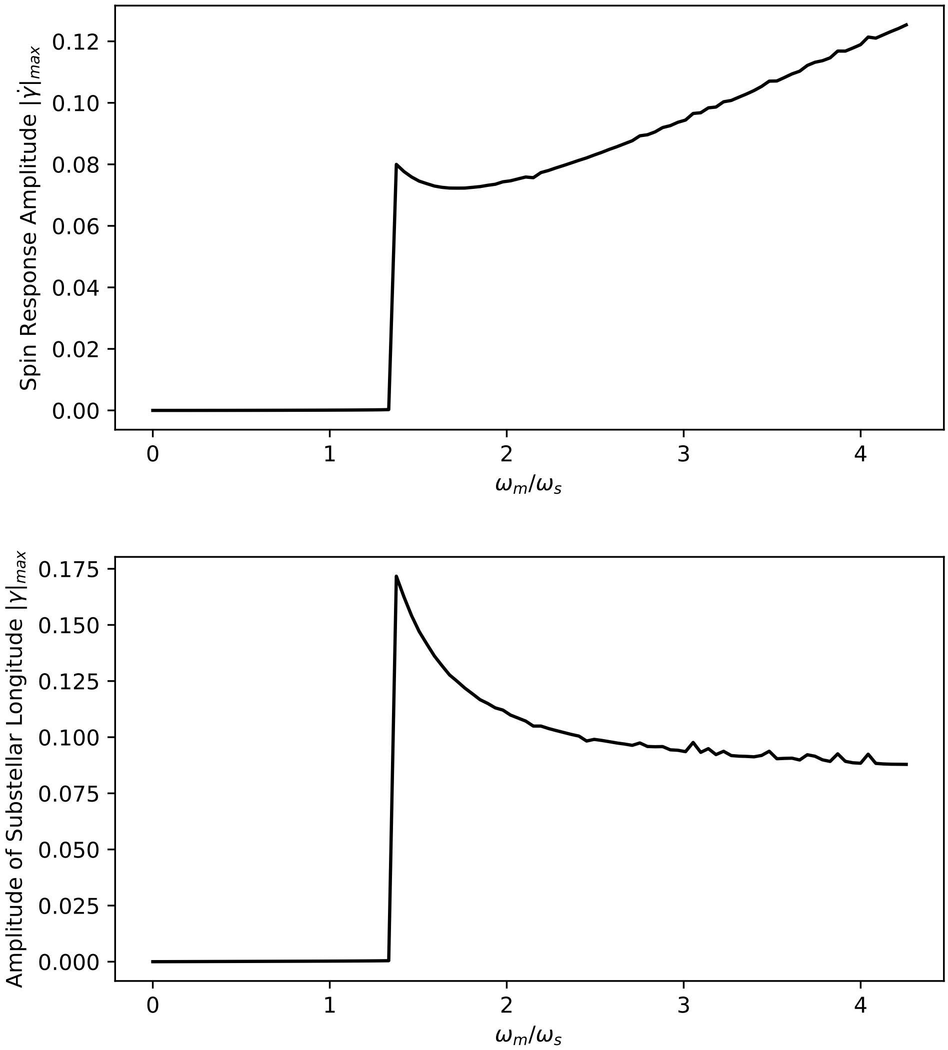

Figure 4.5: Here we present how the spin response varies for our TOI-700 analogue system as we vary ω_M/ω_S by plotting the amplitudes of $\dot{\gamma}$ (top panel) and of γ (bottom panel). For this set of integrations, we choose a relatively low initial condition in ϕ, with $\phi(0) = 0.25$ and $\dot{\phi}(0) = 0$, along with $\gamma(0) = 0$, $\dot{\gamma}(0) = 0$. This implies the planets are very close to a perfect orbital resonance, with a small libration of ϕ within the resonance, resulting in a relatively small forcing. Under our new treatment for tidal damping, we observe a threshold in ω_M/ω_S above which close-to-pure synchronicity is practically broken. We note that our fiducial parameter choices for TOI-700 would yield a ratio of $\omega_M/\omega_S \simeq 1/3$, which would imply near-perfect synchronicity in this particular plot.

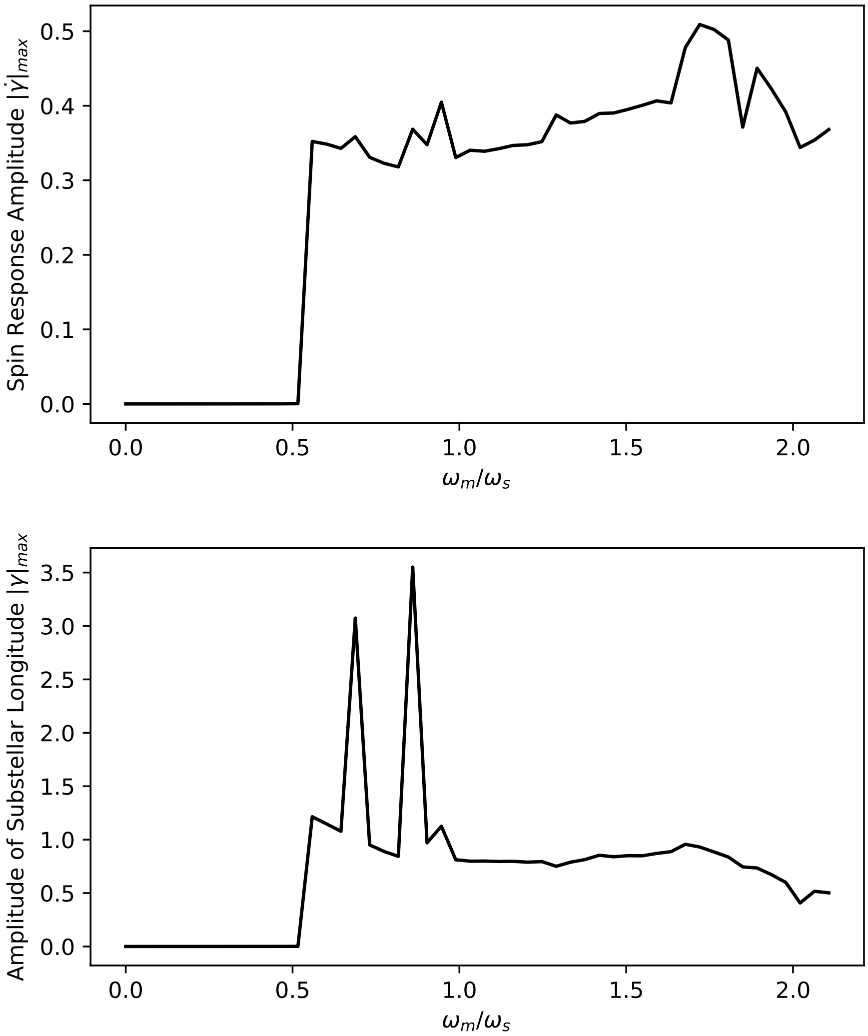

Figure 4.6: Here we present how the spin response varies for our TOI-700 analogue system as we vary ω_M/ω_S by plotting the amplitudes of $\dot{\gamma}$ (top panel) and of γ (bottom panel). For this set of integrations, we choose initial conditions with $\phi(0) = 1.0$ and $\dot{\phi}(0) = 0$, along with $\gamma(0) = 0$, $\dot{\gamma}(0) = 0$. This implies the planets are in resonance with a moderate-to-high amplitude libration of ϕ. We observe a threshold in ω_M/ω_S above which close-to-pure synchronicity is practically broken. We note the differences in this plot as compared to Figure 4.5, with these integrations showing a stronger, yet less predictable, response. The threshold in ω_M/ω_S between near-perfect synchronicity and non-synchronicity is also lower.

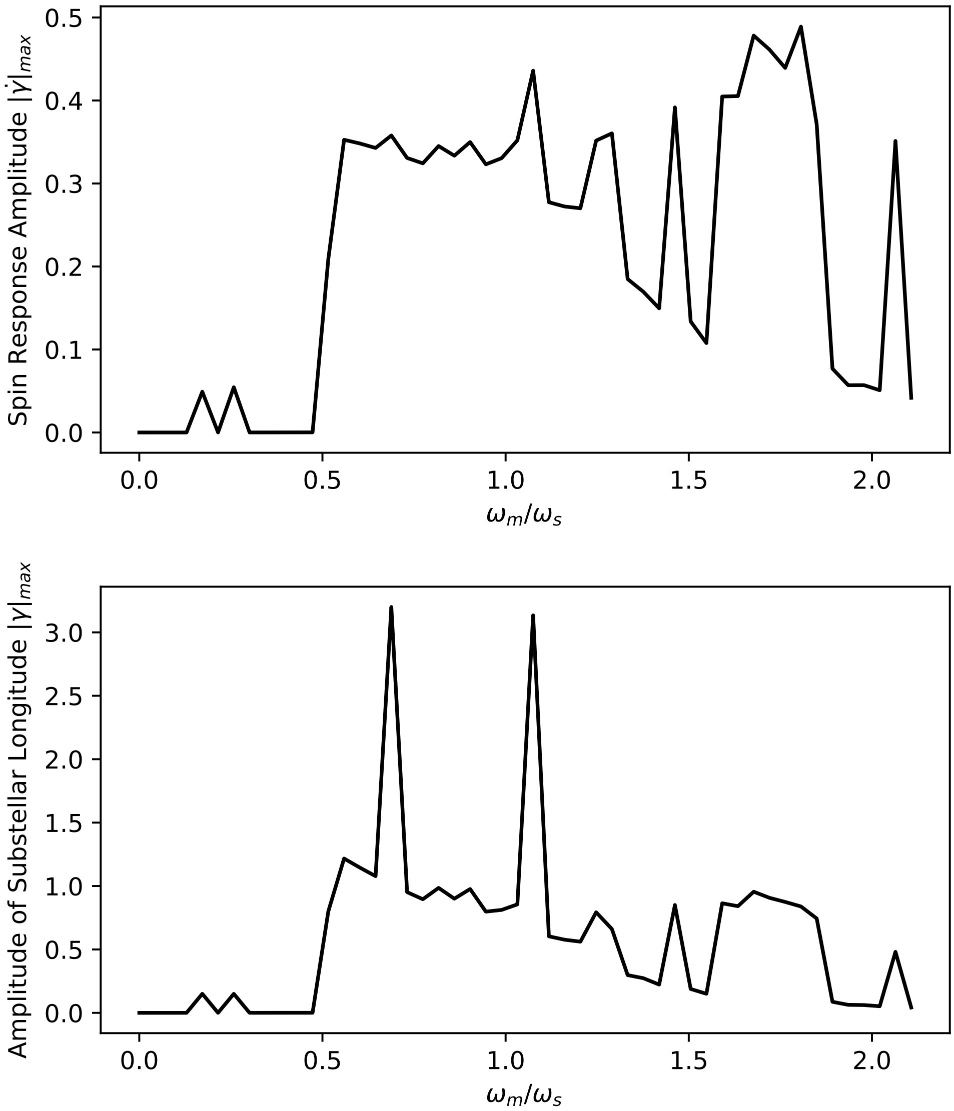

Figure 4.7: Here we present how the spin response varies for our TOI-700 analogue system as we vary ω_M/ω_S by plotting the amplitudes of $\dot{\gamma}$ (top panel) and of γ (bottom panel). We choose initial conditions with $\phi(0) = 1.0$ and $\dot{\phi}(0) = 0$, along with $\gamma(0) = 1.4$ and $\dot{\gamma}(0) = 0$. This is similar to Figure 4.6, except with a different initial condition in γ. We still observe a threshold in ω_M/ω_S above which close-to-pure synchronicity is practically broken. However, there are some simulations which can break out of synchronicity even below this threshold, and behavior is even less predictable at higher ω_M/ω_S.

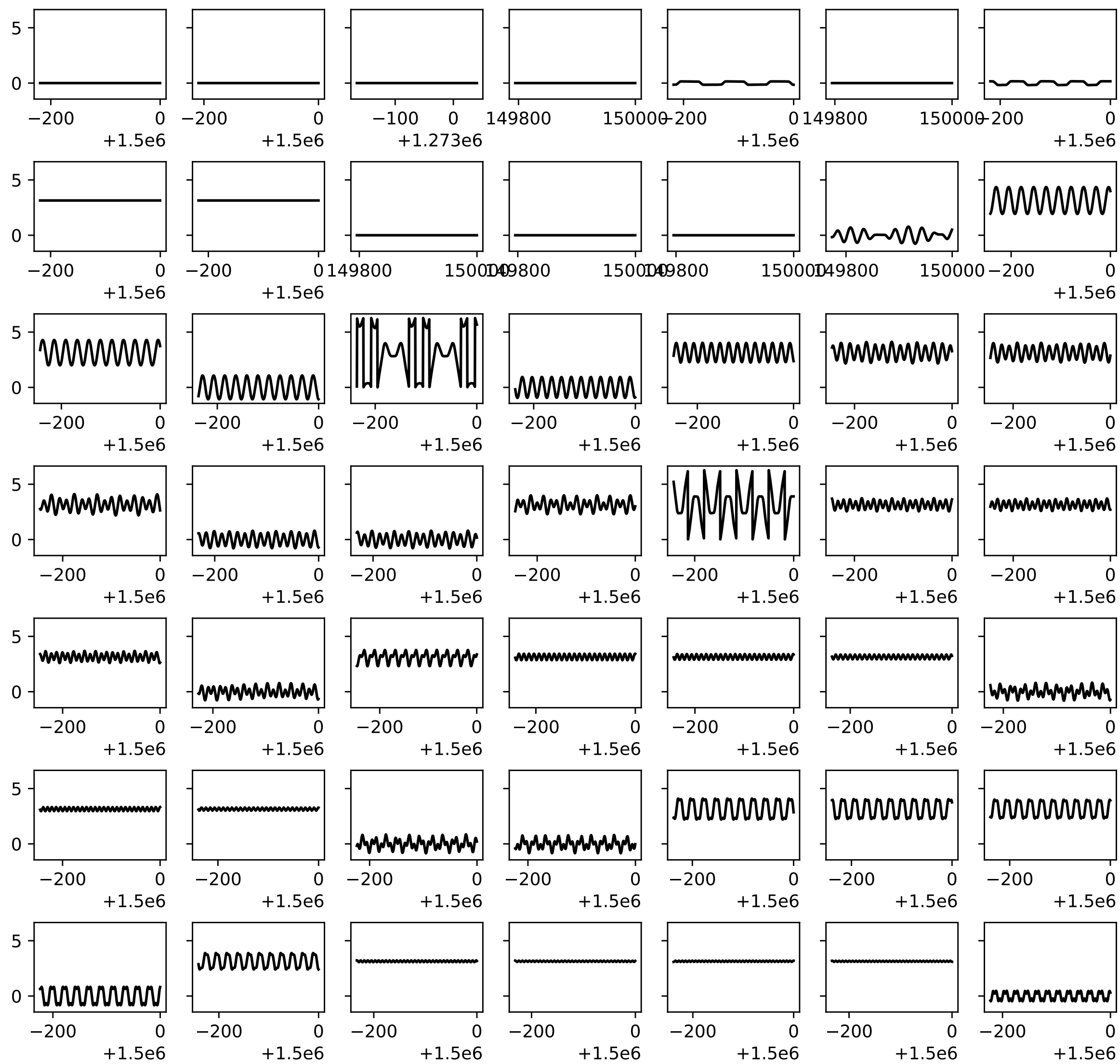

Figure 4.8: γ versus time over ~ 250 years for various integrations which correspond to those used in Figure 4.7. ω_M/ω_S increases from left to right with top left being lowest and bottom right being the highest.

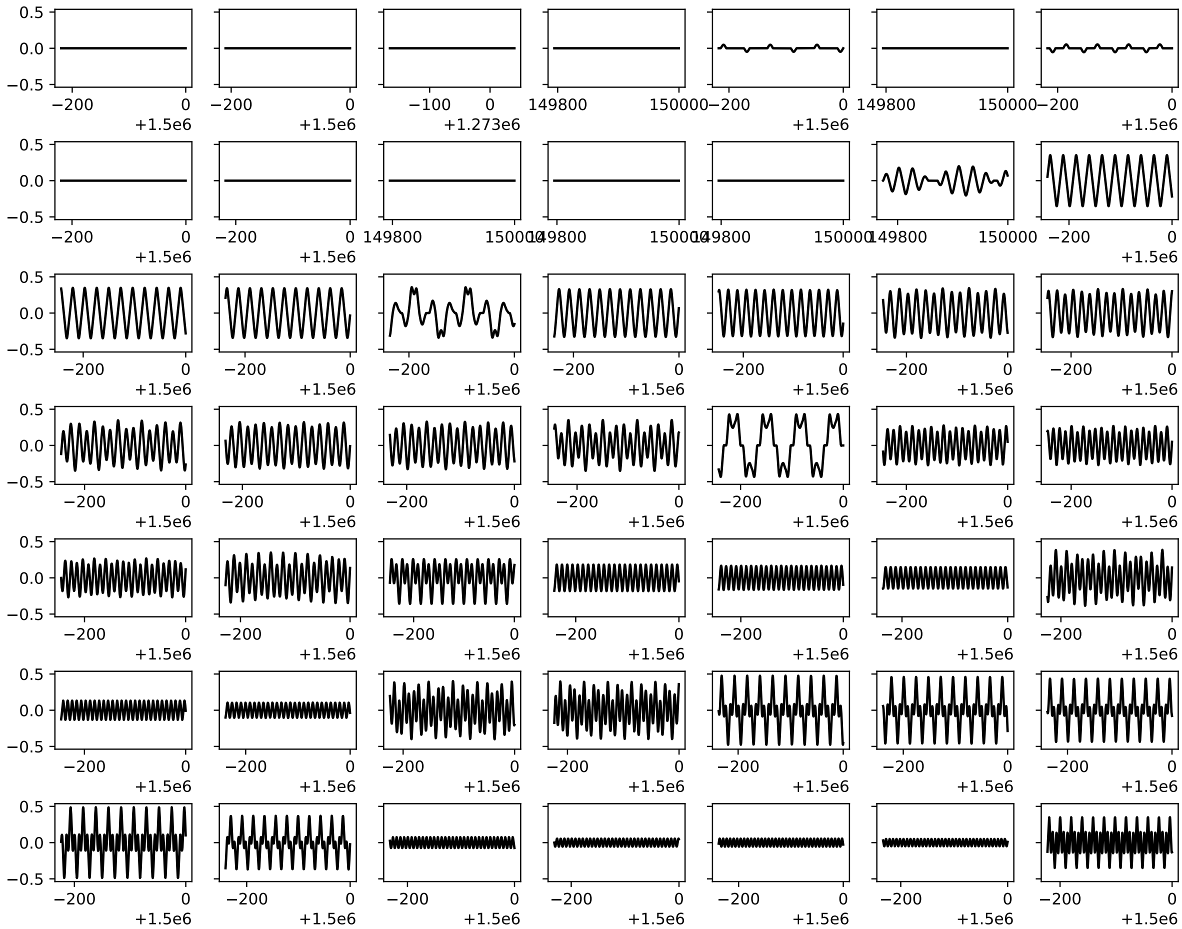

Figure 4.9: $\dot{\gamma}$ versus time over ~ 250 years for various integrations which correspond to those used in Figure 4.7. ω_M/ω_S increases from left to right with top left being lowest and bottom right being the highest.

4.4.2 With Atmospheric and Spin-Orbit Resonance Considerations

We now wish to explore how atmospheric tides can affect the net damping of the spin and the resultant effects on spin. There are two main ways that the atmospheric effects can be relevant in the context of our spin model: 1.) the atmospheric tides can enhance higher order, non-synchronous spin-orbit resonances such that capture in these states is more likely, and 2.) the atmospheric tides can create new equilibria (stable and unstable) as presented in Figure 4.2. We find that the second scenario is not dramatically affected by our spin forcing model, as the stability is enforced over a much broader range in $\dot{\gamma}$, and so will focus on the first scenario. We also note that the atmospheric tides can more typically act to weaken the net damping from the Efroimsky torque when not near a spin-orbit resonance. However, as can also be seen from Figure 4.2, the atmospheric tidal strength tends to become insignificant compared to the Efroimsky torque when approaching synchronicity, and so this weakening is only relevant at larger values of $|\dot{\gamma}|$.

The first scenario is depicted in Figure 4.10, where we observe a stable equilibrium at $\dot{\gamma} = 30.79$ yr^{-1} corresponding to a 2:1 spin-orbit resonant state, with mean motion $n = 61.58$ yr^{-1}. This resonance is observed when only considering the Efroimsky torque, where we observe a chance at capture as the tidal torque rises above 0. We also observe that this resonance is stronger if we consider the effects of atmospheric tides, potentially increasing the odds of capture. In considering the atmospheric tides, we choose to take an N_2, 10 bar atmosphere for a planet residing in the habitable zone, suggesting values of $\omega_0 = 22$ yr^{-1} and $q_0 = 3000$ Pa [Leconte et al., 2015]. If we choose a more Earth-like atmosphere (by choosing a 1 bar atmosphere), then the atmospheric effects become insignificant. As such, we note that, while atmospheres as thick and inhospitable as that of Venus need not be required to have a significant atmospheric torque, atmospheres as thin as that of Earth are likely insufficient to yield significant effects within our systems of interest.

While we observe these stable equilibria under these parameter choices, we also must consider that the forcing on the spin due to $\dot{n}$ may further affect the odds of resonant capture. We may wish to know, for example, if some level of forcing can push the spin out

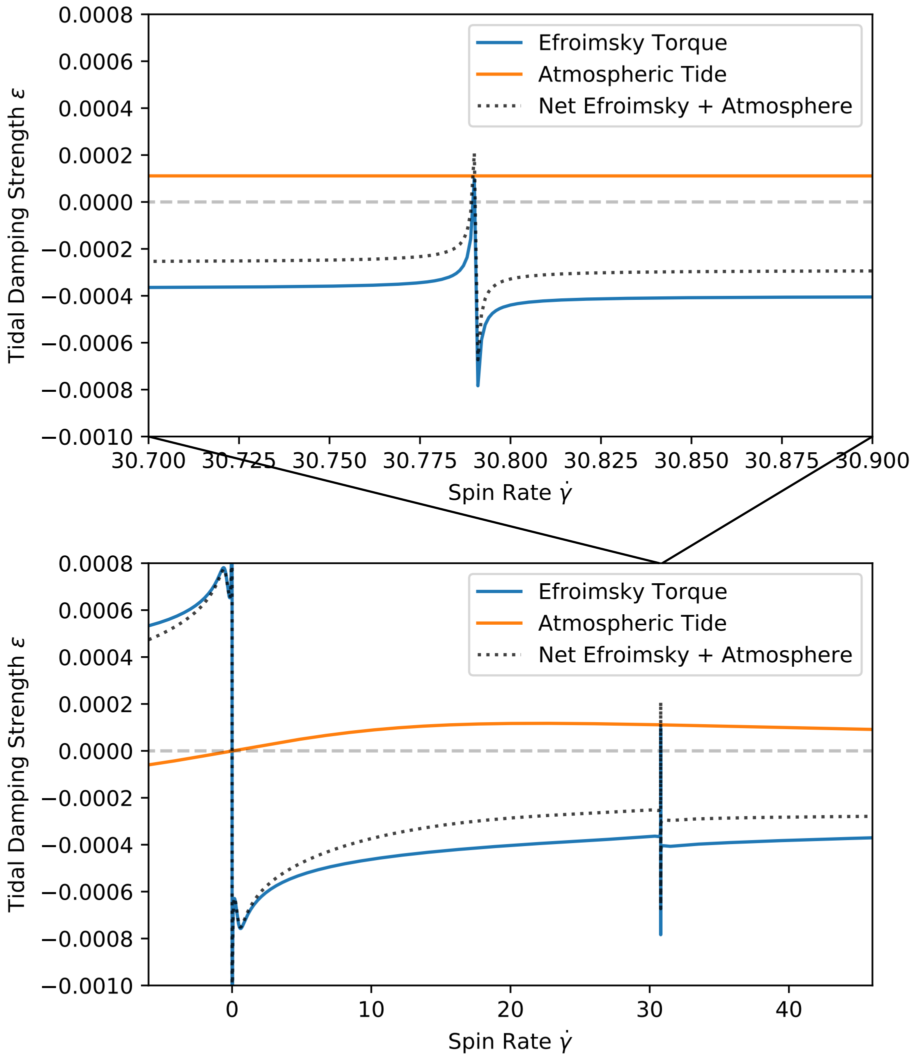

Figure 4.10: Here we show tidal torque strengths for the Efroimsky torque in blue and the atmospheric torque in orange. The bottom panel zooms in on a smaller range in $\dot{\gamma}$ as compared to the top panel. We observe a spin-orbit resonance with the Efroimsky torque, which would be strengthened when considering the atmospheric torque. To calculate the Efroimsky and atmospheric torques, we used parameters $m = 1.0M_{\oplus}$, $r = R_{\oplus}$, $e = 0.05$, $\mu = 8.0 \times 10^{10}$, $q_0 = 3000$ Pa and $\omega_0 = 22$ yr^{-1}, with atmospheric parameters corresponding to a planet in the outer habitable zone with a 10 bar N_2 atmosphere.

of this resonance, causing $\dot{\gamma}$ to further decrease until at or near synchronicity, or else further reinforce the resonance. We therefore allow a variety of forcing conditions by again varying ω_M/ω_S and plot results in the spin response for two damping scenarios from Figure 4.10 where we suppress atmospheric effects and including the atmospheric effects which cause a stronger resonance. These results are shown in Figure 4.11, where we integrate all runs for over 3 million simulation years.

Here we note that there is a resonant capture at $\omega_M = 0$ (corresponding to zero forcing) if we consider atmospheric effects, but not if we consider only the Efroimsky torque without any atmospheric effects. The differences are also apparent for high ω_M, where the forcing becomes very strong. In this regime, we see that the spin response is generally larger when we add atmospheric tides. However, in the lower ω_M regime, we observe little difference. This is because, in this regime where the forcing is relatively smaller, the spin response decreases for both scenarios, with $\dot{\gamma}$ entering a regime near enough synchronicity to where the Efroimsky torque dominates over the atmospheric torque, rendering the atmospheric torque insignificant.

4.5 Implications

We have shown how the complexities of different tidal torques can affect the evolution of the spin of a planet coupled with driving of the spin. The Efroimsky torque adds complexity given how $\dot{\gamma}$ feeds into it, which in turn feeds back into the evolution of $\dot{\gamma}$ along with any forcing. The result is that, given certain choices in parameters, we observe practically pure synchronicity below a certain forcing strength, as the Efroimsky torque gets very large as $\dot{\gamma}$ becomes relatively small. We therefore would need a strong enough forcing to keep $\dot{\gamma}$ elevated enough to sustain itself in a regime where the Efroimsky torque is of lower strength.

We find that the forcing due to proximity to mean motion resonances may be strong enough to significantly affect the spin for Earth-sized planets around very cool dwarf systems if the perturber is massive enough and if the proximity to resonance is such that ϕ varies substantially (i.e. if near the separatrix of the $\phi - \dot{\phi}$ system). This is observed in Figures

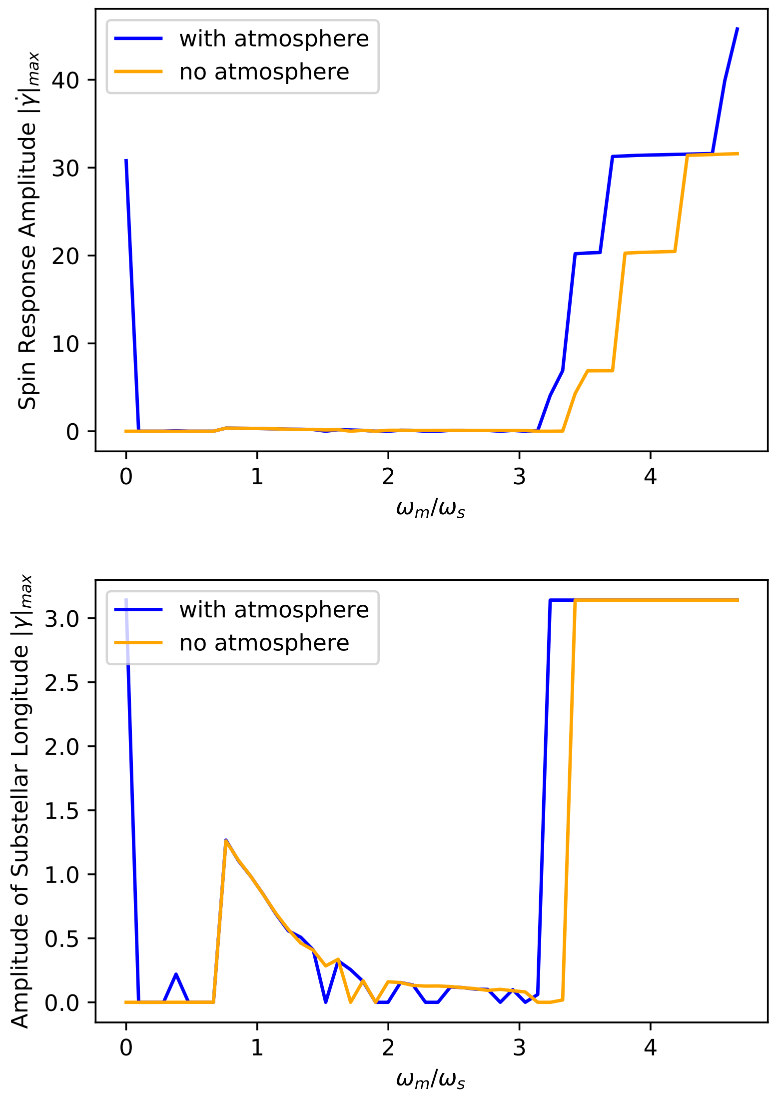

Figure 4.11: Here we depict the spin response as we vary ω_M if we start with a high initial condition in $\dot{\gamma}$ (65 yr^{-1}) for our TOI-700 analogue system and applying tidal damping strengths depicted in Figure 4.10. The net tidal torque yields a possibility for spin-orbit resonant capture at $\dot{\gamma} = 30.79\ \text{yr}^{-1}$, with the resonance being more pronounced if we consider atmospheric effects. In blue, we plot results considering atmospheric effects along with the Efroimsky torque, and in orange we consider just the Efroimsky torque without atmosphere. We note differences between the two are evident for high ω_M and for $\omega_M = 0$ (corresponding to no forcing).

4.5 and 4.6, where we observe a threshold in ω_M/ω_S below which synchronicity tends to occur and above which non-synchronicity occurs with moderate libration or even full stellar coverage. When we increase the libration amplitude in ϕ, we observe the threshold in ω_M/ω_S lowering, depicting how proximity to resonance can be an important factor in determining the likelihood of a synchronous spin state.

We further depicted how atmospheric tidal torques may have the opportunity to dramatically affect the spin. One main point here are that a thick atmosphere can strengthen the probability of capture into higher order resonances under the Efroimsky torque, as can be seen in Figure 4.11. This is due to the fact that atmospheric torques, while typically acting against the standard bodily tidal torque, will actually work to further strengthen a resonance where the Efroimsky torque switches signs to create stable equilibria. We find that the atmosphere would likely have to be quite thick, however, to allow for significant effects from atmospheric torques.

In our integrations, we found that an Earth-like 1 bar atmosphere resulted in insignificant atmospheric torques as compared to the Efroimsky torque, while a 10 bar N_2 atmosphere could allow for more significant effects. Even for a thicker atmosphere, the effects tend to only be significant at higher $\dot{\gamma}$ not near synchronicity, as the Efroimsky torque dominates at smaller $\dot{\gamma}$ whereas the atmospheric torque approaches zero.

We also note that the atmospheric torque can create new stable equilibria, as shown in Figure 4.2. However, we do not expect the driving torques to significantly affect final spin results for these scenarios, as the stable equilibrium is enforced over a much broader range in $\dot{\gamma}$ as compared to standard spin-orbit resonances.

Meanwhile, forcing seems to increase the likelihood for capture into higher order spin-orbit resonances, especially when the resonances are significantly strengthened by the atmospheric torque. Forcing can also result in other stable limit cycles in which the spin argument γ circulates.

For the TOI-700 system, which we used as our case study analogue system in this chapter, our results show that the estimated mass of the perturbing planet TOI-700c implies a ratio of

$\omega_M/\omega_S \simeq 0.3$ with our other fiducial choices in parameters. These parameter choices result in a practically pure synchronous rotation, being just below the ω_M/ω_S threshold barrier when choosing initial conditions of $\dot{\phi} = 0.3$ yr^{-1} (implied from current observations if we set $\phi = 0$), and $\phi = 0$, which results in a circulation in ϕ just beyond the separatrix.

However, choosing different, reasonable parameters can change our ratio of ω_M/ω_S to be either just above the synchronicity threshold, or further below it. The fact that current observations suggest that the resonant angle system of planets d and c is very close the separatrix suggests that, though the perturbing planet likely may not be massive enough to push the spin out of synchronicity, it still may be possible if we shift our assumptions. And if the perturbing planet were larger, then the effects on the spin could almost certainly result in a spin that was effectively non-synchronous.

As this is just the first system discovered by *TESS* with an Earth-sized planet in the estimated habitable, we can expect more discoveries in the near future from missions such as *TESS* of such systems, which may be even more applicable to our spin model.

We also note that the case study we used in this chapter involves a system with two planets in a 7:3 commensurability. The behavior for other resonances should be qualitatively similar *if* the resonant angle ϕ varies at similar strengths. The biggest difference is that the conditions to be interior to the separatrix of the $\phi - \dot{\phi}$ system is more stringent as the order of the commensurability increases; i.e. the range in semi-major axis becomes tighter for a planet to be considered as being *in* resonance with another planet. Thus, lower order resonances would typically be expected to lead to larger mean motion variations primarily because the criteria for a resonance is broader. However, TOI-700, the system used as a case study in this chapter, contained two planets that still happened to be extraordinarily close to a higher-order commensurability, and implied variations in the resonant angle that would still allow for significant spin forcing.

Finally, this chapter indicates that the choice in tidal modeling is an important one. For our previous tidal model used in chapters 2 and 3, for example, we would not observe the threshold in ω_M/ω_S that we observe with the Efroimsky torque in this chapter. While the

Efroimsky torque can become quite strong at smaller $\dot{\gamma}$, we still show that the forcing can excite the spin enough to allow $\dot{\gamma}$ sustain itself under a higher amplitude under the influence of the Efroimsky torque. Finally, this chapter also depicts how forcing, as well as strong atmospheric torques, may actually increase the odds of capture in higher-order spin-orbit resonances.

CHAPTER 5

Conclusions

In the previous chapters, we have introduced a new significant consideration in modeling the spin of planets in the habitable zone of small stars. We have demonstrated the variations in mean motion caused by nearby resonant companions can have potentially significant effects on the resultant spin of planets in such systems. In Chapter 2, we introduced this concept by considering the effects of only one resonant companion on the primary planet of concern, applying a simple tidal damping model for illustrative purposes. In Chapter 3 we added complexity by considering how multiple resonant companions can affect the spin state, introducing chaotic behaviors that result from the long-term unstable behavior of the mean motion under the influence of these multiple companions. Finally, in Chapter 4 we considered further complexities in tidal modeling as well as the potential effects of atmospheric tidal torques, which depicted that there may be thresholds of forcing strength above which we would expect non-synchronous spins and below which we expect almost pure synchronicity. We also showed how spin forcing and significant atmospheric torques can further enforce the stability of higher-order spin-orbit resonances and suggest higher capture probabilities.

Altogether, we have showcased many of the complexities of modeling the spin of habitable zone planets around small, cool stars. Most other studies thus far have largely assumed that planets in such systems are necessarily tidally locked into synchronous spin states, resulting in permanent day-night sides on such planets and raising some doubts on habitability prospects. Our modeling presented here, however, shows that much work still needs to be done on spin evolution for these planets, with more than just pure tidal torques acting on the planets.

In fact, we have demonstrated a strong probability that many relevant planets could be pushed from otherwise synchronous spin states to effectively non-synchronous states due to forcing caused by mean motion variations. The planets may then librate with high amplitude librations, or else even completely circulate, resulting in higher or complete stellar coverage of the planet over time.

We also find current systems for which our model may be relevant, especially in TRAPPIST-1. The number of relevant systems is expected grow dramatically with the new *TESS* mission, which has already discovered systems such as TOI-700. As these systems are discovered, our model can provide insight to the possible spin behaviors of habitable zone planets around such small and cool stars.

Further work is required to, among other things, explore the potential effects on climate and thus prospects for habitability. Effects on climate would depend greatly on the spin period of those planets with full stellar coverage, with shorter periods being more likely to prevent atmospheric collapse. Considerations would also need to be made for planets with stable moderate-to-high amplitude librations, with stellar coverage not being uniformly distributed over time for any particular latitude. Climate modeling is potentially further complicated for planets within a TRAPPIST-1-like system, with our results in Chapter 3 depicting quasi-stable spin states which abruptly switch over time. These avenues of exploration can inspire much more work on planets within these relevant systems, shedding more light on the complexities of spin within compact systems and its effects on climate.

APPENDIX A

REBOUND Samples

We sampled from different initial conditions of REBOUND simulations of the orbital parameters of TRAPPIST-1 in Chapter 3. We chose to sample among a range of different orbital behaviors. Namely, we sampled among simulations with behaviors spanning a range in the forcing strength depicted in equation 3.1 (i.e. simulations spanning a range of different variances in mean motion among the planets), from negligible to strong (see horizontal axes of Figures 3.6, 3.7, and 3.11). REBOUND simulations sampled by file name are listed below and can be found at `https://zenodo.org/record/496153`:

IC111K1.6763e+02mag3.2152e-03.bin

IC100K1.2213e+02mag6.8408e-03.bin

IC125K1.0315e+02mag1.4880e-03.bin

IC235K7.2640e+02mag3.6993e-02.bin

IC123K2.4714e+02mag7.2180e-03.bin

IC119K4.9624e+02mag3.1153e-02.bin

IC73K1.9292e+02mag4.1292e-02.bin

IC190K3.0921e+02mag7.6131e-02.bin

IC163K2.3874e+02mag2.6440e-02.bin

IC98K2.9143e+02mag5.0300e-02.bin

IC290K3.5223e+01mag6.1289e-03.bin

IC294K2.1680e+02mag2.5643e-03.bin

IC93K1.6320e+02mag9.3872e-02.bin

IC101K1.0784e+02mag5.1523e-02.bin

IC162K4.3853e+01mag1.8504e-01.bin

IC239K4.1655e+01mag2.4514e-03.bin

IC240K3.8638e+01mag1.9549e-02.bin

IC70K7.1608e+02mag4.1427e-01.bin

REFERENCES

[Baker and Blackburn, 2005] Baker, G. L. and Blackburn, J. A. (2005). *The Pendulum: A Case Study in Physics*. Oxford University Press, Oxford.

[Ballard and Johnson, 2016] Ballard, S. and Johnson, J. A. (2016). The Kepler Dichotomy among the M Dwarfs: Half of Systems Contain Five or More Coplanar Planets. *Astrophysical Journal*, 816:66.

[Barnes et al., 2013] Barnes, R., Mullins, K., Goldblatt, C., Meadows, V. S., Kasting, J. F., and Heller, R. (2013). Tidal Venuses: Triggering a Climate Catastrophe via Tidal Heating. *Astrobiology*, 13:225–250.

[Bolmont et al., 2017] Bolmont, E., Selsis, F., Owen, J. E., Ribas, I., Raymond, S. N., Leconte, J., and Gillon, M. (2017). Water loss from terrestrial planets orbiting ultracool dwarfs: implications for the planets of TRAPPIST-1. *Monthly Notices of the Royal Astronomical Society*, 464:3728–3741.

[Bolmont et al., 2013] Bolmont, E., Selsis, F., Raymond, S. N., Leconte, J., Hersant, F., Maurin, A.-S., and Pericaud, J. (2013). Tidal dissipation and eccentricity pumping: Implications for the depth of the secondary eclipse of 55 Cancri e. *Astronomy & Astrophysics*, 556:A17.

[Charbonneau and Deming, 2007] Charbonneau, D. and Deming, D. (2007). The Dynamics-Based Approach to Studying Terrestrial Exoplanets. *arXiv e-prints*, page arXiv:0706.1047.

[Chen et al., 2015] Chen, W., Li, J. C., Ray, J., Shen, W. B., and Huang, C. L. (2015). Consistent estimates of the dynamic figure parameters of the earth. *Journal of Geodesy*, 89:179–188.

[Cowan et al., 2012] Cowan, N. B., Voigt, A., and Abbot, D. S. (2012). Thermal Phases of Earth-like Planets: Estimating Thermal Inertia from Eccentricity, Obliquity, and Diurnal Forcing. *Astrophysical Journal*, 757:80.

[Crossfield, 2013] Crossfield, I. J. M. (2013). On high-contrast characterization of nearby, short-period exoplanets with giant segmented-mirror telescopes. *Astronomy & Astrophysics*, 551:A99.

[Dressing and Charbonneau, 2013] Dressing, C. D. and Charbonneau, D. (2013). The Occurrence Rate of Small Planets around Small Stars. *Astrophysical Journal*, 767:95.

[Driscoll and Barnes, 2015] Driscoll, P. E. and Barnes, R. (2015). Tidal Heating of Earth-like Exoplanets around M Stars: Thermal, Magnetic, and Orbital Evolutions. *Astrobiology*, 15:739–760.

[Edvardsson et al., 2002] Edvardsson, S., Karlsson, K. G., and Engholm, M. (2002). Accurate spin axes and solar system dynamics: Climatic variations for the Earth and Mars. *Astronomy & Astrophysics*, 384:689–701.

[Efroimsky, 2012a] Efroimsky, M. (2012a). Bodily tides near spin-orbit resonances. *Celestial Mechanics and Dynamical Astronomy*, 112(3):283–330.

[Efroimsky, 2012b] Efroimsky, M. (2012b). Tidal Dissipation Compared to Seismic Dissipation: In Small Bodies, Earths, and Super-Earths. *Astrophysical Journal*, 746(2):150.

[Efroimsky and Lainey, 2007] Efroimsky, M. and Lainey, V. (2007). Physics of bodily tides in terrestrial planets and the appropriate scales of dynamical evolution. *Journal of Geophysical Research (Planets)*, 112:E12003.

[Efroimsky and Williams, 2009] Efroimsky, M. and Williams, J. G. (2009). Tidal torques: a critical review of some techniques. *Celestial Mechanics and Dynamical Astronomy*, 104(3):257–289.

[Egbert and Ray, 2000] Egbert, G. D. and Ray, R. D. (2000). Significant dissipation of tidal energy in the deep ocean inferred from satellite altimeter data. *Nature*, 405:775–778.

[Eggleton et al., 1998] Eggleton, P. P., Kiseleva, L. G., and Hut, P. (1998). The Equilibrium Tide Model for Tidal Friction. *Astrophysical Journal*, 499:853–870.

[Fabrycky et al., 2014] Fabrycky, D. C., Lissauer, J. J., Ragozzine, D., Rowe, J. F., Steffen, J. H., Agol, E., Barclay, T., Batalha, N., Borucki, W., Ciardi, D. R., Ford, E. B., Gautier, T. N., Geary, J. C., Holman, M. J., Jenkins, J. M., Li, J., Morehead, R. C., Morris, R. L., Shporer, A., Smith, J. C., Still, M., and Van Cleve, J. (2014). Architecture of Kepler's Multi-transiting Systems. II. New Investigations with Twice as Many Candidates. *Astrophysical Journal*, 790:146.

[Fang and Margot, 2012] Fang, J. and Margot, J.-L. (2012). Architecture of Planetary Systems Based on Kepler Data: Number of Planets and Coplanarity. *The Astrophysical Journal*, 761(2):92.

[Ford et al., 2001] Ford, E. B., Seager, S., and Turner, E. L. (2001). Characterization of extrasolar terrestrial planets from diurnal photometric variability. *Nature*, 412:885–887.

[Gilbert et al., 2020] Gilbert, E. A., Barclay, T., Schlieder, J. E., Quintana, E. V., Hord, B. J., Kostov, V. B., Lopez, E. D., Rowe, J. F., Hoffman, K., Walkowicz, L. M., Silverstein, M. L., Rodriguez, J. E., Vanderburg, A., Suissa, G., Airapetian, V. S., Clement, M. S., Raymond, S. N., Mann, A. W., Kruse, E., Lissauer, J. J., Colón, K. D., Kopparapu, R. k., Kreidberg, L., Zieba, S., Collins, K. A., Quinn, S. N., Howell, S. B., Ziegler, C., Halley Vrijmoet, E., Adams, F. C., Arney, G. N., Boyd, P. T., Brande, J., Burke, C. J., Cacciapuoti, L., Chance, Q., Christiansen, J. L., Covone, G., Daylan, T., Dineen, D., Dressing, C. D., Essack, Z., Fauchez, T. J., Galgano, B., Howe, A. R., Kaltenegger, L., Kane, S. R., Lam, C., Lee, E. J., Lewis, N. K., Logsdon, S. E., Mand ell, A. M., Monsue, T., Mullally, F., Mullally, S. E., Paudel, R., Pidhorodetska, D., Plavchan, P., Tañón Reyes, N., Rinehart, S. A., Rojas-Ayala, B., Smith, J. C., Stassun, K. G., Tenenbaum, P., Vega, L. D., Villanueva, G. L., Wolf, E. T., Youngblood, A., Ricker, G. R., Vanderspek, R. K., Latham, D. W., Seager, S., Winn, J. N., Jenkins, J. M., Bakos, G. Á., Briceño, C., Ciardi, D. R., Cloutier, R., Conti, D. M., Couperus, A., Di Sora, M., Eisner, N. L., Everett, M. E., Gan, T., Hartman, J. D., Henry, T., Isopi, G., Jao, W.-C., Jensen, E. L. N., Law, N., Mallia, F., Matson, R. A., Shappee, B. J., Wood, M. L., and Winters, J. G. (2020). The First Habitable Zone Earth-sized Planet from TESS. I: Validation of the TOI-700 System. *arXiv e-prints*, page arXiv:2001.00952.

[Gillon et al., 2017] Gillon, M. T., Amaury, H. M. J., Demory, B. O., Jehin, E., Agol, E., Deck, K. M., Lederer, S. M., de Wit, J., and Burdanov, A. (2017). Seven temperate terrestrial planets around the nearby ultracool dwarf star TRAPPIST-1 JA. *Nature Letters*, 542:456.

[Goldreich and Peale, 1966] Goldreich, P. and Peale, S. (1966). Spin-orbit coupling in the solar system. *Astronomical Journal*, 71:425.

[Goldreich and Peale, 1968] Goldreich, P. and Peale, S. J. (1968). The Dynamics of Planetary Rotations. *Annual Review of Astronomy and Astrophysics*, 6:287.

[Goldreich and Schlichting, 2014] Goldreich, P. and Schlichting, H. E. (2014). Overstable Librations can Account for the Paucity of Mean Motion Resonances among Exoplanet Pairs. *Astronomical Journal*, 147:32.

[Grimm et al., 2018] Grimm, S. L., Demory, B.-O., Gillon, M., Dorn, C., Agol, E., Burdanov, A., Delrez, L., Sestovic, M., Triaud, A. H. M. J., Turbet, M., Bolmont, É., Caldas, A., Wit, J. d., Jehin, E., Leconte, J., Raymond, S. N., Grootel, V. V., Burgasser, A. J., Carey, S., Fabrycky, D., Heng, K., Hernandez, D. M., Ingalls, J. G., Lederer, S., Selsis, F., and Queloz, D. (2018). The nature of the TRAPPIST-1 exoplanets. *Astronomy & Astrophysics*, 613:A68.

[Hadden and Lithwick, 2014] Hadden, S. and Lithwick, Y. (2014). Densities and Eccentricities of 139 Kepler Planets from Transit Time Variations. *Astrophysical Journal*, 787:80.

[Hansen, 2010] Hansen, B. M. S. (2010). Calibration of Equilibrium Tide Theory for Extrasolar Planet Systems. *Astrophysical Journal*, 723:285–299.

[Hansen and Murray, 2013] Hansen, B. M. S. and Murray, N. (2013). Testing in Situ Assembly with the Kepler Planet Candidate Sample. *Astrophysical Journal*, 775:53.

[Hansen and Murray, 2015] Hansen, B. M. S. and Murray, N. (2015). Secular effects of tidal damping in compact planetary systems. *Monthly Notices of the Royal Astronomical Society*, 448:1044–1059.

[Heller et al., 2011] Heller, R., Leconte, J., and Barnes, R. (2011). Tidal obliquity evolution of potentially habitable planets. *Astronomy & Astrophysics*, 528:A27.

[Hut, 1981] Hut, P. (1981). Tidal evolution in close binary systems. *Astronomy & Astrophysics*, 99:126–140.

[Ingersoll and Dobrovolskis, 1978] Ingersoll, A. P. and Dobrovolskis, A. R. (1978). Venus' rotation and atmospheric tides. *Nature*, 275(5675):37–38.

[Joshi et al., 1997] Joshi, M., Haberle, R., and Reynolds, R. (1997). Simulations of the atmospheres of synchronously rotating terrestrial planets orbiting m dwarfs: Conditions for atmospheric collapse and the implications for habitability. *Icarus*, 129(2):450 – 465.

[Kasting et al., 1993] Kasting, J. F., Whitmire, D. P., and Reynolds, R. T. (1993). Habitable Zones around Main Sequence Stars. *Icarus*, 101(1):108–128.

[Kawahara and Fujii, 2011] Kawahara, H. and Fujii, Y. (2011). Mapping Clouds and Terrain of Earth-like Planets from Photometric Variability: Demonstration with Planets in Face-on Orbits. *Astrophysical Journal Letters*, 739:L62.

[Kopparapu, 2013] Kopparapu, R. K. (2013). A Revised Estimate of the Occurrence Rate of Terrestrial Planets in the Habitable Zones around Kepler M-dwarfs. *Astrophysical Journal Letters*, 767:L8.

[Kopparapu et al., 2013] Kopparapu, R. K., Ramirez, R., Kasting, J. F., Eymet, V., Robinson, T. D., Mahadevan, S., Terrien, R. C., Domagal-Goldman, S., Meadows, V., and Deshpande, R. (2013). Habitable Zones around Main-sequence Stars: New Estimates. *Astrophysical Journal*, 765:131.

[Kopparapu et al., 2016] Kopparapu, R. k., Wolf, E. T., Haqq-Misra, J., Yang, J., Kasting, J. F., Meadows, V., Terrien, R., and Mahadevan, S. (2016). The Inner Edge of the Habitable Zone for Synchronously Rotating Planets around Low-mass Stars Using General Circulation Models. *Astrophysical Journal*, 819:84.

[Lainey et al., 2007] Lainey, V., Dehant, V., and Pätzold, M. (2007). First numerical ephemerides of the Martian moons. *Astronomy & Astrophysics*, 465:1075–1084.

[Leconte et al., 2015] Leconte, J., Wu, H., Menou, K., and Murray, N. (2015). Asynchronous rotation of Earth-mass planets in the habitable zone of lower-mass stars. *Science*, 347:632–635.

[Lissauer et al., 2011] Lissauer, J. J., Ragozzine, D., Fabrycky, D. C., Steffen, J. H., Ford, E. B., Jenkins, J. M., Shporer, A., Holman, M. J., Rowe, J. F., Quintana, E. V., Batalha, N. M., Borucki, W. J., Bryson, S. T., Caldwell, D. A., Carter, J. A., Ciardi, D., Dunham, E. W., Fortney, J. J., Gautier, III, T. N., Howell, S. B., Koch, D. G., Latham, D. W., Marcy, G. W., Morehead, R. C., and Sasselov, D. (2011). Architecture and Dynamics of Kepler's Candidate Multiple Transiting Planet Systems. *Astrophysical Journal Supplement*, 197:8.

[Makarov, 2012] Makarov, V. V. (2012). Conditions of Passage and Entrapment of Terrestrial Planets in Spin-orbit Resonances. *Astrophysical Journal*, 752(1):73.

[Margot et al., 2007] Margot, J. L., Peale, S. J., Jurgens, R. F., Slade, M. A., and Holin, I. V. (2007). Large longitude libration of mercury reveals a molten core. *Science*, 316(5825):710–714.

[Margot et al., 2012] Margot, J.-L., Peale, S. J., Solomon, S. C., Hauck, II, S. A., Ghigo, F. D., Jurgens, R. F., Yseboodt, M., Giorgini, J. D., Padovan, S., and Campbell, D. B. (2012). Mercury's moment of inertia from spin and gravity data. *Journal of Geophysical Research (Planets)*, 117:E00L09.

[Millholland et al., 2017] Millholland, S., Wang, S., and Laughlin, G. (2017). Kepler multi-planet systems exhibit unexpected intra-system uniformity in mass and radius. *The Astrophysical Journal Letters*, 849(2):L33.

[Murray and Dermott, 1999] Murray, C. D. and Dermott, S. F. (1999). *Solar system dynamics*. Cambridge University Press, Cambridge.

[Ogilvie, 2014] Ogilvie, G. I. (2014). Tidal Dissipation in Stars and Giant Planets. *Annual Review of Astronomy and Astrophysics*, 52:171–210.

[Petigura et al., 2015] Petigura, E. A., Schlieder, J. E., Crossfield, I. J. M., Howard, A. W., Deck, K. M., Ciardi, D. R., Sinukoff, E., Allers, K. N., Best, W. M. J., Liu, M. C., Beichman, C. A., Isaacson, H., Hansen, B. M. S., and Lépine, S. (2015). Two Transiting Earth-size Planets Near Resonance Orbiting a Nearby Cool Star. *Astrophysical Journal*, 811:102.

[Rein and Liu, 2012] Rein, H. and Liu, S.-F. (2012). Rebound: an open-source multi-purpose n-body code for collisional dynamics. *Astronomy & Astrophysics*, 537:A128.

[Rein and Tamayo, 2015] Rein, H. and Tamayo, D. (2015). Whfast: a fast and unbiased implementation of a symplectic wisdom–holman integrator for long-term gravitational simulations. *Monthly Notices of the Royal Astronomical Society*, 452(1):376–388.

[Rein and Tamayo, 2017] Rein, H. and Tamayo, D. (2017). A new paradigm for reproducing and analysing n-body simulations of planetary systems. *Monthly Notices of the Royal Astronomical Society*, 467(2):2377–2383.

[Shields et al., 2016] Shields, A. L., Ballard, S., and Johnson, J. A. (2016). The habitability of planets orbiting M-dwarf stars. *Physics Reports*, 663:1.

[Spiegel et al., 2008] Spiegel, D. S., Menou, K., and Scharf, C. A. (2008). Habitable Climates. *Astrophysical Journal*, 681:1609–1623.

[Swift et al., 2013] Swift, J. J., Johnson, J. A., Morton, T. D., Crepp, J. R., Montet, B. T., Fabrycky, D. C., and Muirhead, P. S. (2013). Characterizing the Cool KOIs. IV. Kepler-32 as a Prototype for the Formation of Compact Planetary Systems throughout the Galaxy. *Astrophysical Journal*, 764:105.

[Tamayo et al., 2017] Tamayo, D., Rein, H., Petrovich, C., and Murray, N. (2017). Convergent Migration Renders TRAPPIST-1 Long-lived. *Astrophysical Journal*, 840:L19.

[Turbet et al., 2018] Turbet, M., Bolmont, E., Leconte, J., Forget, F., Selsis, F., Tobie, G., Caldas, A., Naar, J., and Gillon, M. (2018). Modeling climate diversity, tidal dynamics and the fate of volatiles on TRAPPIST-1 planets. *Astronomy & Astrophysics*, 612:A86.

[Van Eylen and Albrecht, 2015] Van Eylen, V. and Albrecht, S. (2015). Eccentricity from Transit Photometry: Small Planets in Kepler Multi-planet Systems Have Low Eccentricities. *Astrophysical Journal*, 808:126.

[Van Laerhoven et al., 2014] Van Laerhoven, C., Barnes, R., and Greenberg, R. (2014). Tides, planetary companions, and habitability: habitability in the habitable zone of low-mass stars. *Monthly Notices of the Royal Astronomical Society*, 441:1888–1898.

[Weiss et al., 2018] Weiss, L. M., Marcy, G. W., Petigura, E. A., Fulton, B. J., Howard, A. W., Winn, J. N., Isaacson, H. T., Morton, T. D., Hirsch, L. A., Sinukoff, E. J., et al. (2018). The california-kepler survey. v. peas in a pod: planets in a kepler multi-planet system are similar in size and regularly spaced. *The Astronomical Journal*, 155(1):48.

[Wordsworth, 2015] Wordsworth, R. (2015). Atmospheric heat redistribution and collapse on tidally locked planets. *The Astrophysical Journal*, 806(2):180.

[Wordsworth et al., 2011] Wordsworth, R. D., Forget, F., Selsis, F., Millour, E., Charnay, B., and Madeleine, J.-B. (2011). Gliese 581d is the First Discovered Terrestrial-mass Exoplanet in the Habitable Zone. *Astrophysical Journal*, 733(2):L48.

[Wu and Lithwick, 2013] Wu, Y. and Lithwick, Y. (2013). Density and Eccentricity of Kepler Planets. *Astrophysical Journal*, 772:74.

[Yang et al., 2014] Yang, J., Boué, G., Fabrycky, D. C., and Abbot, D. S. (2014). Strong Dependence of the Inner Edge of the Habitable Zone on Planetary Rotation Rate. *Astrophysical Journal Letters*, 787:L2.

[Yoder and Peale, 1981] Yoder, C. F. and Peale, S. J. (1981). The tides of Io. *Icarus*, 47:1–35.

[Zanazzi and Lai, 2017] Zanazzi, J. J. and Lai, D. (2017). Triaxial deformation and asynchronous rotation of rocky planets in the habitable zone of low-mass stars. *Monthly Notices of the Royal Astronomical Society*, 469(3):2879–2885.